DEVELOPMENT OF DNA NANOSENSORS AS APTASENSOR FOR LYSOZYME AND DNAZYME SENSOR FOR ZINC IONS

Wai Jing Luen

Thesis submitted to the University of Nottingham for the degree of Doctor of Philosophy

Jan 2020

To my beloved parents, Wai Teak Chong and Chua Mui Chen, and my dearest sister and brother, Ching Ying and Jing Shien. Thank you for your understanding and support throughout my PhD life.

ACKNOWLEDGEMENTS

First and foremost, I would like to express my utmost gratitude to my supervisor, Dr New Siu Yee for her continuous patience, guidance and motivation throughout my entire period of research and thesis writing. Without her immense knowledge, persistent encouragement and selfless support, this thesis would not have been possible. I could not have imagined having a better mentor for my PhD study. Besides, I would also like to extend my gratefulness to Professor Lu Yi of University of Illinois Urbana-Champaign for his support and willingness to host me during my overseas laboratory attachment at the United States. The eye-opening experience is truly invaluable and pivotal in making this research a worthful journey.

I would also like to thank my fellow friends, especially Dr Janet Tan Sui Ling, Koh May Zie, and Leong Chia Choong, who throughout our PhD journey together, are willing to listen to all my concerns and provide suggestions whenever needed. Also, thank you for your willingness to share yours with me. Not to forget my undergraduate classmates, Tao Leong, Jean How and Ee Phinn who are always there for me and cheering me up during my ups and downs. Chatting with all of you is truly a pleasure in my life.

In addition, I would also like to express my sincere gratitude to the lab manager, Mr Wong as well as other lab technicians for their kind efforts in guiding and responding to all my queries and problems that I have encountered with the equipment in the laboratories. Your presence makes the lab a better place to work in. Last but not the least, I wish to thank the Graduate School who had shared their previous experience, intellectual support, assistance and suggestions in various ways to make me a better researcher.

DECLARATION

This thesis is based on my original work except for the citations or references which have been duly acknowledged. It has not been previously or concurrently submitted for any degree at either the University of Nottingham Malaysia or any other institution.

_____

Wai Jing Luen

TABLE OF CONTENTS

LIST OF TABLES

LIST OF FIGURES

LIST OF EQUATIONS

LIST OF ABBREVIATIONS

8-Oxo-dG	8-hyrdoxy-2'-deoxyguanosine
A	Adenosine
Abs	Absorbance
Ag	Silver
Aptasensor	Aptamer-based biosensor
Au	Gold
$AuCl_4^-$	Tetrachloroaurate
AuNPs	Gold nanoparticles
Ba^{2+}	Barium ion
BRET	Bioluminescence resonance energy transfer
BSA	Bovine serum albumin
C	Cytosine
$C_2H_4O_2S$	Mercaptoacetic acid
C_2H_7NS	Cysteamine/ 2-Aminoethanethiol
$C_5H_9NO_3S$	Acetylcysteine
Ca^{2+}	Calcium ion
CAMB	Catalytic and molecular beacon
citAuNPs	Citrate-capped gold nanoparticles
CRC	Critical redispersion concentration
CRET	Chemiluminescence resonance energy transfer
CTAB-AuNRs	Hexadecyltrimethylammonium bromide-coated gold nanorods
Cu	Copper
cysAuNPs	Cysteamine-coated gold nanoparticles
DI H_2O	Deionised water
DLS	Dynamic light scattering
DNA	Deoxyribonucleic acid
D_r	Dispersion ratios
dsDNA	Double-stranded DNA
EDL	Electrical double layer
E-DNA biosensor	DNA-based electrochemical biosensor
ELISA	Enzyme-linked immunosorbent assay
etc	Et cetera
FRET	Fluorescence resonance energy transfer
G	Guanine
H_2O_2	Hydrogen peroxide
$HAuCl_4$	gold(III) chloride
HCl	Hydrochloric acid
HIV	Human immunodeficiency viruses
HNO_3	Nitric acid
HRTEM	High-resolution transmission electron microscope
HSA	Human serum albumin
i.e.	In other words,
ISL	Inverse sensitivity limit
ISL	Inverse sensitivity limit
K^+	Potassium ion
L	Luminescence
LBA	Lysozyme-binding aptamer
Li^+	Lithium ion
LOD	Limit of detection

LSPR	Localised surface plasmon resonance
Mg^{2+}	Magnesium ion
Mode A	Aggregation mode
Mode R	Redispersion mode
Na^{+}	Sodium ion
$NaBH_4$	Sodium borohydride
Pb^{2+}	Lead ion
PBS	Phosphate buffered saline
PCR	Polymerase chain reaction
PCS	Photon correlation spectroscopy
PDDA	Polydiallyldimethylammonium chloride
PDMS	Polydimethylsiloxane
PET	Photoinduced electron transfer
pI	Isoelectric point
PIFE	Protein induced fluorescence enhancement
pKa	Negative log of acid dissociation constant
PNPP	p-nitrophenyl phosphate
R^2	Correlation coefficient
rA	Adenosine RNA
RET	Resonance energy transfer
RNA	Ribonucleic acid
S	Sulphur
SELEX	Systematic evolution of ligands by exponential enrichment
SEM	Scanning electron microscope
SNR	Signal-to-noise ratio
SPR	Surface plasmon resonance
ssDNA	Single-stranded DNA
STEM	Scanning-transmission electron microscope
Strep-Lucia	Streptavidin-labelled Lucia luciferase
T	Thymine
TBA	Thrombin-binding aptamer
TEM	Transmission electron microscope
T_m	Melting temperature
TMB	3,3',5,5'-tetramethylbenzidine
UV	Ultraviolet
UV-Vis	Ultraviolet-Visible
VEGF	Vascular endothelial growth factor
Zn^{2+}	Zinc ion
ZP	Zeta potential

ACHIEVEMENTS AND PUBLICATIONS

Presentation(s)

2nd International Conference on Molecular Diagnostics and Biomarker Discovery Conference, 2-4 May 2017, Institute for Research in Molecular Medicine (INFORMM), Universiti Sains Malaysia, Penang, Malaysia. Poster presentation.

3rd Annual Postgraduate Research Symposium, 8 August 2017, Department of Biomedical Sciences, University of Nottingham Malaysia, Selangor, Malaysia. Poster presentation. Won the Best Poster Award.

3 Minutes Thesis, 12 September 2017, Graduate School, University of Nottingham Malaysia, Selangor, Malaysia. Oral presentation.

23rd Chinese American Chemical Society - Great Lakes Chapter (GLCACS) Annual Conference, 27 April 2019, Abbott Laboratories, Illinois, United States. Oral presentation.

Publication(s)

Wai JL and New SY. Cysteamine-Coated Gold Nanoparticles for Bimodal Colorimetric Detection with Inverse Sensitivity: A Proof-of-Concept with Lysozyme. RSC Advances. (Published)

Wai JL, Zheng J, New SY, Yi L. A Bioluminescence Resonance Energy Transfer (BRET) Driven DNAzyme for Ratiometric Detection of Metal Ions. (Writing-in-progress)

Collaboration and Attachment

Oversea laboratory attachment at University of Illinois Urbana-Champaign under supervision of Prof. Yi Lu for 16 months. Pioneering and collaborating on two major projects involving DNAzymes-based biosensors for environmental monitoring and biomedical diagnostics.

ABSTRACT

DNA nanotechnology based on DNA aptamers and DNAzymes is highly beneficial because they provide more stable, programmable and manageable alternatives to their native counterparts (*i.e.* antibodies and enzymes) on top of being cost-effective.

One of the widely reported features of DNA-aptamer based biosensors is by coupling it with gold nanoparticles (AuNPs), due to the unique opto-electronic characteristics of the latter. While the positively charged cysteamine-coated gold nanoparticles (cysAuNPs) present an ideal candidate to directly interact with negatively charged DNA, the fundamental understanding and precise modulation on their interaction for biosensing purposes are still largely unexplored. By carefully studying the interaction between cysAuNPs and lysozyme-binding aptamer (LBA), a colorimetric aptasensor has been developed for lysozyme detection. Despite inducing aggregation initially, further increasing the amount of LBA above critical redispersion concentration (CRC) was found to redisperse cysAuNPs, as proven by UV-visible spectroscopy and zeta-sizer study. The changing dispersion states of cysAuNPs was further exploited to construct a bimodal colorimetric aptasensor, with modes A (aggregation) and R (redispersion) utilising LBA at concentrations below and above CRC, respectively. Both modes were found to be complementarily: mode A having a linear range of 37.5 - 180 nM of lysozyme with a limit of detection (LOD) of 2.29 nM; whereas mode R can detect lysozyme linearly in the range of 500 - 4000 nM with a LOD of 375 nM. Synergistic screening *via* both modes also display a remarkable selectivity towards lysozyme against other control proteins. Besides, detection of lysozyme *via* mode R also demonstrated a novel analytical concept of inverse sensitivity, with exceptional signal-to-noise ratio (SNR) of 72.56.

From another perspective, DNAzymes are frequently coupled with fluorescence resonance energy transfer (FRET) in the development of metal ion sensors. Despite allowing analysis being performed ratiometrically, FRET is hindered by several pivotal limitations, preventing such DNAzymes-driven metal ion sensors to be translated into practical scenarios. Bioluminescence resonance energy transfer (BRET) provides a good solution in line with that premise as it does not require an excitation stimulus. An 8-17 DNAzyme and its cofactor, Zn^{2+} ions, have been chosen for proof-of-concept study, with the BRET pair consists of Lucia luciferase and Cy3 fluorophore. The implementation of BRET was verified by observing a second luminescence peak from co-excited Cy3. Further structural and experimental optimisations have resulted in an improved BRET ratio at 0.43. The DNAzyme-driven BRET-based biosensor also showed great selectivity towards Zn^{2+} ions by inducing a noticeable BRET percentage changes and was able to quantify Zn^{2+} from 100 to 3200 nM in buffered solution. Compared to other reported Zn^{2+} sensors, the DNAzyme biosensor described here was able to quantify > 300 equivalent concentration of Zn^{2+} ions, yet still having a low LOD estimated at 62.58 nM. The study here represents a milestone that for the first time, a previously unexplored technique of BRET has been successfully implemented in DNAzyme system for metal ion sensing.

In summary, the works detailed here have provided an insight on the further development of DNA nanotechnology with regards to biosensing purposes. These successful applications of both DNA aptamers and DNAzymes, when coupled with cysAuNPs and BRET, respectively, have not only addressed their currently associated limitations, but also opens up more possibility of utilising them as biosensing platforms to reliably detect biomarkers and metal ions in the near future.

CHAPTER 1

INTRODUCTION

1.1 General overview

DNA is always known as a molecule responsible for storing and transmitting genetic information from generation to generation in all biological systems. Built on this premise, the principle idea of DNA nanotechnology is to take the DNA out of its initial biological context and utilise it for various purposes, either in biological or non-biological frameworks. Since the first proposal by Seeman in 1980s to utilise nucleic acids as building blocks in constructing self-assembled nanomaterials (Seeman, 1982), DNA nanotechnology has always been a fast-growing field. Nowadays, it has even far exceeded the original biological function of DNA as a mere storage of genetic information. Their feasibility in terms of sequence programmability, structural flexibility and unique chemical properties have synergistically made them a very powerful component for nanostructure assembly (Seeman, 2017; Ke, Castro and Choi, 2018), molecular recognition (Xing *et al.*, 2014; Alizadeh *et al.*, 2018; Zhang, Lai and Juhas, 2019), and reaction catalysis (Hollenstein, 2015; Liu, Chang and Li, 2017). Nevertheless, despite constant global efforts to further develop DNA nanotechnologies, their full potential is yet to be uncovered.

DNA aptamers are short, single-stranded DNA molecules that can be folded specifically to recognise particular targets with both high affinity and specificity (Zhang, Lai and Juhas, 2019). Their antibody-like behaviour is often harnessed for the functionalisation of gold nanoparticles (AuNPs) in developing colorimetric biosensors targeting various molecules-of-interest (Li *et al.*, 2011; Z. B. Chen *et al.*, 2013; Peng *et al.*, 2013). Represented by citrate-reduced gold nanoparticles (citAuNPs), AuNPs are nanosized gold that depending on their dispersion state, can undergo transition

between ruby red (dispersed) and bluish grey (aggregated) in colour (Xia *et al.*, 2016). Such unique colour-changing behaviour makes them a remarkable reporter probe in biosensors development to indicate the presence of particular molecules-of-interest. However, during DNA functionalisation, conventional citAuNPs are negatively charged as-synthesised and thus requires laborious protocols such as salt aging to bring both DNA aptamers and citAuNPs into close proximity to enable their interactions (Mirkin *et al.*, 1996). Furthermore, expensive thiolation on DNA is also needed to provide a mean of conjugation through the formation of covalent Au–S bond. To circumvent these bottlenecks, cysteamine-stabilised gold nanoparticles (cysAuNPs) appear to be a good alternative. Given that they are positively charged upon synthesis (Niidome *et al.*, 2004), cysAuNPs can interact with non-modified DNA with ease. On top of their improved stability due to intrinsic cysteamine-stabilisation *via* Au–S bonds, the advantages of cysAuNPs has been slowly gaining more attention in recent years. Coupled with the goal of addressing the current limitations of the mainstream citAuNPs, a beneficial advancement would be to further the investigation and exploitation on the electrostatic interaction between cysAuNPs and DNA aptamers to rationally design an aptamer-based biosensor (aptasensor). In the light of above, Chapter 3 focuses on the development of a bimodal cysAuNPs-based aptasensor using lysozyme and lysozyme-binding aptamer (LBA) as study models. Physical characterisations on the cysAuNPs were first conducted, indicating a nanoparticles system physically similar to the conventional citAuNPs with the exception of reversed zeta potential. The positively charged cysAuNPs were then allowed to interact with LBA at various concentrations. The subsequent LBA concentration-dependent response were studied in the forms of cysAuNPs aggregation and redispersion through ratiometric analysis on their resulting UV-Vis absorbance spectra. The unprecedented observation of cysAuNPs redispersion in

presence of excess LBA was documented with the proposal of critical redispersion concentration (CRC), a theoretical concentration of DNA required to induce dispersion instead of aggregation on cysAuNPs. Built on the premise that the binding between lysozyme and LBA would negate the electronegativity of the latter, a colorimetric and ratiometric aptasensor has been rationally designed for lysozyme detection. A bimodal detection with different dynamic ranges and promising limits of detection (LOD) has been achieved by applying LBA at the concentration of either below or above CRC, paving a path for tuneable detection. Apart from having remarkable sensitivity performance, the bimodal screening can also complement each other to rule out false positive results, therefore achieving good selectivity even in the presence of mixed control proteins. The significance of this work is further ascertained by the successful implementation of inverse sensitivity, a novel analytical concept of having increased responsive signal despite decreasing concentration of targeted analyte.

Another aspect of DNA nanotechnology is DNAzyme. Instead of having antibody-like properties as DNA aptamers, DNAzymes are a family of short and single-stranded DNA that possess certain catalytic capabilities, thus making them "enzyme-like". Upon activation by cofactors, DNAzymes can catalyse various enzymatic reactions, most notably in RNA transesterification that effectively cleave a RNA or RNA-DNA chimera strand into two shorter strands at specific site (Breaker and Joyce, 1994; Silverman, 2016). While most DNAzyme constructs are double-helix initially, the RNA-cleavage will lead to a drastic drop in their melting temperature, thus leading to strand dehybridisation between the enzyme and substrate strands. Due to their metal-dependent activities, DNAzymes are frequently incorporated into metal ion sensors with the implementation of fluorescence resonance energy transfer (FRET). A DNAzyme-driven FRET-based metal ion sensor typically utilises the

change in fluorescence, either an increase or decrease, to reflect the assembly or disassembly of the DNAzyme construct. However, such sensing platforms suffer from pivotal bottlenecks including photobleaching, signal contamination, and the requirement of excitation energy (mostly an external light source) that unfavourably hinder their practical usability. In line with the goal of translating DNAzymes technology into truly sustainable portable sensor for metal ion detection, one can infer that it is of utmost importance to explore other possible reporting techniques to complement with the unique molecular activities of DNAzymes in presence of specific metal ion cofactors. Therefore, Chapter 4 of this present thesis is to address the aforementioned FRET-related limitations by incorporating DNAzymes with bioluminescence resonance energy transfer (BRET) instead, as demonstrated by the study models of DNAzyme 8-17 and its metal ion cofactor, Zn^{2+} ions (Li *et al.*, 2000). BRET was achieved by modifying the DNAzyme 8-17 enzyme strand (8-17E) with a Lucia luciferase, a coelenterazine-utilising luciferase derived from marine copepods, through streptavidin-biotin conjugation whereas a Cy3 fluorophore was labelled at the DNAzyme 8-17 substrate strand (8-17S). Only when fully hybridised, the close proximity between Lucia and Cy3 will enable a strong BRET to co-excite the Cy3 in presence of coelenterazine. In principle, the BRET efficiency can be ratiometrically analysed by comparing the luminescence of Lucia and fluorescence of Cy3, indicating the presence and concentration of Zn^{2+} ions. To study the feasibility of a DNAzyme-driven BRET system, the event of BRET was first verified by comparing the DNAzyme construct consisted of only 8-17E or 8-17S, followed by a completed complex of 8-17E/S and the complex in presence of Zn^{2+} ions. Then, the biosensor conditions were optimised in terms of strand modifications, molar ratio of 8-17E/S as well as Lucia/Cy3. The optimised DNAzyme biosensor was first incubated with various monovalent and divalent metal ions, and the results showed very promising

selectivity performance as only Zn^{2+} ions can induce a noticeable change in BRET percentage (Δ BRET (%)) compared to control without any metal ions. An excellent sensitivity performance is also evidenced that a linear range of Zn^{2+} ions detection was observed with good R^2 value. Notably, considering that there is no signal amplification, the DNAzyme biosensor presented here demonstrated an outstanding quantification of > 300 equivalent concentration of Zn^{2+} in addition to its low LOD. The achievement of BRET implementation hereby represents a major advancement in the field of DNAzyme technology as it successfully expanded its horizon to another previously unexplored sensing platform.

1.2 Problem statement, hypothesis and objective

As mentioned previously, biosensors derived from DNA aptamers and DNAzymes are mostly solely available in laboratory settings at present time due to their respective associated disadvantages which prevent them to be deployed for practical purposes like on-site and real-time detection. New generation of such biosensors are thus needed with proper consideration to avoid such limitations. Therefore, the main objective of this study is to explore and expand the current scope of DNA nanotechnologies, by rationally designing a DNA aptamer-based and another DNAzyme-based biosensor for the detection of biomarkers and metal ions, respectively.

Together with their individual hypothesis, the specific objectives serving as prerequisites in achieving the main objectives are listed below, separated into two major groups each dedicated to DNA aptamer and DNAzymes.

For DNA aptamer-based biosensor, it is hypothesised that the electrostatic interaction between cationic cysAuNPs and anionic DNA is of advantage to prevent

the common limitation faced by citAuNPs, which can even be exploited for the detection of targeted analyte. The specific objectives are as following:

1. To study the effect of LBA aptamer on the dispersion states of cysAuNPs across a wide range of concentration.
2. To construct a cysAuNPs-derived aptasensor for lysozyme detection based on the optimised LBA concentrations.
3. To evaluate the sensitivity and selectivity performance of the proposed aptasensor for colorimetric detection of lysozyme in buffered solution.

On the other hand, for DNAzyme-based biosensor, it is hypothesised that BRET can effectively substitute FRET to avoid the disadvantages, thus further expanding the practical usability of DNAzymes for metal ion detection. The specific objectives are as following:

1. To design a BRET-compatible 8-17 DNAzyme system and verify its working principle.
2. To maximise the BRET efficiency and to evaluate its performance for luminescence detection of Zn^{2+} ions in buffered solution.

1.3 Overview of thesis structure

Following on Chapter 1, Chapter 2 is comprised of literature review to provide a fundamental understanding of this thesis. First focusing on the background information of biosensors, their basic principle, components, classifications as well as a brief history on the technological advancement in the field will be introduced. The main aspects in DNA biosensors will also be reviewed, including the typical properties associated with DNA, such as complementary base pairing and melting temperature. Their applications in biosensing will also be appraised based on the

underlying mechanisms, such as direct hybridisation/ dehybridisation, DNA aptamers and DNAzymes. From another perspective, an overview of nanomaterials will be presented, focusing on AuNPs to highlight the common routes for their synthesis, preparations and modifications. Their physico-chemical properties will also be described together with the commonly associated characterisation techniques. Lastly, luminescence-based sensing will be discussed, focusing on the resonance energy transfer related techniques such as FRET and BRET.

Chapter 3 consists of the development of a colorimetric aptasensor based on cysAuNPs for the detection of lysozyme. In this chapter, the synthesis and characterisation of cysAuNPs together with their interaction with LBA will be presented. Then, the proposed aptasensor will be investigated for its capability in detecting lysozyme in buffered solution both quantitatively and qualitatively.

Chapter 4 documents the development of a luminescence BRET biosensor based on 8-17 DNAzyme for the detection of Zn^{2+} ions. In this chapter, the proof-of-concept will first be described through verification of BRET on top of the assembly of the DNAzyme system. Following that, further optimisation to obtain highly efficient BRET will be detailed. Finally, the now optimised DNAzyme biosensor will be particularised in terms of its ability to qualitatively and quantitatively indicate the presence of Zn^{2+} ions in buffered solution.

Last but not the least, to end this thesis, Chapter 5 and 6 will provide some general conclusions and future remarks, respectively.

CHAPTER 2

LITERATURE REVIEW

2.1 General background of biosensors

Sensor in analytical chemistry, refers to an analytical device that is used for the detection of molecule-of-interest/ targeted analyte either for identification or quantification purposes (Petrukhin and Maksimenko, 2008). Typically, a sensor is consisted of a recognition probe that can recognise the presence of targeted analyte. The recognition event will then be translated into quantifiable signal by a reporter probe that corresponds to the amount of the targeted analyte (Lowe, 1984) as illustrated in Figure 2.1.

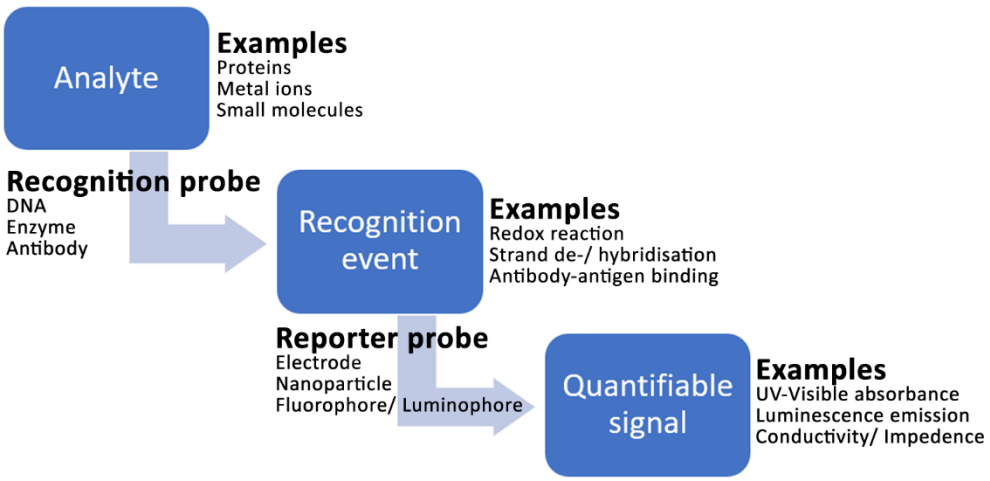

Figure 2.1. The general principle of biosensors with regard to recognition and reporter probes that synergistically generate a measurable output to indicate the presence of molecule-of-interest or targeted analyte.

To be classified as biosensor, either one or both recognition and reporter probes consist of biological elements. Historically, the term “biosensor” was first proposed by Cammann in year 1977 in spite of many previously proposed sensors that had started to exploit biological activities, especially enzymatic reactions for

detection purposes (Cammann, 1977). Depending on the biological components involved as either recognition or reporter probes, biosensors can be categorised into several major types (Table 2.1).

Table 2.1. Example of major classifications of biosensors based on recognition and reporter probes

Classification of Biosensor	
Recognition Probe	**Reporter Probe**
DNA	Optical
Enzyme	Electrochemical
Antibody	Acoustic
Microbial	Thermal

2.2 Recognition probes

Biosensors from earlier years are usually antibody-based that exploit antigen-antibody interaction to achieve the determination of targeted analytes instead of radioactivity (Luppa, Sokoll and Chan, 2001; Lequin, 2005). Classical group of antibody-based biosensors are enzyme-linked immunosorbent assays (ELISA) in which the presence of the targeted analyte (known as antigen) is recognised by an antibody and the recognition is subsequently converted into a measurable feedback by an enzyme. ELISA can be divided into four formats, namely direct, indirect, competitive and sandwich ELISA with their fundamental detection mechanism remains the same. Using indirect ELISA as example illustrated in Figure 2.2, on an ELISA microplate, the antigen that have been pre-immobilised on the surface of the microplate wells will first be recognised by their specific primary antibodies, followed by enzyme-labelled secondary antibodies targeting the primary antibodies. After extensive washing to remove all unbound components, the enzymatic reaction from

the remaining bound enzyme on the secondary antibodies will typically generate optical signals (*i.e.* absorbance or fluorescence) by hydrolysing their respective substrate to indicate the presence of the antigen (Aydin, 2015; Thiha and Ibrahim, 2015; Liang *et al.*, 2016). Commonly used enzymes are alkaline phosphatase and horseradish peroxidase which can provide optical feedback when hydrolyses certain substrates, such as the colorimetric compounds of p-nitrophenyl phosphate (PNPP) (Chen *et al.*, 2017) and 3,3',5,5'-tetramethylbenzidine (TMB) (Uppalapati *et al.*, 2016), respectively.

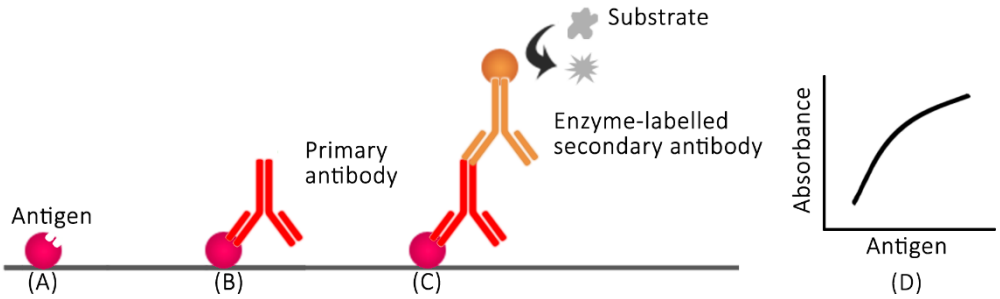

Figure 2.2. Principle of indirect ELISA. **(A)** Immobilised antigen. **(B)** Antigen recognition by primary antibody. **(C)** Further recognition by enzyme-labelled secondary antibody and the hydrolysis of substrate by the enzyme. **(D)** Spectroscopic analysis to indicate the concentration of antigen.

The versatility of ELISA has made it a gold standard as clinical diagnostic tool for the detection over a wide range of targeted analytes. Despite being highly specific, sensitive and efficient when performed by experienced researchers, those biosensors generally associated with a few critical bottlenecks including expensive immunological reagents, high possibility of false results, and hard-to-obtain or hard-to-maintain antibodies especially when monoclonal antibodies were required (Aydin, 2015; Sakamoto *et al.*, 2018).

Due to the huge technological advancement in the field over the past few decades, both DNA-based and enzyme-based biosensors have arisen to represent

the conceptual epicentre to the field of biosensors nowadays (Zhai, Cui and Yang, 1997; Oliveira Brett, 2005; Kavita, 2017; Piro and Reisberg, 2017; C. Liu *et al.*, 2018), with their performances often being compared to ELISA. As this thesis is built on the fundamentals of DNA-based biosensors, it will be focused in following context.

2.2.1 DNA biosensors

With the importance of biosensors slowly gaining more attention in recent decades, further development for detection in more complicated scenarios urged for considerable exploration into other biosensor designs. Instead of relying on the conventional antibodies as in the case of ELISA, DNA nanotechnologies have been widely adapted nowadays.

The implementation of nucleic acids as recognition or reporter probes are being studied extensively due to their exceptional physical, chemical as well as biological activities that promise rapid, reliable and low cost testing (Berney *et al.*, 2000; Kavita, 2017). As a recognition probe, the application of DNA usually derived from three major principles, including (1) DNA-DNA/RNA hybridisation and dehybridisation, (2) DNA-target binding and (3) DNA catalytic reaction which will be discussed accordingly.

2.2.1.1 DNA hybridisation based

Due to Watson-Crick DNA base pairing, each purine always preferably binds to one pyrimidine, for example guanine (G) with cytosine (C) as well as adenosine (A) with thymine (T) for DNA or uracil (U) for RNA. These complementary base pairings, held by hydrogen bonds, have formed the basis for biorecognition in DNA hybridisation biosensors.

2.2.1.1.1 Direct hybridisation and dehybridisation

Only DNA or RNA targets with matching sequences can effectively hybridise with their complementary counterpart whereas a mismatched or non-matching sequence will have less to no hybridisation during the recognition event. Given that DNA is highly flexible, long ssDNA prone to self-fold into various structural configurations, especially secondary structures such as hairpin or random coil which can complicate their hybridisation with the incoming target. Therefore, ssDNA that serves as recognition probe is typically short, with ideally 40 base pairs or less (Kavita, 2017).

Since the first introduction of DNA-based electrochemical biosensor, or E-DNA biosensors by Millan and Mikkelsen in 1993 (Millan and Mikkelsen, 1993), a layer of short ssDNA is typically immobilised onto the transducer or electrode surface. Changes in various electrical signals (*i.e.* chronopotentiometric tranduction, impedance or conductivity) can be expected in the presence of targeted analyte when they hybridise with the immobilised probes, primarily altering the ionic exchange rate on the electrode surface (Wang *et al.*, 1996; Tichoniuk, Ligaj and Filipiak, 2008; Rahman *et al.*, 2015; Gu *et al.*, 2018). The hybridisation event can also be converted into other quantifiable signals, including optical (Chen *et al.*, 1998; Peter *et al.*, 2001) and chemiluminescence (Wu *et al.*, 2010; Liu *et al.*, 2016; Zhang *et al.*, 2018).

2.2.1.1.2 Toehold-mediated strand displacement

Apart from the matching sequence, DNA hybridisation is also dependent on their melting temperature (T_m). T_m hereby refers to the temperature in which half of the DNA oligonucleotides lost their intermolecular bonds, resulting in denaturation, dehybridisation or structural relaxation (Wartell and Benight, 1985). In terms of

dsDNA, they will disassociate into two individual ssDNA whereas for ssDNA, they will undergo structural relaxation to unwind into linear form, subsequently adapting a random coil configuration (Khandelwal and Bhyravabhotla, 2010). In other words, T_m is a direct indication of the tendency of DNA to remain stable in particular configurations, such as double helix and hairpin structure. For instance, a dsDNA with a high T_m means that the dsDNA is more thermodynamically stable against dissociation.

Among all physico-chemical factors (including base stacking, hydrophobic, electrostatic and van der Waals interactions) (Sundaralingam and Ponnuswamy, 2004), hydrogen bonding is the most dominant force that stabilises the double helix DNA structures during complementary base pairing. Reducing the number of complementary base pairing such as shortening the binding arm (hybridising sequence) will lead to drastic drop in the T_m, effectively causing dehybridisation between two DNA strands or prohibit their hybridisation even when they are fully complementary to one another.

In terms of DNA biosensors, it is often exploited in a technique called toehold-mediated strand displacement. During the process, the recognition DNA probe is pre-hybridised to a blocking strand with a hanging segment exposed, thus the name toehold. In the presence of targets, the incoming DNA target (invading strand) will first initiate the hybridisation with the toehold, and consequently substitute the blocking strand. This results in either immediate displacement of the blocking strand, or a sharp reduction in the T_m of the remaining partially hybridised blocking strand. In both cases, the blocking strand will be released, hence displaced from the DNA probe. Other derivatives including strand displacement cascade

(Teichmann, Kopperger and Simmel, 2014; Li *et al.*, 2019) and hybridisation chain reaction (Dirks and Pierce, 2004; Evanko, 2004).

2.2.1.2 DNA-target binding based

Apart from hybridising with complementary sequences, DNA can also bind with molecules other than its complementary strand, a characteristic that is also exploited in biosensing applications. In recent decades, DNA-target binding has been revolutionised by the introduction and subsequent blooming studies of DNA aptamers in 1990s. They are typically single-stranded oligonucleotides with polynucleotide lengths of lesser than 100 bases that upon folding into specific tertiary structures, present antibody-like properties such as capability to bind to their targets with high affinity and specificity (Ellington and Szostak, 1990; Gold and Tuerk, 1990). In fact, the first study of aptamer came in the form of RNA aptamer which can provide HIV resistance by binding to its viral protein, thereby physically inhibiting the following viral RNA-protein binding required for viral replication (Sullenger *et al.*, 1990).

Nowadays, DNA aptamers are mostly discovered via systematic evolution of ligands by exponential enrichment (SELEX) technique whereby a series of selection and amplification processes are taken to isolate a high-affinity oligonucleotide strands from pools of variants against a molecule-of-interest (Jayasena, 1999). During SELEX, a combinatorial library of synthetic DNA oligonucleotides with approximately 10^{15} different sequences were incubated with targeted analyte, allowing specific sequences to interact and bind with it. Then, washing steps will be performed for the separation of bound and unbound strands, while the remaining bound strands will undergo PCR amplification to replenish their amount. At each cycle of DNA-target incubation, separation, elution and amplification, the

identification for selected aptamers will be repeated under increasingly stringent conditions (increasing ionic concentration or ionic strength), ultimately narrowing the pool of DNA aptameric strands down to a single one with highest affinity against particular target (Figure 2.3). Typically, a DNA aptamer selective to a targeted analyte can be identified within 10 to 15 cycles.

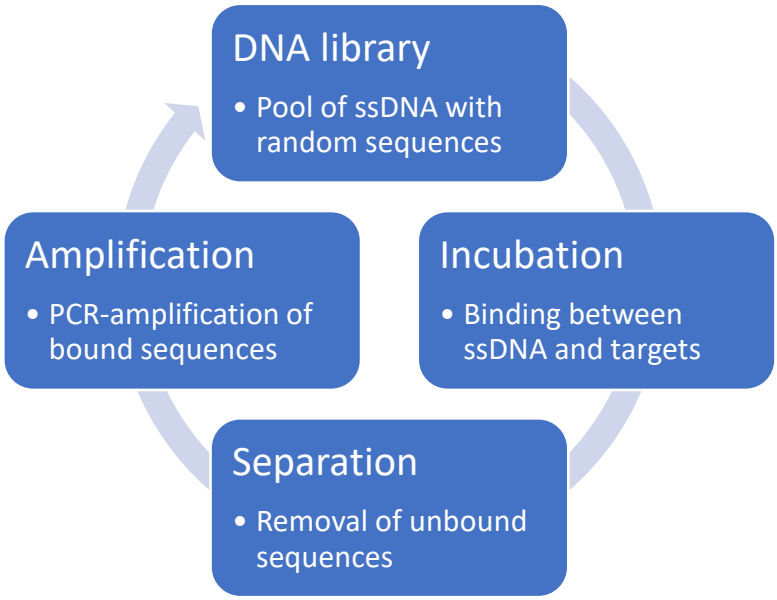

Figure 2.3. Scheme of aptamer identification through SELEX. At each cycle, the ssDNA pool will undergo repeated selection procedures under increasingly stringent conditions until a final sequence is identified to bind with the targeted analyte at highest affinity.

Despite can be used to screen for DNA aptamers selective to virtually any molecules-of-interest, from ions (Wang *et al.*, 2006), and toxins (Alizadeh *et al.*, 2018) to cells (Catuogno and Esposito, 2017; Rahimizadeh *et al.*, 2017) or even microorganisms (Zhao *et al.*, 2018; Shin *et al.*, 2019), SELEX and its derivatives have also been associated with several critical disadvantages that limited their true potential to be widely adapted in most laboratories to identify new aptamers. Due to the requirements of repeated screening using radioactive labelling, highly maintained experimental environment, and well trained personnel, performing SELEX in most non-specialised laboratories is undesirably labour-intensive, time-

consuming, expensive and not environmentally compatible (Stoltenburg, Reinemann and Strehlitz, 2005).

Instead, many aptamers-related studies were actually carried out based on pre-established aptamers, such as anti-thrombin or thrombin-binding aptamer (TBA) (Avino *et al.*, 2012; Deng *et al.*, 2014) and anti-lysozyme or lysozyme-binding aptamer (LBA) (Vasilescu *et al.*, 2016) that have been studied intensively and extensively as study models for the proof-of-concept development of biosensors. Although behaving like antibodies, aptamers are much stable, cheaper, easily available and thus gaining more and more credibility nowadays to serve as a potential alternative in tagging particular molecules, primarily for diagnostic or therapeutic purposes (Song, Lee and Ban, 2012).

2.2.1.3 DNA catalytic reaction based

DNA has been thought to be just a repository of genetic information for a very long time, until the ground-breaking discovery of DNA aptamers that can structurally adapt in order to recognise and bind to their specific targets (Ellington and Szostak, 1990; Gold and Tuerk, 1990). However, another significant milestone in functional DNA technologies was made in year 1994, when Breaker and Joyce reported a RNA-cleaving DNA enzyme for the first time (Breaker and Joyce, 1994). Herein, such catalytic DNA strands are called as DNAzymes, owing to their enzymatic capability.

Unlike the natural ribozymes, native DNAzymes have yet to be reported and are thus obtained synthetically. Nevertheless, their discovery has encouraged following efforts in designing or identifying new species with various reaction-catalysing activities. Being essentially strands of DNA oligonucleotides, DNAzymes are more stable and efficient solid-phase synthesis of specially designed DNAzymes

makes them more cost-effective than designing and producing actual enzymes for various applications (Liu, Chang and Li, 2017).

Most DNAzymes were identified from *in vitro selection*, another term usually given to SELEX when addressing DNAzymes, referring to a series of variation, selection and replication processes that only interacting DNA strands were retained and amplified over increasing levels of stringency (Breaker and Joyce, 1994; Wang *et al.*, 2017). However, instead of screening for remaining bound DNA aptamers, *in vitro selection* isolates DNA catalyst based on their ability to undergo certain reactions, that are their RNA-cleaving activities, in either column binding or gel retardation approach (Achenbach *et al.*, 2004).

In a column binding setup, the pool of double stranded oligonucleotides (either DNA-DNA, RNA-RNA or DNA-RNA with one of it assuming the role of enzymatic strand to cleave the other, named as substrate strand) will be attached to the stationary phase via the non-covalent biotin-streptavidin binding. Only under certain conditions (that is in the presence of specific metal ion functioning as cofactor), the reactive and potential DNAzymes will carry out their RNA cleavage activity. When the RNA substrate strand is cleaved into two shorter strands, the reduced T_m on the now-separated binding arms resulted in dehybridisation of the double helix DNA-RNA chimera, effectively releasing the oligonucleotide strands from stationary phase to be eluted out (Achenbach *et al.*, 2004). In this case, only non-active species will be retained as opposed to SELEX during DNA aptamer studies.

On the other hand, during a gel retardation protocol, the now separated strands of enzyme and substrate strands will move at different rates compared to the non-active species. Similar to typical gel electrophoresis, as the active species are smaller (dehybridised) and shorter (substrate strand gets cleaved into two shorter

strands), they can travel faster through the gel than other non-active species. Although there are numerous DNA derived “enzymes” that can catalyse a wide range of chemical reactions, such as DNA (Cuenoud and Szostak, 1995) and RNA ligation (Flynn-Charlebois *et al.*, 2003), the RNA-cleaving DNAzymes have always been the centred theme (Silverman, 2016).

Among the DNAzymes discovered so far, the DNAzyme “8-17” remains as the classical example of DNAzymes that has been most extensively studied and applied to date. The activity of 8-17 DNAzyme is dependent on its cofactors, with its highest activity reported with Pb^{2+}, followed by Zn^{2+} and finally Mg^{2+} ions (Kim *et al.*, 2007). Since the first report of RNA-cleaving DNAzyme (Breaker and Joyce, 1994), there are a few following reports that documented additional DNAzymes with similar activities. Among them, 8-17 appears to be the core motif in driving the RNA-cleaving reaction (Bruesehoff *et al.*, 2012), that it has been repeatedly identified under various conditions during *in vitro selection* (Faulhammer and Famulok, 1996; Santoro and Joyce, 1997; Li *et al.*, 2000).

The enzymatic motif of 8-17 DNAzyme consists of a stem and a bulge loop (collectively termed as catalytic core) opposite to the adenosine cleavage site, held by binding arms at both sides. Despite the 8-17 DNAzyme is widely believed to cleave the RNA by catalysing the RNA transesterification in the presence of divalent metal ions (Figure 2.4), the fundamental understanding of their structural features or even the underlying reaction mechanisms remain elusive even to date. It has only been recently documented that the reaction is apparently driven by a general pH-sensitive acid-base catalysis mechanism whereby the G14 of the bulge loop opposite to the RNA cleavage site is involved in a proton transfer reaction during the cleavage (Cepeda-Plaza, McGhee and Lu, 2018). As the end product, the reaction produces a

separated 2’3’-cyclic phosphate and another 5’-hydroxyl termini, effectively cleaving the RNA strand into two shorter strands (Grimpe, 2011).

Over the years, continuous studies have indirectly refined the structure of the original 8-17 DNAzyme. In year 2000, Lu group reported the 17E, an 8-17 variant with highly conserved catalytic core sequence, that can even work on a DNA-RNA chimera strand (adenosine RNA is preserved as cleavage site) and has improved Zn^{2+}-dependent activity (Li *et al.*, 2000).

Nowadays, given its high similarity on top of promising selectivity against both Pb^{2+} and Zn^{2+} metal ions, 17E is commonly reported as 8-17 DNAzyme. To make use of these DNAzymes in biosensors development, researchers often exploit the RNA cleavage in reducing the overall T_m of the hybridising strands.

As depicted in Figure 2.4, the initial T_m of the assembled DNAzyme is calculated to be well above 40 ^oC (excluding the Hoogsteen base pairing of G•T). It is presumed that only certain metal ion cofactors (such as Pb^{2+} and Zn^{2+}) can fit into the catalytic core to facilitate the RNA transesterification. After cleavage, both binding arms will have their T_m reduced to below 25 ^oC with some even lower than the typical room temperature of 20 ^oC. The reduction in T_m consequently leads to strand dehybridisation, disassembling the DNAzyme complex. This has formed the basis in many biosensing platforms for metal ions detection, including catalytic and molecular beacon (CAMB) (Zhang *et al.*, 2010; Song *et al.*, 2012), resonance energy transfer (RET) (Li and Lu, 2000; Yang *et al.*, 2018), and enzymatic-based metal ions DNAzyme biosensors (Zhang *et al.*, 2015).

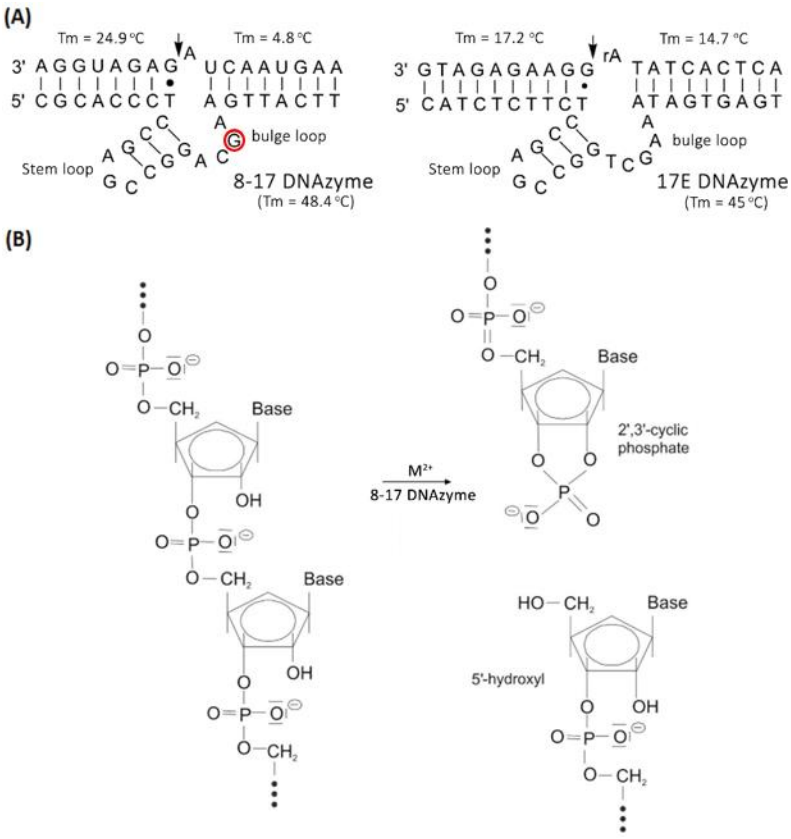

Figure 2.4. (A) The sequences and structures of 8-17 (left) and 17E (right) DNAzymes, respectively with G14 on 8-17 being circled in red. The substrate strand for 8-17 DNAzyme is an RNA whereas for 17E, it is a DNA-RNA chimera strand with rA (adenosine RNA) being the only RNA base. The arrows, lines, and dots represent the cleavage sites, Watson-Crick base pairings and Hoogsteen base pairings, respectively. **(B)** Proposed mechanism of 8-17 DNAzyme driven RNA transesterification (Achenbach *et al.*, 2004)

2.3 Reporter probes

2.3.1 Nanotechnology and nanomaterials

Nanotechnology is a novel field that has been expanding exponentially throughout recent decades and its impacts can be easily spotted on multiple areas especially economy, environment, electronics and biosciences (Coté, Lec and Pishko, 2003; de Lima, Seabra and Durán, 2012; Wang and Yu, 2013). A simple definition for nanotechnology is the application of nanomaterials through a series of fabrication, manipulation and functionalisation processes.

Conventionally, nanomaterials with an average diameter of smaller than 100 nm are classified as nanoparticles (Zeng *et al.*, 2011). Due to their exceptional advantages compared to respective bulk counterpart, nanoparticle research is now an active field of study with attention centred on metal derived nanoparticles. Among them, gold nanoparticles (AuNPs) are among the most extensively studied candidates and therefore, represent the focus in this section.

2.3.1.1 Gold nanoparticles (AuNPs)

Gold, traditionally regarded as a symbol of power and wealth, together with others like silver, is one of the irrefutably important metal elements throughout the entire human civilisation. Since the beginning of commerce history, gold has been a universal means of financial transactions and reserve due to its reliable value (Rahman and Rebrov, 2014).

In spite of the idea of existence of non-bulk gold has been proposed in 1676, the first systematic synthesis of AuNPs and its subsequent study was pioneered by Michael Faraday in 1857 (Faraday, 1857). Through the preparation of colloidal gold solution via the reduction of aqueous tetrachloroaurate ($AuCl_4^-$) by phosphorus in a two-phase system, he described the optical properties of these AuNPs that their colour appearance can be reversibly changed from bluish-purple to green when mechanical compression was applied on a thin film prepared from the AuNPs (Faraday, 1857; Daniel and Astruc, 2004).

Since then, many works have been conducted to advance the study of AuNPs and various synthesis approaches have been reported, from as simple as “mix-and-stir” to a series of chemical and/or physical processes (Merza *et al.*, 2012; Saha *et al.*, 2012; Elia *et al.*, 2014). Application wise, an important breakthrough that should not be overlooked is the contribution of Chad Mirkin, who introduced and pioneered the

idea of utilising nanoparticle-biomolecule conjugates as colorimetric reporter probe in year 1996. By conjugating AuNPs with DNA oligonucleotides via thiol linkages, he successfully assembled the nanoparticles rationally into macroscopic materials (Mirkin *et al.*, 1996) and later with his research group, they even developed a colorimetric assay to selectively detect oligonucleotides (Elghanian *et al.*, 1997). His researches eventually established the fundamental framework that most following works, especially for biosensing and bio-imaging, are made possible with or without modification built on the premise of his initial DNA-AuNPs nanostructure.

To date, AuNPs still remain as a major research interest with a significant number of related papers being published from time to time. The areas where AuNPs hold key potential for further advancements and are constantly under reviews included but not limited to biosensing and diagnostics (Dykman and Khlebtsov, 2011; Zeng *et al.*, 2011), drug delivery (Arvizo, Bhattacharya and Mukherjee, 2010), cancer therapy (Jain, Hirst and O'Sullivan, 2012; Muddineti, Ghosh and Biswas, 2015), environmental pollutant detection (Wang and Yu, 2013) and chemical process catalysis (Daniel and Astruc, 2004). Nonetheless, the full potential of AuNPs is not entirely uncovered yet and thus more development and improvement in the related knowledge and application can be anticipated.

2.3.1.2 Synthesis, preparations and modifications

There are numerous protocols being proposed to prepare AuNPs with various characteristics and surface modifications such as particle sizes, surface charges and conjugated ligands. While the exact conditions for each method might be different, the underlying mechanisms to form AuNPs usually relies on the same basic principle, that is the chemical reduction of the gold ions from Au^{3+} to Au^{0} and subsequent stabilisation of the as-prepared nanoparticles.

The common synthetic, modification and functionalisation routes which are well established hitherto are citrate reduction, the Burst-Schiffrin method, place exchange, physical particle modification and polymer stabilization techniques. Each technique has its own pros and cons while citrate reduction and Brust-Schiffrin systems concurrently represent the current mainstream in AuNPs preparation and are widely employed by research groups.

2.3.1.2.1 Citrate reduction

Citrate reduction is generally considered as the most classical, convenient and simplest way to prepare monodispersed AuNPs which was first reported by Turkevich *et al* in 1951. Typically, trisodium citrate reduces the gold ions and subsequently stabilises the resulting AuNPs. Given that citrate is not a strong reducing agent per se, constant reflux throughout the reaction is needed to provide the heat energy required in driving the reduction process (Turkevich, Stevenson and Hillier, 1951). The as-synthesised colloidal solution is usually referred as citrate-reduced gold nanoparticles (citAuNPs).

With simple “one-pot” synthesis, citAuNPs with good monodispersity can be prepared and the resulting diameter (particle size) can be controlled by varying the molar ratio of gold: citrate (Frens, 1973; Ghosh and Chattopadhyay, 2013). However, due to the citrate having three pKa values (i.e. 3.06, 4.74 and 5.40), the resulting citAuNPs will be limited to having a negative surface charge. The resulting colloidal solution might also be contaminated by unreacted, excessive reactants (Kimling *et al.*, 2006).

Besides, citAuNPs are also prone to undesired salt-induced aggregation although further studies have been conducted to make use of this feature for downstream applications (Aung *et al.*, 2014; Lukman *et al.*, 2014). This is due to the

fact that the citrate–gold bonding is mediated via monocarboxylate bridging, dicarboxylate bridging and monocarboxylate monodentate modes (Al-Johani *et al.*, 2017). The weak bonds are susceptible to environmental changes such as ionic strength, ionic concentration and pH variation. In fact, recent study has reported that the performance of citrate reduction is highly pH-dependent that slight variation in the pH during synthesis can cause a drastic 46% reduced yield despite same size and morphology of the citAuNPs (Contreras-Trigo *et al.*, 2018).

2.3.1.2.2 Brust-Schiffrin system (thiol ligand conjugation)

Brust-Schiffrin system is another well-known method pioneered by Brust and Schiffrin together with their team that AuNPs are conjugated with thiol-containing molecules via a strong Au–S bond to achieve stabilisation purpose upon synthesis. In their two-phase reduction system, chloroauric acid is transferred to toluene by tetraoctylammonium bromide and subsequently reduced in the presence of dodecanethiol (Brust *et al.*, 1994). In most cases, the reduction is carried out by a strong reducing agent, that is sodium borohydride.

Compared to citAuNPs, the AuNPs stabilised by thiol ligands are more stable due to the covalent Au–S bond. Besides, while citrate-reduction has been well-established to prepare AuNPs with high monodispersity and controlled shape, reduction *via* sodium borohydride generally gives high yield with smaller size (Oliveira *et al.*, 2020). As virtually any thiol ligands can be conjugated (Templeton *et al.*, 1998; Negishi *et al.*, 2004; Su *et al.*, 2013), this system allows facile functionalisation of the AuNPs with different characteristics (Brust *et al.*, 1995; Daniel and Astruc, 2004). Subsequent studies also achieved improvements such as single-phase system (Yee *et al.*, 1999; Zheng, Li and Huang, 2004), alternative

reducing agents (Yee *et al.*, 1999) and mixed monolayer-coating in producing a wide variety of AuNPs (Itoh *et al.*, 2004).

Due to thiol ligands conjugation, the opportunity for synthesising AuNPs with various surface chemistry for various applications can be fulfilled. For instance, AuNPs can be characterised with different surface charges depending on the types of ligands being conjugated, unlike the citrate-coated AuNPs which are limited to negative charge. As first demonstrated by Niidome's group, AuNPs conjugated with 2-aminoethanethiol, also known as cysteamine, exhibit positive surface charge (Niidome *et al.*, 2004; Su *et al.*, 2013). Being the shortest aminothiol, cysteamine offers both thiol and amine groups that enable strong binding to gold surface with a net positive surface charge (Su *et al.*, 2013; M. Wang *et al.*, 2016). The resulting colloidal system is referred as cysteamine-stabilised gold nanoparticles (cysAuNPs).

Despite being novel, the early applications of cysAuNPs prepared by direct capping of cysteamine during synthesis are still limited, mostly as a direct reporter probe in various sensing platforms, such as colorimetry (Cao and Li, 2011; Sharma *et al.*, 2018) and electrochemical based biosensors (Ramírez-Segovia *et al.*, 2014; Asadzadeh-Firouzabadi and Zare, 2017). Nevertheless, given their opposite surface charges and surface chemistry that direct to a path different than the conventional citAuNPs, cysAuNPs are slowly gaining attention in recent years with more forthcoming studies expected in near future.

2.3.1.2.3 Ligand exchange technique

In short, place exchange technique is the gradual displacement and substitution of ligands on the AuNPs by other ligands after their synthesis (Hostetler *et al.*, 1996; Hostetler, Templeton and Murray, 1999). With dynamic competition

between the ligands, mixed or completely substituted monolayer coating on the AuNPs can be achieved after optimisation (Donkers, Lee and Murray, 2004).

Among the possible ligand exchange, thiolated DNA were often used to conjugate with AuNPs by substituting the citrate ligands. The weak bonding of citrate–gold allows easy replacement by stronger thiol–gold bonds. Such post-synthetic modifications on citAuNPs is frequently applied in analyte detection (Chen *et al.*, 2013), AuNPs self-assembly (Lalander *et al.*, 2010; Gür *et al.*, 2016) and DNA-directed biological functionality (Heo *et al.*, 2015). Although DNA-functionalised AuNPs are considerably stable (Heo *et al.*, 2015), they are limited by same negative electrostatic charges of DNA and citAuNPs. This is because such electrostatic repulsion has to be screened off delicately through a procedure known as salt aging, a time-consuming and laborious technique whereby salt ions were slowly added to mask off the repulsive surface charges of the citAuNPs and DNA in order for them to conjugate in close proximity (Mirkin *et al.*, 1996; Liu and Lu, 2006).

Recently, efforts to address such issues have finally been materialised with the introduction of diverse approaches to prepare DNA-functionalised AuNPs, such as mononucleotide-mediated (Zhao, Lin and Hsing, 2009), pH-assisted (Zhang *et al.*, 2012; Zhang, Servos and Liu, 2012) and freezing-directed (Liu and Liu, 2017a) conjugation. However, such techniques are still relatively immature compared to salt-aging with more studies and optimisations being expected. Moreover, these procedures involve excessive reagents or drastic changes in reaction conditions (*i.e.* pH or temperature), which can complicate the downstream applications.

2.3.1.2.4 Polymer stabilisation

As the name suggested, polymer stabilisation is the stabilisation of AuNPs by coating them with polymer as outer shell. Four principle techniques are widely used:

(1) “grafting from” (growth of polymer chain from initiators pre-attached onto AuNPs), (2) “grafting to” (coating of AuNPs with thiol-containing polymers), (3) physisorption (physical engulfment of AuNPs by polymers without specific chemical bonds) and (4) post-modification (modification with polymers after AuNPs synthesis) (Saha *et al.*, 2012).

2.3.1.2.5 Physical synthesis, modification and separation

Apart from above-mentioned chemical synthesis, physical approaches have also been developed to manipulate the structure and properties of AuNPs, including but not limited to thermolysis (Nakamoto, Kashiwagi and Yamamoto, 2005; Erk *et al.*, 2012), digestive ripening (Prasad *et al.*, 2002, 2003), conventional ripening (Zhong *et al.*, 1999; Maye *et al.*, 2000), UV irradiation (Sau *et al.*, 2001), laser irradiation (Muttaqin, Nakamura and Sato, 2015), microwave irradiation (Augustine, Nampoori and Kailasnath, 2014), ultrasonication (Okitsu *et al.*, 2001; Lee *et al.*, 2012) and radiolysis (Henglein and Meisel, 1998). Post-production separation such as size chromatography has also been applied to physically separate the AuNPs with high monodispersity (Wei, 1999; Liu, 2012).

While those mentioned above are concurrently considered “conventional” due to their frequent reports and reviews throughout the years, there are a few novel and unorthodox synthetic protocol for AuNPs. The first is the so-called “green synthesis” whereby AuNPs were prepared through reduction using various plant extracts such as *Salvia Officinalis*, *Lippia Citriodora* and *Punica Granatum* (Elia *et al.*, 2014). Other reported plants included black cardamom (Singh and Srivastava, 2015) and several species of citrus fruits (Sujitha and Kannan, 2013) which might be highly potential but not fully exploited yet.

Moving away from “green synthesis”, one particularly interesting way to synthesise AuNPs is dipping a stainless-steel mesh into the tetrachloroauric acid under acidic condition for hours (Han *et al.*, 2013, 2014). It was suggested that the progressive corrosion of the stainless-steel surface can release sufficient number of electrons to drive the Au^{3+} reduction. Despite in-depth studies are required, these novel and relatively “unconventional” methods should pave another new route to further encourage and extend the current application possibility of AuNPs.

2.3.1.3 Properties and characterisations

As the AuNPs are prepared in nanometer scale, they show prominent quantum size effect which are so inimitable and attracts enormous interest worldwide for both scientific and commercial purposes. In order to precisely study the AuNPs, many analysis techniques have been developed and used to characterise them, subsequently trying to gain more insights into their quantum properties in order to apply them.

Among all other parameters, the first and therefore most influential criterion in assessing the as-prepared AuNPs is their particle sizes undoubtedly. Despite being in nanometer, the precise diameter of the AuNPs have been repeatedly studied and reported to play part in determining their morphology, biological and chemical properties (Xia *et al.*, 2016; Liu *et al.*, 2016). By applying AuNPs of various particle sizes, the resulting bio-distribution profile will be different as evident in lab mice and rats (Sonavane, Tomoda and Makino, 2008; Hirn *et al.*, 2011).

On the other hand, assembling AuNPs with different sizes through complementary oligonucleotides acting as bridge will lead to a chiro-plasmonic assemblies because of the double helix nature of DNA. Indeed, Liu and co-workers (Liu *et al.*, 2016) reported an 8-hyrdoxy-2’-deoxyguanosine detection using AuNPs

held together via a dsDNA bridge (each strand is thiolated and conjugated to the differently sized AuNPs) that presence of the target would disassemble the DNA-AuNPs nanostructure, providing a mean of detection based on the chirality of AuNPs.

Thanks to the successful breakthrough inventions in imaging field (Haguenau *et al.*, 2003), the physical diameter of AuNPs are now frequently measured microscopically, such as transmission electron microscope (TEM) (Han *et al.*, 2013) and scanning electron microscope (SEM) (Chen *et al.*, 2013). High-resolution transmission electron microscope (HRTEM) can also be applied to obtain clearer images which are then processed digitally to measure the average core diameters of AuNPs (Liu *et al.*, 2007).

Dynamic light scattering (DLS), also known as photon correlation spectroscopy (PCS) is another technique to measure the hydrodynamic particle sizes (or Stokes radius), a hypothetical sphere encircling each AuNP like an intermedium layer between the physical core and the solvent capable of altering the path of traveling photons (Goldburg, 1999). When a monochromatic laser is illuminated through the colloidal solution, the resulting intensity and distribution of scattered light in the form of frequency shift are measured (Hackley and Clogston, 2011). This frequency shift correlates to the Brownian motion, with larger nanoparticles moving slower than smaller nanoparticles, providing a mean to back-calculate and estimate their size distribution.

Apart from measuring hydrodynamic particle size, the convenient presentation of size distribution when performing DLS also serve as a direct reflection on the monodispersity profile of the AuNPs which can be coupled with the microscopic techniques mentioned earlier for higher accuracy in understanding the physical parameters of the nanoparticles.

From another perspective, zeta potential (ZP) is also an important criterion in describing nanoparticles, AuNPs in this context. ZP can be referred as the effective surface charge, the electric potential of the interfacial layer between AuNPs and its immediate environment (Doane *et al.*, 2012). As nanoparticles with a net surface charge can attract and hold their counterions, there is always an electrical double layer (EDL) between their surface and the surrounding medium. This EDL arises from their intrinsic surface charge and the ions present in the environment, therefore, can be influenced by the parameters of the dispersing medium, such as pH, ionic concentration and ionic strength (Clogston and Patri, 2011).

Conventionally, most AuNPs are synthesised with strong surface charges conferred by the surface ligands to enable effective electrostatic repulsion in order to withstand their thermodynamically unstable high surface energy, thus achieving stability against unwanted aggregation (Wang *et al.*, 2006; Heo *et al.*, 2015; Xia *et al.*, 2016). This means that a stronger ZP will impose more effective electrostatic repulsion and therefore, the key to fulfil long-term stability. Considering that AuNPs have high Hamaker constant (Bishop *et al.*, 2009), their high tendency for Van der Waals attraction requires a strong ZP to counter it, typically with a ZP of more than 30 mV or less than -30 mV (Bhumkar *et al.*, 2007). Furthermore, in-depth studies also evidently found that the cytotoxicity mechanisms (Schaeublin *et al.*, 2011) and bio-distributions (Hirn *et al.*, 2011; Schleh *et al.*, 2012; Elci *et al.*, 2016) of AuNPs are highly associated with their ZP which directly affects how these AuNPs interact with the surrounding environments.

For examples, exploiting the interaction between cationic AuNPs (such as cysAuNPs) and anionic DNA aptamer has enabled the possibility to develop novel detection assay as demonstrated in detection of lysozyme (Su *et al.*, 2013), mercury

(Qi *et al.*, 2017), melamine (Zheng *et al.*, 2017), estradiol (Li *et al.*, 2018), tetracycline (Luo *et al.*, 2015) and oxytetracycline (Su *et al.*, 2016). To gauge the ZP, specialised instruments such as zeta potential analyser or zetasizer system are employed which measure the electrophoretic light scattering of the nanoparticles, a variant of DLS that applies an oscillating electric field to drive the movement of nanoparticles instead of relying on their Brownian motion.

Apart from the parameters mentioned, another critical characteristic of AuNPs is their quantum size effect as a direct result of their small diameters. Surface plasmon resonance (SPR) is a quantum phenomenon first demonstrated in year 1968 whereby the conductive electrons on a metallic surface are collectively oscillating at resonant frequency when excited by incident light at specific wavelengths (Bhumkar *et al.*, 2007; Daghestani and Day, 2010).

For metals, the excitation of plasmons can only occur in nanosized materials when the electric field of incident light is able to penetrate the metal and subsequently polarise the conduction electrons for resonance (Amendola *et al.*, 2017). To assess the SPR phenomenon, UV-Vis spectroscopy proved itself to be a convenient way by performing a spectral scanning on AuNPs to identify the maximum absorbance band across a broad wavelength of light. UV-Vis spectroscopy is an analytical technique used to measure the absorbance of a given sample by analysing the light intensity passing through the sample in contrast to a reference sample.

In terms of AuNPs, the nanoparticles can absorb light at certain wavelengths due to SPR. Conventionally, the observed absorbance band is also known as localised surface plasmon resonance (LSPR) band while the exact maxima can be referred as LSPR peak. With such small sizes, the occurrence of SPR is more prominent in AuNPs

but the exact phenomenon can be affected by the precise diameter of the nanoparticle that even a few nanometer can make a difference in the resulting SPR profile (Xia *et al.*, 2016).

For example, most dispersed AuNPs show a LSPR band centring around 520 nm but gradual increase in sizes will cause a corresponding red-shift of the band (Xia *et al.*, 2016). Significantly increased core diameter of AuNPs will further move the SPR band towards red region, that is 670 nm (Su *et al.*, 2013).

Besides, SPR profile can also be used to indicate the monodispersity of AuNPs whereby highly monodispersed sample will display a sharp and prominent SPR band while less monodispersed sample will generally show a broadened band at longer wavelength region (Bhumkar *et al.*, 2007; Dhumale *et al.*, 2012). The SPR phenomenon is also reflected on the solution appearance, for instance, dispersed AuNPs will appear as ruby red in colour but progressively change to bluish grey if the dispersed AuNPs are getting larger in sizes, especially after aggregation. Indeed, the SPR phenomenon of AuNPs is so potential that many of their derivative sensors are based on the SPR profiling, including biological, chemical and physical sensing (Dhumale *et al.*, 2012; Saha *et al.*, 2012; Liu *et al.*, 2018; Chang *et al.*, 2019).

2.3.2 Resonance energy transfer (RET)

RET refers to an interactive mechanism between two light-sensitive molecules (known as chromophores) in which the donor chromophore gets excited and transfers the energy to an acceptor chromophore when they are in close proximity (Jones and Bradshaw, 2019). The transfer of excitation energy is mediated by a distance dependent, radiationless and long-range dipole-dipole interaction (Hussain, 2009) with the theoretical model first proposed correctly by Theodor Förster in 1940s (Förster, 1946, 1948). During RET, the excess energy released during

relaxation of electrons from exited state to a lower energy electronic state from the donor chromophore is transferred to the electrons of a nearby acceptor chromophore in the form of transmitted photon (Jones and Bradshaw, 2019). As a result, RET can lead to two possible outcomes: (1) co-excitation of acceptor chromophore or (2) total quenching of the donor chromophore (Figure 2.5). While depending on the exact acceptor being used, RET typically change the fluorescence spectra of the sample. Fluorescence quenching can also happen if all of the energy was being transferred to the acceptor without re-emission, with the acceptor commonly referred as quencher in this case (Marras, 2002).

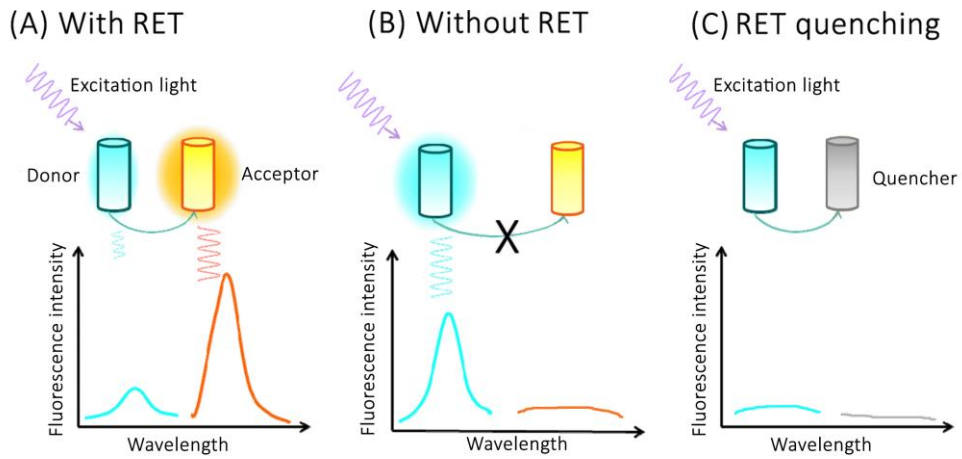

Figure 2.5. Schematic idea of two chromophores under various conditions. **(A)** with RET. **(B)** Without RET. **(C)** with RET quenching with the resulting fluorescence spectra.

In practical scenario, RET can be divided into three classes, known as fluorescence resonance energy transfer (FRET), bioluminescence resonance energy transfer (BRET) and chemiluminescence resonance energy transfer (CRET). Their fundamental mechanisms are the same, with the only difference being the chromophores involved. As the donor and/ or acceptor chromophores, FRET typically uses only fluorescence molecules (fluorophores), including fluorescence dyes such as Cy3 and fluorescein (Huang *et al.*, 2016; Wen *et al.*, 2018; Ren *et al.*, 2019; Sapkota *et*

al., 2019) and nanomaterials such as quantum dots and nanoparticles (Wu *et al.*, 2006; Gao *et al.*, 2011; Wang *et al.*, 2017; Bülbül *et al.*, 2018). However, due to the requirement of highly energised excitation light source, the use of fluorescence dyes are often associated with drawbacks such as photobleaching (Song *et al.*, 1995; Satsoura *et al.*, 2007; Vicente *et al.*, 2007) and signal contamination (Chen *et al.*, 2007; Liao, Song and Liu, 2015; Bene and Damjanovich, 2019).

In addition to fluorophores, both BRET and CRET involves the catalytic oxidation of certain luminescence substrates in which bioluminescence proteins such as luciferases and fluorescent proteins (Li *et al.*, 2012; Brown, Blumer and Hepler, 2015; Machleidt *et al.*, 2015; Aper, Dierickx and Merkx, 2016; Arts *et al.*, 2016; Engelen *et al.*, 2017; Rainey and Patterson, 2019) was applied in BRET whereas CRET can make use of typical HRP-driven or novel DNA-based HRP-mimicking luminol chemiluminescence systems (Huang *et al.*, 2006, 2012; Zhao, Huang, Liu, *et al.*, 2010; Zhao, Huang, Shi, *et al.*, 2010; Freeman, Liu and Willner, 2011; Mun *et al.*, 2014; Bi *et al.*, 2015). Typically, BRET and CRET does not require an excitation source since the chromophore donor is capable of producing the energy through the substrate oxidation and thus represent the effort to circumvent the FRET-related limitations aforementioned.

Applications of RET can be easily seen throughout biosensor development that exploit their distance-sensitive response to indicate presence of targeted analyte, including a wide variety of biomolecules (Medintz *et al.*, 2003; Xu *et al.*, 2014; Huang *et al.*, 2016; Zhang *et al.*, 2017; Wen *et al.*, 2018; Umrao *et al.*, 2019), metal ions (Liu *et al.*, 2011; Wu *et al.*, 2017; Yang *et al.*, 2018; Feng *et al.*, 2019), etc. Biosensors with successful RET implementation are actively being developed as they allow ratiometric analysis by comparing the fluorescence of donor and acceptor

chromophores which can theoretically provide better reliability and repeatability compared to conventional sensors.

CHAPTER 3

BIMODAL COLORIMETRIC DNA APTAMER SENSOR BASED ON CYSTEAMINE-COATED GOLD NANOPARTICLES: A PROOF-OF-CONCEPT WITH LYSOZYME

3.1 Chapter overview

In this chapter, the application of DNA aptamer is explored together with gold nanoparticles (AuNPs), each representing one of the centred themes in the fields of DNA and material nanotechnologies, respectively. Using cysteamine-coated gold nanoparticles (cysAuNPs) and a lysozyme-binding aptamer (LBA), the purpose of this study is to investigate and exploit the electrostatic relationship between the oppositely charged cysAuNPs and LBA in developing an aptasensor for lysozyme detection. After understanding the correlation between LBA concentration and dispersion behaviour of cysAuNPs, a bimodal aptasensor is developed for sensitive and selective detection of lysozyme in buffered samples. Lastly, the chapter will be concluded with significant achievements of this study and suggestion for possible future works, underlining the potential and prospects of cysAuNPs as an alternative to the conventional citrate-capped gold nanoparticles (citAuNPs).

3.2 Introduction

Lysozyme is a small enzyme consists of 129 amino acids and usually carries a net +8 charge over a wide range of pH due to its high isoelectric point (pI ≈ 11) (Blake *et al.*, 1965; Gorbenko, Ioffe and Kinnunen, 2007). It is a ubiquitous protein found in many living organisms, usually responsible for innate antimicrobial activity (Cheng, Ge and Yu, 2007; Salazar and Asenjo, 2007; Kozuka *et al.*, 2015).

Lysozyme catalyses the hydrolysis of β-1,4-glycosidic bond between N-acetylmuramic acid and N-acetylglucosamine. Such lytic action results in degradation

of the cell wall mucopolysaccharides of Gram-positive bacteria (Nash *et al.*, 2006; Rodríguez and Rivas, 2009). However, abnormal concentration and distribution of lysozyme in human body has also been reported as promising pathological biomarker. For example, increased concentration of lysozyme in cerebrospinal fluid can be associated with neurological diseases such as Alzheimer (Helmfors *et al.*, 2015).

An elevated concentrations of lysozyme in serum and urine can also indicate chronic myelomonocytic leukaemia due to lysozyme-induced nephopathy (Moscinski, Kasnic and Saker, 1992; Santoriello *et al.*, 2017; Patel, Miles and Deininger, 2019). It is also a prognostic factor and potential therapeutic target in several carcinomas (Vizoso *et al.*, 2001; Serra *et al.*, 2002; Wang *et al.*, 2016).

In food industries, lysozyme is also widely used either as food processing or preserving agent, as seen in the production of cheese, beer, etc (Silvetti *et al.*, 2010; Chen, Sun and Li, 2011; Kondeková *et al.*, 2014). Given its biological and industrial importance with established structural understanding, lysozyme is clearly an excellent model of analyte to be studied for the development of novel detection assay.

The current mainstream analytical approaches for lysozyme detection are chromatography and ELISA that typically associated with expensive, lengthy and complicated procedures. To overcome these, many lysozyme sensors have been designed based on various methods, mainly derived from electrochemistry (Cheng, Ge and Yu, 2007; Li *et al.*, 2010; Chen *et al.*, 2011; Ocaña *et al.*, 2015; Ortiz-Aguayo and del Valle, 2018), colorimetry (Chen *et al.*, 2008; Wang *et al.*, 2011; Su *et al.*, 2013; Yao *et al.*, 2016; Lou, Qiang and Chen, 2017), and fluorescence techniques (Wang and Liu, 2009; Liao *et al.*, 2013; Liu *et al.*, 2014).

With these achievements, aptamers appear to hold great potential as recognition probe to identify the presence of lysozyme instead of conventional antibodies. As discussed in Chapter 2.2.1.2, DNA aptamers are short strands of antibody-like oligonucleotides that can bind to their target with high selectivity once folded into appropriate structures. The LBA used in this study was derived from the anti-lysozyme DNA aptamer first reported by Cox *et al.* with a dissociation constant of 31 nM in year 2001 to demonstrate an automated SELEX protocol (Cox and Ellington, 2001). It was then further studied by Kirby *et al.* to incorporate into an electronic tongue sensor arrays for higher screening throughput and reusability (Kirby *et al.*, 2004).

In terms of AuNPs, the traditional citAuNPs cannot directly interact with most anionic molecules due to their same electrostatic charge as mentioned in Chapter 2.3.1.2. Taking DNA as example, it has to be first thiolated to enable a strong covalent Au–S bond, providing a mean of anchoring point for possible conjugation. In order to bring the citAuNPs and thiolated DNA into close proximity to enable their interaction, a salt aging technique developed by Mirkin and co-workers (Mirkin *et al.*, 1996) is typically involved by gradually adding salt or NaCl for electrostatic masking purpose (Liu and Liu, 2017b). However, the protocol per se is laborious and time-consuming due to the weak binding energy of Au–carboxylate resulting in electrostatic repulsion between both negatively charged citAuNPs and DNA has to be screened off very delicately during the salt aging to avoid irreversible aggregation (Liu and Lu, 2006).

With that in regards, considerable efforts have been devoted in modulating the interaction between DNA and AuNPs to achieve surface functionalisation. For instance, Hsing and co-workers (Zhao, Lin and Hsing, 2009) presented a new method

to synthesise DNA-functionalised AuNPs *via* mononucleotide-mediated conjugation. In later years, Liu and co-workers (Zhang *et al.*, 2012; Zhang, Servos and Liu, 2012) introduced pH-assisted and freezing-directed (Liu and Liu, 2017a) routes to prepare DNA-modified citAuNPs. However, excessive reagents or drastic changes in reaction conditions (*i.e.* pH or temperature) are required, which can be unfavourable for downstream applications.

This chapter thus aims to address the aforementioned bottlenecks by studying non-citAuNPs, *i.e.* cysAuNPs and subsequently harnessing their electrostatic interactions with non-modified DNA in sensor development. Being the shortest aminothiol, cysteamine offers both thiol and amine groups that enable strong binding to gold with a net positive surface charge (Su *et al.*, 2013; Wang *et al.*, 2016). Therefore, cysAuNPs can interact directly with DNA without any electrostatic masking required. While the simplicity of preparation and generality of cysAuNPs are comparable to that of citAuNPs, the former is relatively stable due to the stronger Au–S bonds as aforementioned (Niidome *et al.*, 2004; Zheng *et al.*, 2013). In terms of optical property, cysAuNPs show similar LSPR behaviour that display a colour transition between ruby red (dispersed state) and bluish grey (aggregated state) in respond to altered intermolecular distance.

Given their interesting properties, cysAuNPs have been incorporated into various assays for different sensing purposes, including colorimetric (Cao and Li, 2011; Su *et al.*, 2013, 2016; Luo *et al.*, 2015; Mura *et al.*, 2015; Qi *et al.*, 2017; Zheng *et al.*, 2017; Li *et al.*, 2018; Sharma *et al.*, 2018; Yadav, Patel and Lad, 2018) and electrochemical platforms (Ramírez-Segovia *et al.*, 2014; Asadzadeh-Firouzabadi and Zare, 2017). In the context of cysAuNPs-derived aptasensors, they are mainly based on the following general principles:

i. in the absence of targets, electrostatic attraction between oppositely charged DNA aptamers and cysAuNPs leads to close proximity of the particles and aggregate them;

ii. in the presence of targets, the specific recognition between DNA aptamers and targets would negate the electrostatic interaction between the aptamers and cysAuNPs, leading to dispersed particles.

Keeping this in mind, the concept is further developed here by systematically measuring the dispersity of cysAuNPs over a wide range of LBA concentrations. On top of the expected outcome where cysAuNPs aggregated in the presence of LBA, redispersion of cysAuNPs has been observed when LBA achieves a critical redispersion concentration (CRC), attributed to the formation of anionic LBA layer surrounding each cysAuNP. CRC hereby refers to the threshold in which any LBA concentration above CRC would lead to redispersion of cysAuNPs rather than aggregation. This inspires a bimodal colorimetric aptasensor to detect lysozyme by modulating the concentration of LBA (Figure 3.1) based on the following principles:

i. mode A (A = aggregation), where concentration of LBA that could aggregate cysAuNPs was employed. The presence of targets (*i.e.* lysozymes) would reduce the aggregation of cysAuNPs as aforementioned;

ii. mode R (R = redispersion) with excess LBA at CRC regime. Adding lysozymes to the redispersed cysAuNPs would lead to two observations: (1) formation of lysozyme/LBA complexes would deplete the free LBA adsorbed onto the particle surface, subsequently cysAuNPs aggregate due to electrostatic masking; (2) further increased amount of lysozyme would result in exhausted LBA layers, hence cysAuNPs re-establish their positive charges and repel each other.

In both modes, the changes in dispersity of cysAuNPs is reflected by the red shift of their LSPR bands. This allows a ratiometric detection of lysozyme by measuring the absorptions on the relevant wavelengths. With positively charged and amino-rich surface as-synthesised, the unique features of cysAuNPs make them a very interesting and promising alternative to conventional citAuNPs by paving new path in the sensing field, especially with regards to DNA nanotechnology as demonstrated here in this work.

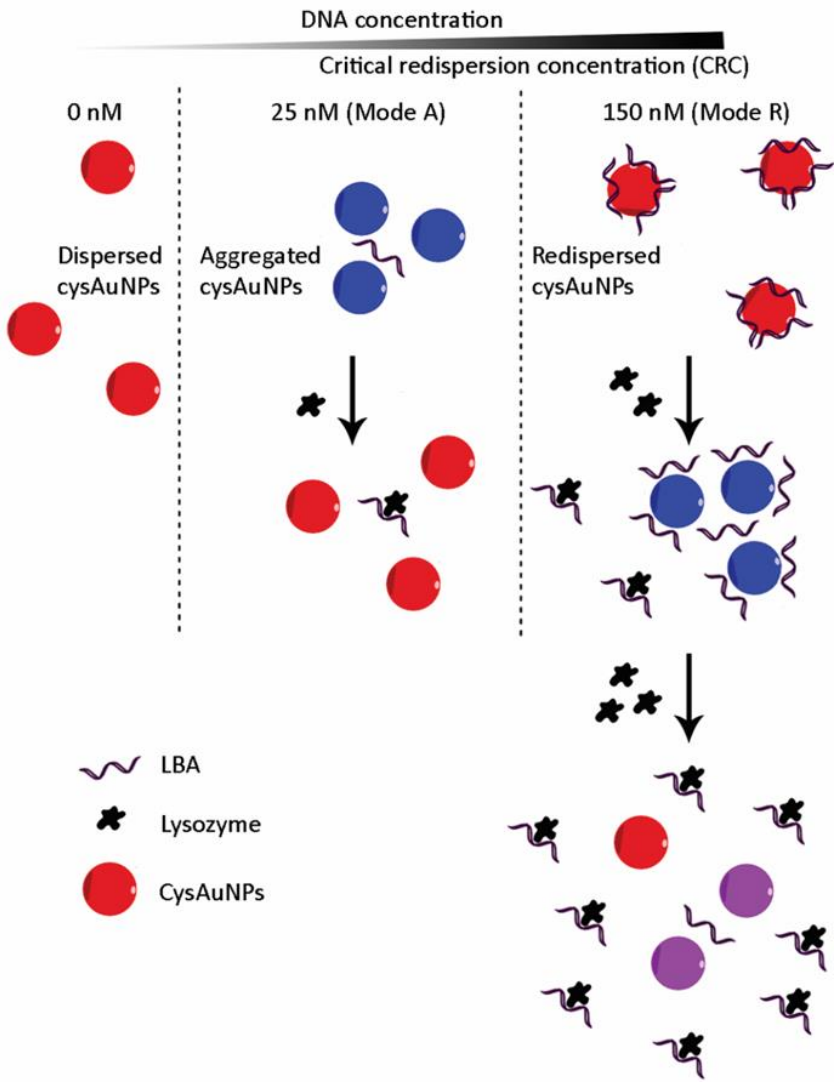

Figure 3.1. Proposed cysAuNPs-based aptasensor with bimodal responses (modes A and R). The dispersion states of cysAuNPs are represented by their colours, which include red (dispersed), purple (partially aggregated) and blue (aggregated), respectively. Note: Different LBA concentrations are used for different modes. Components are not drawn to scale.

3.3 Experimental section

3.3.1 Instrumentation

An Epoch™ microplate spectrophotometer was used to measure the UV-Vis absorbance spectra (Biotek Instrument, USA). DNA heating was performed on a ThermoMixer® C (Eppendorf, Germany). DNA quantification was performed using a NanoDrop™ One (Nanodrop, USA). Dynamic light scattering and zeta potential analyses were conducted on a Malvern Nanoseries Zetasizer (Malvern, UK). Scanning-transmission electron microscopy (STEM) images were taken on a Quanta 400F (FEI Company, USA) at 15 kV under high vacuum, with the samples being air-dried on formvar-coated copper grids without specific fixation.

3.3.2 Chemicals

Lysozyme, cytochrome C, insulin, vascular endothelial growth factor (VEGF), bovine serum albumin (BSA), mercaptoacetic acid ($C_2H_4O_2S$), acetylcysteine ($C_5H_9NO_3S$), and gold(III) chloride ($HAuCl_4$) solution were purchased from Sigma-Aldrich (St. Louis, USA). 2-aminoethanethiol or cysteamine (C_2H_7NS) was obtained from Tokyo Chemical Industry Co., Ltd (Kyoto, Japan). Sodium borohydride ($NaBH_4$) was purchased from Nacalai Tesque Inc. (Kyoto, Japan). 1x phosphate buffered saline (PBS) buffer at pH 7.4 was used. All reagents and chemicals were of analytical grade and used without further purification after reconstituted as recommended by the respective suppliers. Deionised water (DI H_2O) with measured conductivity of 18.2 MΩ.cm was used throughout all experiments. Unless otherwise stated, all experiments were conducted at room temperature (20 ^oC).

3.3.3 Sequences and preparation of DNA oligonucleotide

The DNA oligonucleotide, LBA, with sequence of 5'- ATC TAC GAA TTC ATC AGG GCT AAA GAG TGC AGA GTT ACT TAG -3' was synthesised by Integrated DNA Technologies, Inc (Singapore). All oligonucleotides were reconstituted in DI H_2O and stored in -20 ^oC freezer as recommended by manufacturer and used without further purification. The concentrations of the oligonucleotides were measured using UV-Vis spectrophotometry prior to each usage.

3.3.4 Preparation and characterisations of CysAuNPs

Prior to synthesis, all glassware was rinsed with aqua regia (HNO_3:HCl of 3:1 (v/v)), then washed extensively with DI H_2O and air-dried overnight. The cationic cysAuNPs were synthesised according to published protocol with slight modifications (Niidome *et al.*, 2004; Su *et al.*, 2013). In brief, 400 µL C_2H_7NS (213 mM) was mixed with 40 mL of $HAuCl_4$ (1.42 mM) solution under gentle stirring in dark. After that, 10 µL of fresh cold $NaBH_4$ (10 mM) was added under vigorous stirring for another 10 min, followed by mild stirring for 30 min. The solution was then stored in dark at room temperature for overnight before use. After that, an aliquot of as-prepared cysAuNPs was taken for characterisations purpose, including STEM, dynamic light scattering and zeta potential analyses. All cysAuNPs were used within two months.

3.3.5 Colorimetric assays

The LBA was first diluted to the desired concentration in buffer. Then, the LBA was heat treated at 90 ^oC for 5 min and slowly cooled down to room temperature. As general screening procedure in a 96-well plate, 5 µL of sample solution containing LBA was incubated with 95 µL of cysAuNPs for 5 min under mild mixing on a rotary shaker. The samples were then photographed against a white

background and subjected to UV-Vis measurement to obtain their respective absorbance spectra from 400 to 900 nm with 1 nm interval.

3.3.6 Evaluation of sensitivity of lysozyme sensor

Two different concentrations of LBA (25 and 150 nM of final concentrations) were used to detect lysozyme via modes A and R, respectively. The LBAs were prepared fresh and heat-treated as mentioned above, then incubated with various concentrations of lysozyme for 1 hour. After that, 5 µL of the mixture was added into 95 µL of cysAuNPs for 5 min in a 96-well plate under mild mixing on a rotary shaker. The samples were then photographed and subjected to UV-Vis absorbance measurement as previously described.

3.3.7 Evaluation of selectivity of lysozyme sensor

Different proteins were used to incubate with LBA apart from lysozyme ($M_{(r)}$: 14.6 kDa; pI: 11), including cytochrome C ($M_{(r)}$: 11.7 kDa; pI: 9.6), insulin ($M_{(r)}$: 5.73 kDa; pI: 5.3), VEGF ($M_{(r)}$: 19.3 kDa; pI: 6.6) and BSA ($M_{(r)}$: 66.43 kDa; pI: 4.7) for 1 hour. 5 µL of the protein/LBA mixture were then mixed with 95 µL of cysAuNPs on a rotary shaker for 5 min. The samples were then photographed and subjected for UV-Vis absorbance measurement.

3.3.8 Data analysis

The obtained UV-Vis absorbance spectra were analysed ratiometrically for their dispersion ratios (D_r) by comparing the absorbances at 526 and 700 nm as shown in below:

Dispersion ratio = $\frac{\mathrm{Abs}_{526}}{\mathrm{Abs}_{700}}$ ..... (3A)

The obtained data were then further analysed for their signal-to-noise ratio (SNR) and limit of detection (LOD) using the equations given below:

$$SNR = \frac{R_L}{\sigma} \quad \text{..... (3B)}$$

$$LOD = 3.3 \times \frac{\sigma}{S} \quad \text{..... (3C)}$$

where R_L = signal response of least known concentration

σ = standard deviation of noise of blank sample (no analyte)

S = slope of the linear regression model obtained

3.4 Results and discussion

3.4.1 Characterisation of CysAuNPs

CysAuNPs were first prepared in one-pot synthesis reaction *via* sodium borohydride reduction in the presence of cysteamine without post-synthesis modification (Liang *et al.*, 2011; Ma *et al.*, 2013; Kang *et al.*, 2016). In accordance with other reports, the as-synthesised cysAuNPs in this study were ruby-red in colour with the characteristic of LSPR band peaked at 526 nm (Figure 3.2) (Kim *et al.*, 2009; Zheng *et al.*, 2013).

The STEM image reveals homogenously dispersed spherical particles, with an average physical diameter of 28 nm (Table 3.1). The stability of cysAuNPs is further evidenced from their zeta potential measured at 44.3 mV, implying that the particles are highly dispersed by virtue of electro-repulsive force among protonated cysteamine ligands (pka = 8.3). While it is well known that citAuNPs are highly susceptible to aggregation in presence of thiol-containing molecules, such as mercaptoacetic acid (Alkilany *et al.*, 2014), cysAuNPs are expected to have better

tolerance due to their covalent Au–S bonds upon synthesis. As shown in Figure 3.3, the cysAuNPs could tolerate a high concentration of thiol-containing molecules, including both mercaptoacetic acid and acetylcysteine, up to 12.5 µM, respectively.

In terms of structural coordination, cysteamine is known to cap onto the AuNPs through strong Au–S bond conferred by the thiol group presumed to be in a *trans* conformation as illustrated in Figure 3.4. However, the possibility of Au–N coordinative bond from amino group *via gauche* conformation should not be neglected as it could play a certain role in the interaction between cysAuNPs and DNA (Aina *et al.*, 2010; Xia *et al.*, 2012; Radenković *et al.*, 2017). The slow transition of cysteamine ligands from *trans* to *gauche* conformation has been recently simulated by Puangmali and co-workers (Toomjeen *et al.*, 2019). They reported that different ionic forms of cysteamine (*i.e.* protonated, zwitterionic and deprotonated) will have different conformation profiles, with the protonated form present predominantly as *trans* configuration. Their simulations also demonstrated the preference of protonated cysteamine on AuNPs over the other two ionic forms in their study using cysAuNPs to detect 8-oxo-dG.

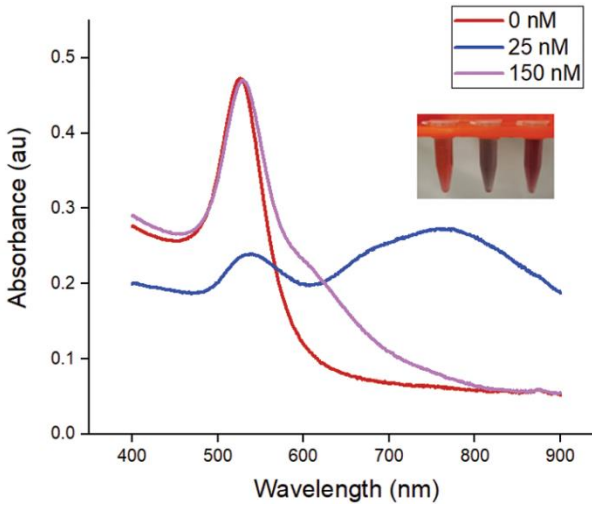

Figure 3.2. UV-Vis absorbance spectra of cysAuNPs in the absence and presence of LBA with both concentrations below and above CRC. Inset: the corresponding photographs of cysAuNPs in response to different final concentrations of LBA (left to right: 0, 25, 150 nM).

Table 3.1. Summary of STEM images and zeta sizer results of cysAuNPs under different conditions: **(A)** blank PBS buffer, **(B)** incubated with 25 nM of LBA and **(C)** incubated with 150 nM of LBA, respectively

Parameter	Sample	(A) Blank cysAuNPs	(B) CysAuNPs with 25 nM LBA	(C) CysAuNPs with 150 nM LBA
STEM image (scale bar = 200 nm)		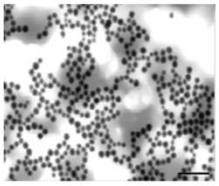	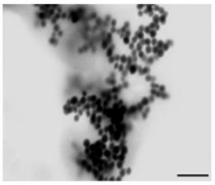	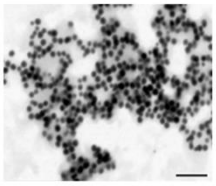
Hydrodynamic size (nm)		45.52 ± 0.41	Severely aggregated	46.33 ± 0.41
PDI		0.15 ± 0.01	Severely aggregated	0.35 ± 0.05
Zeta potential (mV)		44.3 ± 1.37	17.5 ± 1.95	-21.6 ± 2.10

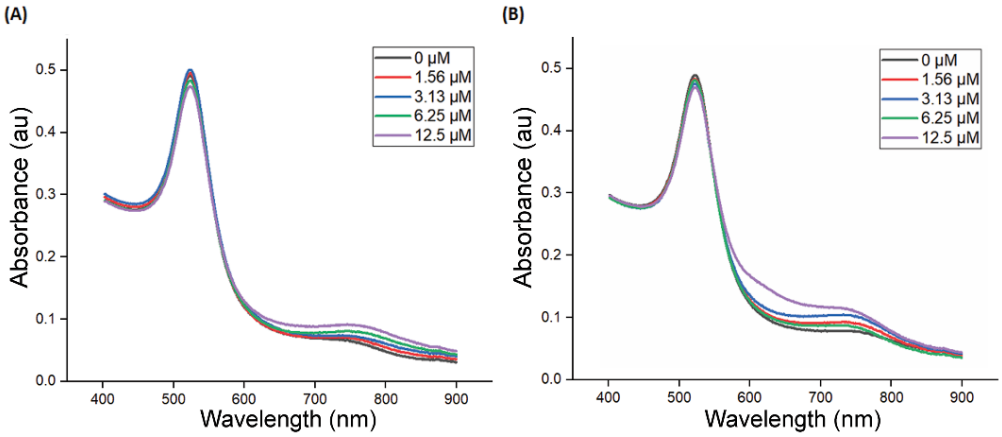

Figure 3.3. UV-Vis absorbance spectra of cysAuNPs in the presence of **(A)** mercaptoacetic acid and **(B)** acetylcysteine at their respective final concentration as indicated in the legend (1.56, 3.13, 6.25, and 12.5 µM).

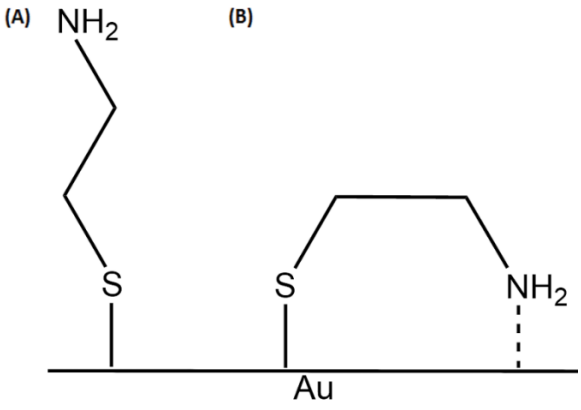

Figure 3.4. Possible structural arrangements of cysteamine being conjugated onto the surface of AuNPs in the form of **(A)** *trans*, and **(B)** *gauche* conformations.

3.4.2 Interaction between LBA and CysAuNPs

Similar as other single-stranded DNAs (ssDNAs) reported elsewhere (Su *et al.*, 2013, 2016; Luo *et al.*, 2015; Qi *et al.*, 2017; Zheng *et al.*, 2017; Li *et al.*, 2018), the polyanionic LBA wraps onto cysAuNPs at pH 7.4, leading to electrostatic masking that disrupt the initial stabilisation provided by cysteamine ligands. As the nanoparticles aggregate, the interparticle distance between each cysAuNPs decreases along with increasing LBA concentration. Ratiometric analysis on the resulting red shift of LSPR band on their absorbance spectra can thus be carried out to indicate the dispersion ratio of cysAuNPs in response to LBA concentration based on equation 3A. The cysAuNPs aggregation is also coupled with a gradual colour transition from ruby red to bluish grey (Figure 3.5). The colour transition is also evidenced by the red shift in their UV-Vis absorbance spectra shown in Figure 3.6.

Owing to LBA-induced electrostatic masking, the aggregation of cysAuNPs is supported by the decreased in zeta potential of cysAuNPs in presence of 25 nM (where cysAuNPs aggregated and appeared blue) with significant reduction from 44.3 to 17.5 mV. As the zeta potential is now lower than +30 mV (typical threshold assigned for strong electro-repulsive nanoparticles stabilisation) (Clogston and Patri, 2011), the colloidal system collapses due to strong interparticle Van der Waals attraction (Bishop *et al*., 2009; Liu and Liu, 2017b).

Moving forward, as the amount of LBA increases to 50 nM and above, the cysAuNPs starts to retain their colloidal stability. The change from aggregation to dispersion is accompanied by increased dispersion ratio and gradual colour transition from blue to red as illustrated in Figure 3.5 with the individual spectrum shown in Figure 3.6. From the gradual response of cysAuNPs towards increment of LBA, the CRC was determined at 150 nM, where the particles redispersed and appeared red.

Interestingly, the zeta potential of cysAuNPs with LBA above CRC was also reverted to -21.6 mV. This implies that the excess LBA adsorbs onto the surface of cysAuNPs and hence renders them negatively charged. Additionally, both the hydrodynamic particle size and STEM image of cysAuNPs at CRC regime are comparable to that of blank particles, further confirming the re-stabilisation of cysAuNPs (Table 3.1).

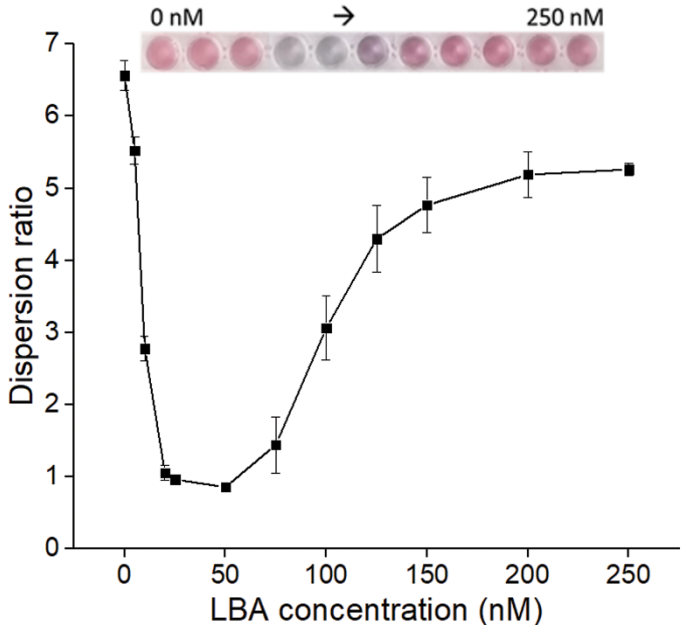

Figure 3.5. Dispersion ratio plot of cysAuNPs in response to increasing concentration of LBA. Results were presented as mean ± S.D. (n = 3). Inset: the corresponding photographs show gradual colour changes of cysAuNPs samples upon mixing with LBA.

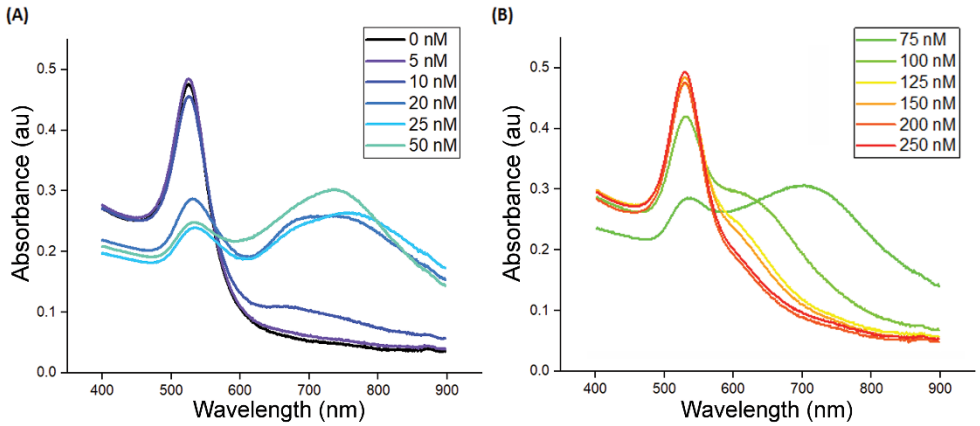

Figure 3.6. UV-Vis absorbance spectra of cysAuNPs incubated with different final concentrations of LBA. **(A)** CysAuNPs aggregate as concentration of LBA increases from 0 to 50 nM. **(B)** CysAuNPs disperse as concentration of LBA increases from 75 to 250 nM.

3.4.3 Detection of lysozyme in buffered solutions

3.4.3.1 Sensitivity performance

After establishing the relationship between cysAuNPs and LBA, two concentrations of LBA have been chosen for bimodal detection of lysozyme, *i.e.* modes A and R. In mode A, LBA with a final concentration of 25 nM (below CRC) was employed. At this stage, cysAuNPs aggregate due to their electrostatic interaction with LBA. In the presence of lysozyme, the LBA binds to its target to form a rigid lysozyme/LBA complex, mimicking the antigen/antibody binding (Jayasena, 1999). The formation of such complex would negate the amount of effective negative charge on LBA to electrostatically interact with cysAuNPs (Su *et al.*, 2013). Hence, cysAuNPs retain their stability, as reflected by the recovery of LSPR band at 526 nm with increasing concentrations of lysozyme (Figure 3.7).

By analysing the dispersion ratio, a good response along with lysozyme concentrations was observed, accompanied with a colour transition from bluish grey to red and the linear detection range was established from 37.5 to 180 nM. The LOD was calculated as 2.29 nM based on equation 3C, which is considerably lower than the lysozyme content reported in submandibular saliva (*i.e.* 353 – 468 nM) (Yeh *et al.*, 1997) and in colostrum milk (*i.e.* 4.7 μM) (Goldblum *et al.*, 1982).

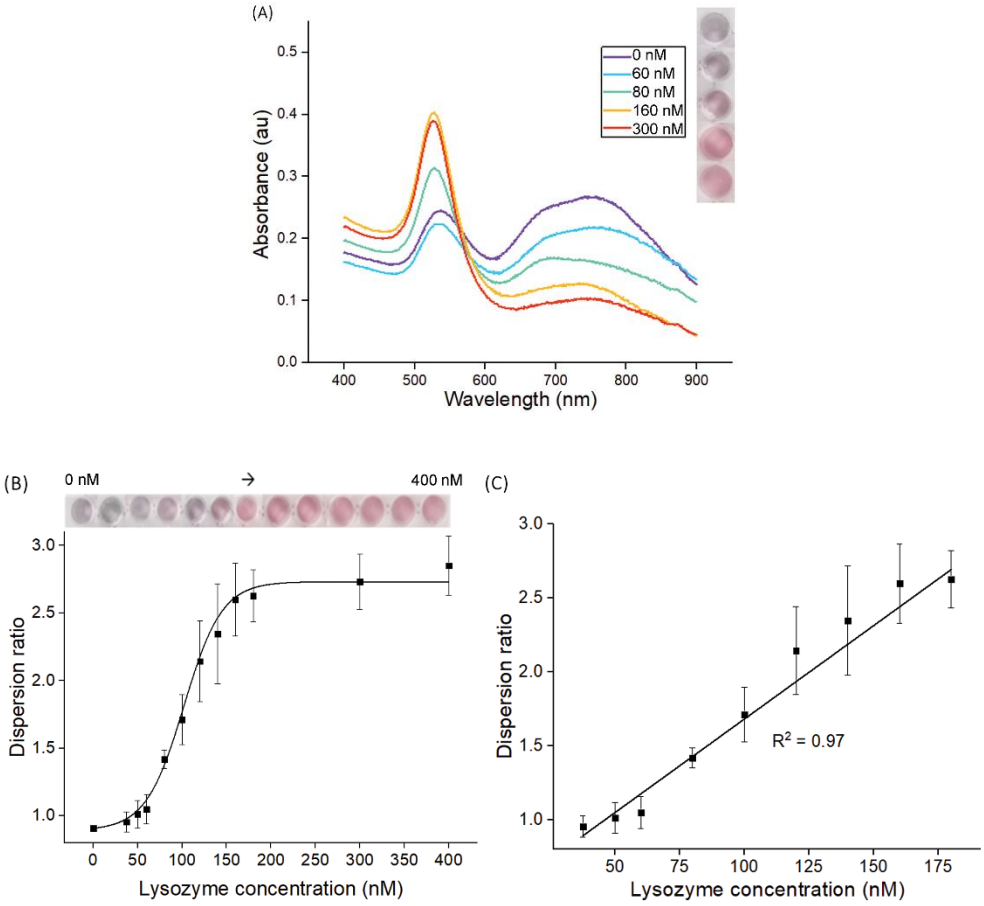

Figure 3.7. (A) The UV-Vis absorbance spectra and **(B)** dispersion ratio plot of the cysAuNPs aptasensor in mode A with different concentrations of lysozyme with **(C)** the linear regression fitting model. Results were presented as mean ± S.D. (n = 3). Certain spectra were selected to highlight the blue shift and re-establishment of LSPR band at 526 nm. Insets show the progressive colour changes of cysAuNPs in response to increasing concentrations of lysozyme. Note that due to huge number of samples in a 96-well plate, different photography lighting and angles may influence the overall appearance of some sample images.

On the other hand, a final concentration of 150 nM LBA was used in mode R to represent concentration above CRC. At this stage, cysAuNPs were in dispersion stage due to additional LBA coated on nanoparticles and rendered them negative electrostatic repulsion. In this mode, the presence of lysozyme would competitively disrupt the electrostatic adsorption of LBA onto cysAuNPs, causing aggregation as evidenced by the red shift in their UV-Vis absorbance spectra in Figure 3.8 (A and B). This leads to decreased dispersion ratios as indicated in the blue regime shown in Figure 3.8 (C).

Since adding lysozyme would aggregate cysAuNPs, the dispersion ratio experiences a sharp decrease, indicating that the equilibrium of cysAuNPs and LBA is highly sensitive to their relative concentrations. However, as the concentration of lysozyme further increases, the response is inverted, in line with recovery of dispersion ratio as indicated by the red regime of Figure 3.8 (C). This interesting phenomenon is due to the further formation of lysozyme/LBA complexes that has depleted the LBA available to aggregate cysAuNPs. Hence, the particles regain their electro-repulsive positive charge conferred by the cysteamine ligands.

Noteworthily, such response curve demonstrates an inverse sensitivity behaviour, *i.e.* lower analyte yields higher response. In this case, the dispersion ratio at inverse sensitivity limit (ISL; *i.e.* the observed LOD in red regime at 375 nM) is 0.918, implying the highest aggregation level of nanoparticles. As the blue regime is so narrow and reversed to that in red, response below the ISL is almost negligible. Such observation and assumption would therefore lead to a linear range of detection from 500 to 4000 nM with good R^2 value (Figure 3.8 (D)) and significantly improved SNR of 72.56 at the ISL, a whopping 24-fold higher than the typically required SNR of 3 for most sensors at their respective LOD (Long and Winefordner, 1983; Shrivastava and Gupta, 2011).

In fact, the novel idea of inverse sensitivity was actually first proposed by Rodrıguez-Lorenzo *et al.* (Rodríguez-Lorenzo *et al.*, 2012) using enzyme-directed silver deposition on gold nanostars to detect cancer biomarker. Later on, Pallares *et al.* (Pallares *et al.*, 2015; Pallares, Thanh and Su, 2018) further developed the concept using hexadecyltrimethylammonium bromide-coated gold nanorods (CTAB-AuNRs) for quantification of extracellular DNA and circulating cell-free DNA.

The discovery of this inverse sensitivity concept is ground-breaking because one can quantify low concentration of analyte with higher reliability due to exceptional SNR. The aptasensor reported here indeed demonstrated the first implementation of inverse sensitivity for colorimetric detection using spherical AuNPs. While the performance of CTAB-AuNRs could be affected by aspect ratio of the nanorods (Pallares, Thanh and Su, 2018), utilising cysAuNPs per se is more controllable considering they are round shaped with stronger Au-S conjugation.

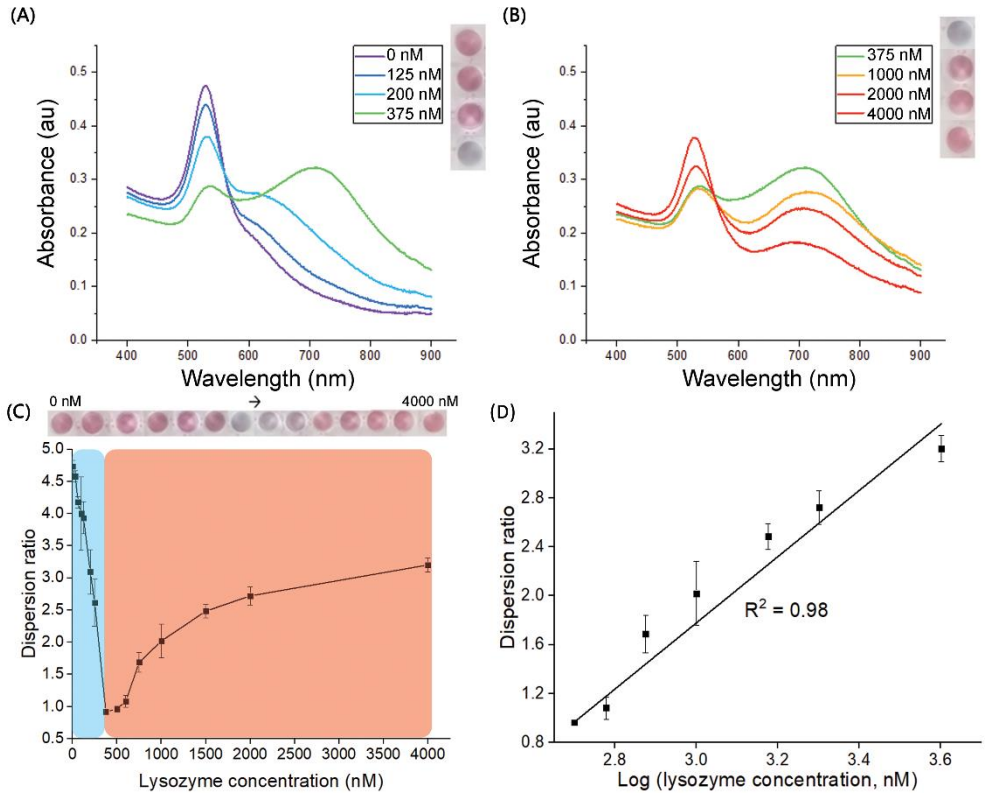

Figure 3.8. UV-Vis absorbance spectra and dispersion ratio plot of the cysAuNPs aptasensor in mode R with different concentrations of lysozyme. The spectra were selected to highlight **(A)** the increased aggregation and then **(B)** redispersion of cysAuNPs that also correspond to **(C)** the blue and red regimes in their observed dispersion ratio with **(D)** the linear regression fitting model from 500 to 4000 nM (concentration in logarithmic scale). Results were presented as mean ± S.D. (n = 3). Insets show the progressive colour changes of cysAuNPs in line with increasing concentrations of lysozyme.

Overall, the aptasensor demonstrated good sensitivity for lysozyme detection. Compared to other colorimetric aptasensors for lysozyme detection (Table 3.2), the work reported here presents several advantages in general, including versatility of bimodal sensing modes, wide and tuneable detection range, lower LOD as well as exceptional SNR. These are achieved through carefully modulating the concentration of LBA to enable bimodal sensing which is yet to be reported in others.

Table 3.2. Comparison of the reported colorimetric aptasensors for lysozyme detection

Materials	**LOD (nM)**	**Linear range (nM)**	**Reference**
Polydiallyldimethylammonium chloride (PDDA), citAuNPs	4.4	4.4 – 200	(Yao *et al.*, 2016)
cysAuNPs	35	35– 1050	(Su *et al.*, 2013)
Human serum albumin (HSA)-modified citAuNPs	50	100 – 1000	(Chen *et al.*, 2008)
Core-shell Cu@AuNPs, 3,3,5,5-tetramethylbenzidine - hydrogen peroxide (TMB-H_2O_2)	60	100 – 1000000	(Lou, Qiang and Chen, 2017)
Polydimethylsiloxane (PDMS)-AuNPs, Ag	0.0069	0.69 – 69	(Wang *et al.*, 2011)
cysAuNPs	2.29	37.5 – 180 (Mode A)	This work
	375	500 – 4000 (Mode R)	

3.4.3.2 Selectivity performance

To evaluate if the aptasensor is selective towards lysozyme, several control proteins with different sizes and isoelectric points were tested. As indicated by their respective UV-Vis absorbance spectra in Figure 3.9, only samples containing lysozyme are dispersed in mode A and aggregated in mode R; whereas the others

show the opposite results. Despite so, an exception was observed for BSA samples, where the cysAuNPs were indeed dispersed in both modes, implying that these bulky proteins may provide electro-steric stabilisation to the cysAuNPs. Notably, BSA has been widely used in passivating gold surfaces, particularly in positively charged nanomaterials such as CTAB-AuNRs (Tebbe *et al.*, 2015; Yasun *et al.*, 2015). Avila *et al.* (Cardoso Avila *et al.*, 2017) have also reported the preparation of AuNPs co-coated with both cysteamine and BSA as mixed layer, by incubating cysAuNPs with BSA. The high binding affinity of BSA towards metal surfaces could be attributed to its high-molecular-weight charges, as well as the prevalence of carboxylate, thiol, amine, and imidazole groups within the protein structure (Brewer *et al.*, 2005; Chakraborty *et al.*, 2011; Tsai *et al.*, 2011; Tebbe *et al.*, 2015). Despite that, the positive error of BSA could be easily identified and eliminated based on its outlier dispersion ratios in both modes (Figure 3.10).

By calculating the averaged dispersion ratios of all the other control proteins +/- 3 S.D. for modes A and R, respectively, cut-off values could be set to distinguish lysozyme from the rest. The difference in mixed protein samples containing multiple control proteins with or without lysozyme could even be observable by naked eyes under optimised condition as illustrated in Figure 3.11. Therefore, the findings reveal that the selectivity of this aptasensor is attained since only lysozyme samples produced distinguishable results from other control proteins and performing bimodal screening can eliminate false positive outcome.

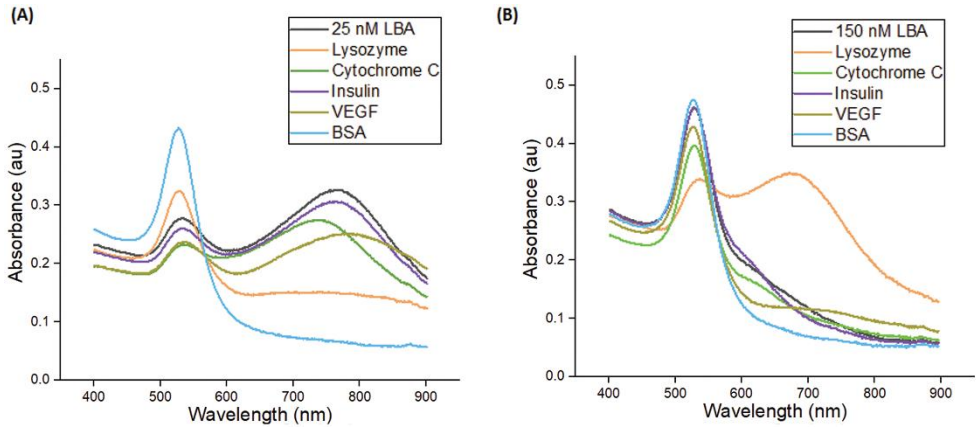

Figure 3.9. UV-Vis absorbance spectra of the aptasensor in **(A)** mode A and **(B)** mode R in the presence of lysozyme and control proteins individually. The concentrations of proteins were tested at 180 and 375 nM for modes A and R.

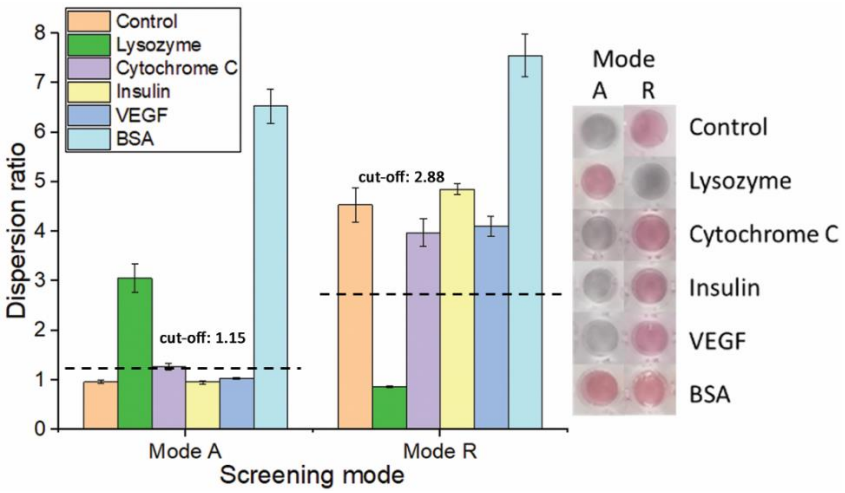

Figure 3.10. Selectivity performance of the proposed aptasensor towards lysozyme in both modes A and R. Results were presented as mean ± S.D. (n = 3). Inset: photos correspond to the samples.

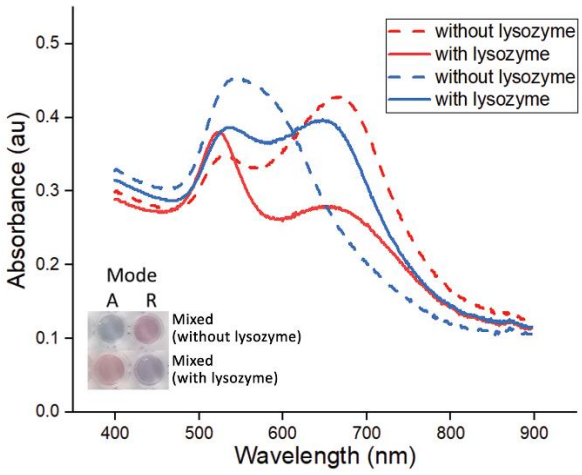

Figure 3.11. UV-Vis absorbance spectra of the aptasensor for lysozyme detection in mixed samples containing the control proteins (cytochrome C, insulin and VEGF) (red lines: mode A; blue lines: mode R). Mode A contains 540 nM of control proteins and 180 nM of lysozyme, whereas mode R contains 1125 nM of control proteins and 375 nM of lysozyme.

3.4.3.3 Comparison between modes A and R

As compared to mode R, mode A enables a more straightforward detection approach since the former requires careful screening to identify the CRC regime of DNA aptamer. However, the detection range of mode A is generally narrower, in accordance with other studies using cysAuNPs as aptasensor to detect melamine (1 – 24 nM) (Zheng *et al.*, 2017) and 17 β-estradiol (3.67 – 312.06 nM) (Li *et al.*, 2018). This can be attributed to the number of aptamers available in mode A which is relatively lesser than that in mode R. Furthermore, as demonstrated in the selectivity test, mode A is also more susceptible to false positive result when bulky protein is assayed.

Having bimodal screening modes in a single assay has undoubtedly provided a complementary approach with greater versatility. On top of having the merit to choose the suitable screening mode, one can further validate the sensing results using the same batch of detection probes (*i.e.* cysAuNPs in this case). As

demonstrated in the selectivity study, erroneous result can be eliminated with high accuracy. Furthermore, since modes A and R can be used for different concentration ranges of lysozyme, it provides a mean of tuneable dynamic range of detection.

3.5 Conclusion and future direction

As a summary, this chapter addresses the electrostatic relationship between DNA aptamer and cysAuNPs from the perspective of consequent nanoparticles aggregation or redispersion. The first observation is in line with other literatures whereby incubating cysAuNPs with DNA aptamer resulted in aggregation. However, this study documented an unprecedented trend of cysAuNPs redispersion when the DNA concentration was further increased upon CRC. Inspired by this observation, a bimodal colorimetric aptasensor has been rationally designed through manipulation on the electrostatic interaction among DNA aptamer, target and cysAuNPs using lysozyme and LBA as study models. While the concept of bimodal detection behaviour is relatively new, this study also shows the first demonstration of inverse sensitivity on spherical AuNPs when lower concentration of target gives rise to higher signal response.

The achievement demonstrated here is important as it signifies that once the technology is fully developed, an aptasensor could be designed without theoretical LOD to detect as little analyte as possible as long as the relevant instrument can analyse the increasing response with high resolution. Despite more studies are needed to further understand the fundamental chemistry between DNA aptamer and cysAuNPs (e.g. their coordination mechanisms), the findings here substantiate their huge potential to be incorporated as a colorimetric aptasensor.

As for the future prospect, the aptasensor proposed here could be employed for real sample testing, such as human serum or saliva samples. Performance

comparison with ELISA could also be conducted to confirm the validity and feasibility of this aptasensor. Besides, as this study is currently limited only to lysozyme detection, the generalisability of this aptasensor could also be evaluated by studying other targets with their respective DNA aptamers. With that in regards, thrombin appears to be a good candidate given that it has two different DNA aptamers (TBA15 and TBA29) that recognise different moieties on the protein (Bock *et al.*, 1992; Deng *et al.*, 2014), thus potentially allowing the development of a sandwich type aptasensor derived from the current design.

Last but not the least, the study here demonstrates that cysAuNPs could present many other possible routes for diverse reactions and applications that are otherwise not achievable by the mainstream citAuNPs with ease.

CHAPTER 4

A DNAZYME-DRIVEN SENSOR FOR METAL IONS DETECTION BASED ON BIOLUMINESCENCE RESONANCE ENERGY TRANSFER (BRET)

4.1 Chapter overview

This chapter explores another aspect of DNA nanotechnology in the form of DNAzymes, a family of "enzyme-like" oligonucleotides. The main aim of this study is to address the conventional limitations of DNAzyme systems associated with FRET (including excitation light source, noisy background, photobleaching). This is done by introducing BRET, where a bioluminescent luciferase was employed to generate light emission required to co-excite an adjacent acceptor fluorophore. To investigate the feasibility of this BRET sensor, the DNAzyme "8-17" and its targeted analyte, Zn^{2+} ion, have been chosen as model for proof-of-concept study. After a series of optimisations, the DNAzyme-driven BRET-based sensor was evaluated for its performance in identifying and quantifying Zn^{2+} ions in buffered solution. The chapter then concludes with highlights on the importance of this study, coupled with future outlook of BRET-based DNAzyme in contrast to the conventional FRET-based systems.

4.2 Introduction

Zinc, usually exists as divalent cation Zn^{2+}, is one of the both biologically and industrially important elements. It is the second most abundant metals to be found in human body, required by more than 300 enzymes from all six classes (*i.e.* oxidoreductases, transferases, hydrolases, lyases, isomerases and ligases) to function properly, which can be collectively named as zinc metalloenzymes (McCall, Huang

and Fierke, 2000; Outten, 2001; Cai and Chou, 2005). Zinc is also involved in regulatory proteins in the form of zinc finger motif for a wide variety of biological functions (Laity, Lee and Wright, 2001; Cassandri *et al.*, 2017). In terms of industrial significance, zinc is heavily applied in galvanization of iron or steel and the preparation of other alloys. Its nanomaterial form, *i.e.* zinc oxide nanoparticles, are also extensively used in various fields including but not limited to cosmetics, electronics or chemical catalysis (Kołodziejczak-Radzimska and Jesionowski, 2014).

Nonetheless, the huge demand of zinc has resulted in excessive mining activities that subsequently lead to several environmental concerns, particularly for their hazardous effects on aquatic ecosystems and human health (Zhang *et al.*, 2012; X. F. Li *et al.*, 2019). Over-exposure to zinc or abnormal zinc homeostasis has been reported to cause many adverse effects, including skin corrosion (Singh *et al.*, 2011), attenuated energy production (Lemire, Mailloux and Appanna, 2008), carcinogenesis (Zaichick, Sviridova and Zaichick, 1997; Costello and Franklin, 1998; Leitzmann *et al.*, 2003; Wang *et al.*, 2019), immunodeficiency (Prasad, 2008; Nishida *et al.*, 2009), growth retardation with osteogenic issues (King, Shames and Woodhouse, 2000; Inoue *et al.*, 2002), neurodegenerative disorders (Cuajungco and Lees, 1997; Frederickson *et al.*, 2000; Grabrucker, Rowan and Garner, 2011), etc. With that in mind, a reliable method to detect and quantify the amount of zinc presents in a given sample is clearly demanded.

Given the importance of zinc, there are numerous Zn^{2+}-sensors developed over the years. In particular, the luminescence type can be categorised into two groups, namely intensity and ratiometric probes. The intensity probes rely on photoinduced electron transfer (PET) between a fluorophore and a Zn^{2+}-chelating organic molecule. The coordination of Zn^{2+} ion inhibits the PET quenching of the

unmetalated fluorophore, leading to restoration of fluorescence emission (Carter, Young and Palmer, 2014). Some of the classical examples of intensity probes include 8-aminoquinoline derivatives (Nasir *et al.*, 1999; Nowakowski and Petering, 2011; Nowakowski *et al.*, 2015) and Zinpyr family (*i.e.* small molecule zinc sensor derived from dichlorofluorescein) (Walkup *et al.*, 2000; Burdette *et al.*, 2001, 2003; Zhang *et al.*, 2008).

On the other hand, ratiometric probes are derived on the principle of FRET in which the energy is being transferred from a donor to another proximate acceptor fluorescent molecule, resulting it being co-exited and re-emitting the fluorescence, as previously discussed in Chapter 2.3.2. In practical, it usually involves two separate emission wavelengths and their relative intensities can then provide a ratiometric value that corresponds to the concentration of analyte. For Zn^{2+} ion sensing, the two fluorescent domains are connected *via* a Zn^{2+}-binding moiety, e.g. eCALWY (Vinkenborg *et al.*, 2009) and ZapCY (Qin *et al.*, 2011) (*i.e.* fluorescent proteins-based FRET sensors developed by different research groups). The Zn^{2+}-binding moiety would undergo structural conformation change upon binding with Zn^{2+} ions, subsequently affecting intermolecular distance between the FRET pair and FRET efficiency.

As previously introduced in Chapter 2.2.1.3, DNAzyme is a novel double-stranded oligonucleotide that requires specific cofactors, such as metal ions, to hydrolyse its internal phosphodiester bond, making it a good candidate to construct a metal ion sensor (Santoro and Joyce, 1997; Hollenstein, 2015). Most of the DNAzyme-derived sensors for metal ions sensing nowadays utilise FRET (Li and Lu, 2000; Zhang *et al.*, 2010; Wu *et al.*, 2017; Yang *et al.*, 2018; Feng *et al.*, 2019; Wang *et al.*, 2019), which generally suffer from limitations such as photobleaching as well

as signal contamination from high background and scattered light. Moreover, FRET-based sensors require an external light source to excite the donor fluorophore, which can be cost ineffective as commercialised excitation light sources such as laser are expensive and hard to maintain. Altogether, these unfavourably hinder the technology to be translated into true portable sensor for metal ion detection.

This study aims to circumvent the aforementioned bottlenecks by exploring other reporting techniques. Instead of FRET, BRET was being incorporated into a Zn^{2+}-dependent DNAzyme system as a proof-of-concept study. The DNAzyme "8-17" was chosen as a sensing platform for Zn^{2+} ions, with its enzyme and substrate strands (termed as 8-17E and 8-17S individually) each modified by a bioluminescence protein and fluorophore. The 3' biotinylated 8-17E was further conjugated with a streptavidin-Lucia fusion protein (referred as Strep-Lucia), in which the Lucia luciferase can emit a strong bioluminescence when its luciferin substrate, coelenterazine, is supplied. On the other hand, 8-17S was labelled with a Cy3 fluorophore at its 5' terminal to bring the fluorophore in close proximity with Strep-Lucia when the DNAzyme complex (i.e. hybridised 8-17E/S) was fully assembled. The general sensing principle is as below (Figure 4.1):

1) Without Zn^{2+} ions, the Strep-Lucia emits bioluminescence at 480 nm in the presence of coelenterazine. The close proximity between Strep-Lucia and Cy3 enables BRET between the two, resulting co-excited Cy3 to emit a second fluorescence emission at 560 nm.
2) With Zn^{2+} ions, 8-17S is cleaved and the DNAzyme complex disassembles due to reduced T_m. The now displaced substrate strands with Cy3 fluorophore becomes distant to Strep-Lucia moiety, disfavouring BRET between them and reducing the fluorescent intensity of Cy3 emission.

3) In both scenarios, the BRET efficiency is primarily determined by the proximity between Strep-Lucia and Cy3 fluorophore, which is reflective of the assembly of DNAzyme complex. By measuring the relative intensities of Strep-Lucia and Cy3 ratiometrically, the presence and concentration of Zn^{2+} ions can be reliably determined.

While being principally similar to FRET, this DNAzyme-driven BRET-based biosensor requires no external excitation light but a simple supply of the coelenterazine. This provides a mean of controllable reaction with minimal signal degradation over time. While it is highly translatable into a portable detection sensor and eliminate the expensive instrumental setup, the feature of ratiometric measurement retains its accuracy, making this a highly promising and practicable metal ion biosensor in real application.

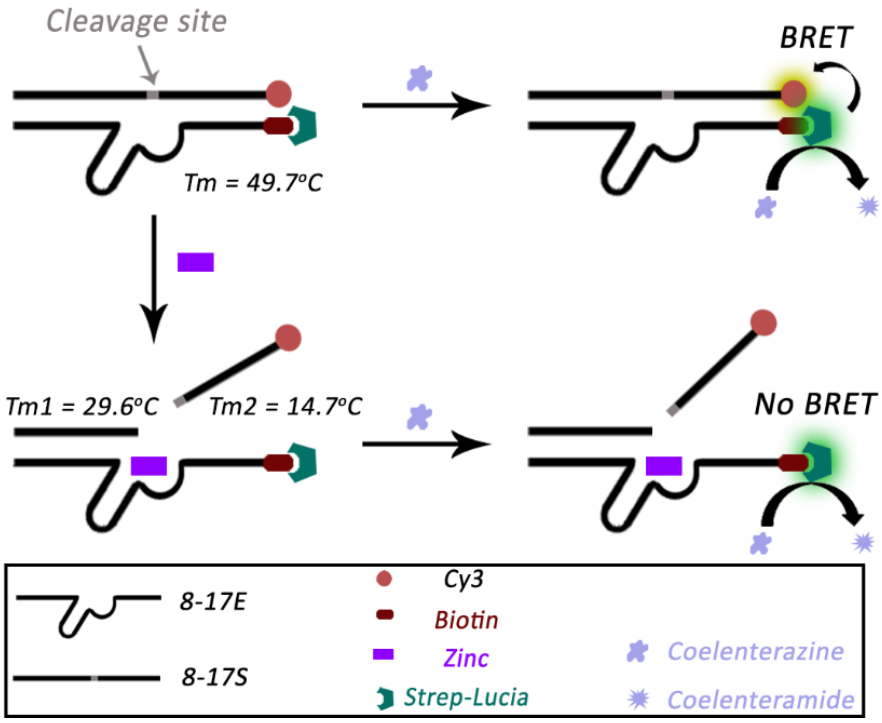

Figure 4.1. Sensing mechanism of DNAzyme-driven BRET-based sensor for Zn^{2+} detection proposed in this present work.

4.3 Experimental section

4.3.1 Instrumentation

The Agilent Cary 8454 UV-Vis spectrophotometer was used to obtain absorbance spectra. A Horiba FluoroMax-P fluorometer was used for the bioluminescence/ fluorescence measurements. DNA heating was performed on an Eppendorf ThermoMixer® C.

4.3.2 Chemicals

All chemicals purchased from Sigma-Aldrich were of analytical grade and used without further purification. 1x Tris-HCl (pH 7.4) was prepared with its pH calibrated using a pH meter. Strep-Lucia (100 µg/ml, 37 kDa) and its coelenterazine-based luminescence assay reagent Quanti-Luc™ were obtained from InvivoGen. All reagents were reconstituted as recommended by the respective suppliers. DI H_2O with measured conductivity of 18.2 MΩ.cm was used throughout all experiments. Unless otherwise stated, all experiments were conducted at room temperature (20 ^{o}C).

4.3.3 Oligonucleotides sequences

All DNA and DNA-RNA chimeric oligonucleotides were synthesised by Integrated DNA Technologies, Inc. All oligonucleotides were reconstituted in DI H_2O and stored at -20 ^{o}C freezer as recommended by manufacturer and used without further purification. The concentrations of the oligonucleotides were measured using UV-Vis spectrophotometry prior to each usage. The oligonucleotides used in this chapter are as following:

Table 4.1. List of DNA and DNA-RNA chimeric strands used in this study. The cleavage site and stem loop motif were colour coded in grey and yellow, respectively. Other modifications were underlined with respective footnote annotations for ease of reading

Oligonucleotides	Sequence (5' – 3')
3S	ACT CAC TAT rAGG AAG AGA TGG A/3Cy3Sp/
5S	/5Cy3/ACT CAC TAT rAGG AAG AGA TGG A
0E	TCC ATC TCT TCT CCG AGC CGG TCG AAA TAG TGA GT/3Bio/
9E	TCC ATC TCT TCT CCG AGC CGG TCG AAA TAG TGA GT/iSp9//3Bio/
18E	TCC ATC TCT TCT CCG AGC CGG TCG AAA TAG TGA GT/iSp18//3Bio/
3TE	TCC ATC TCT TCT CCG AGC CGG TCG AAA TAG TGA GT TTT/3Bio/
6TE	TCC ATC TCT TCT CCG AGC CGG TCG AAA TAG TGA GT TTTTTT/3Bio/

[1]rA = adenosine RNA

[2]3Cy3Sp and 5Cy3 = Cy3 fluorophore labelling

[3]3bio = Biotin labelling

[4]iSp9 and iSp18 = triethylene and hexa-etheylene glycol derived carbon spacer

4.3.4 BRET assays

Both 8-17E and 8-17S were first heat treated at 95 °C for 5 min and slowly cooled to room temperature in an optimised molar ratio of E:S = 1:2. 100 µl of the resulting DNAzyme complex (hybridised 8-17E/S) was then mixed with 50 µl of buffer solution containing Zn^{2+} ions and subsequently incubated at room temperature for 30 min. After that, 50 µl of Strep-Lucia solution was added to conjugate with the biotinylated DNAzyme in an optimised molar ratio of DNAzyme:Strep-Lucia = 1:1. 50 µl of Quanti-Luc™ solution (containing coelenterazine) was added right before luminescence measurement to minimise signal degradation. The total volume of the final sample solution was 250 µl.

4.3.5 Optimisation of assay

The assay has been optimised for the following parameters prior to Zn^{2+} detection: (i) DNAzyme strands modifications, *i.e.* Cy3 position on 8-17S (i.e. 3S and 5S) and spacers on 8-17E (i.e. 0E, 9E, 18E, 3TE and 6TE); (ii) molar ratio of 8-17S and 8-17E; and (iii) molar ratio of DNAzyme:Strep-Lucia.

4.3.6 Evaluation of selectivity of zinc sensor

Various metal ions (Li^{+}, Na^{+}, K^{+}, Ba^{2+}, Ca^{2+}, Mg^{2+} and Pb^{2+}) were used to react with DNAzyme on top of Zn^{2+} ions and the resulting luminescence spectra were compared. The final concentration of DNAzyme, Strep-Lucia and metal ions were fixed at 10, 10 and 3000 nM, respectively for standardised comparison of BRET signals.

4.2.7 Evaluation of sensitivity of zinc sensor

DNAzyme complexes were prepared as above and the concentrations of DNAzyme and Strep-Lucia were set as 10 nM, respectively as optimised conditions. The BRET was monitored with increasing concentrations of Zn^{2+} ions (100, 200, 600, 1600, 2400, 3200, 5000, 10000, and 20000 nM) in final sample solution.

4.3.8 Data analysis

OriginPro v. 2018b was used to analyse the data. All luminescence spectra were smoothed using Savitzky–Golay filter with 10 points of window and subsequently normalised to their respective peak values for comparison purpose. All graphs were presented as mean with standard deviation at n = 3.

The measured luminescence spectra were then analysed for their respective BRET ratio by comparing the luminescence intensity at 480 and 560 nm using the formula shown in equation (4A). The obtained BRET ratio was then further analysed

for changes in BRET (Δ BRET in %) by comparing the BRET of the control (without Zn^{2+} ions) and that of sample (with Zn^{2+} ions), to represent BRET before and after reaction based on equation (4B).

BRET ratio = $\frac{L_{560}}{L_{480}}$ ..... (4A)

Changes in BRET (Δ BRET %) = $\frac{BRET_c - BRET_s}{BRET_c}$ x 100 ..... (4B)

Limit of Detection (LOD) = 3.3 x σ/S ..... (4C)

where L = Luminescence intensity (at either 480 or 560 nm)

$BRET_c$ = BRET ratio of control (before reaction)

$BRET_s$ = BRET ratio of sample (after reaction)

σ = standard deviation of blank solutions

S = slope of the calibration curve

4.4 Results and discussion

4.4.1 Verification of BRET

To confirm the occurrence of BRET between Strep-Lucia and Cy3 labelled on 8-17E and 8-17S strands, respectively, DNAzymes with only 8-17E, 8-17S or both were prepared to represent conditions before and after full DNAzyme assembly in the presence of Strep-Lucia. As shown in Figure 4.2, it is clear that BRET only occurred when both 8-17E and 8-17S were present and hybridised into a full DNAzyme complex. With only 8-17E, there was no BRET since no Cy3 was present to re-emit the luminescence. On the other hand, in the case of 8-17S alone, BRET cannot be achieved despite the presence of both Strep-Lucia and Cy3 fluorophore. This is due to the absence of biotinylated 8-17E to provide an attachment site for Strep-Lucia to be in close proximity with Cy3. Therefore, in both conditions, there was only one luminescence band observed at 480 nm, corresponding to sole emission of Strep-Lucia supplied with coelenterazine. However, when both 8-17E and 8-17S were present together with Strep-Lucia, a second luminescence band appeared at 560 nm, indicating the co-excitation of Cy3 due to BRET. The calculated melting temperature of full DNAzyme complex was 49.7 ^{o}C. Upon cleavage induced by 3200 nM final concentration of Zn^{2+}, each shorter binding arm will have its melting temperature reduced to 14.7 and 29.6 ^{o}C, respectively, effectively displacing the Cy3-labeled strand at room temperature (Figure 4.1). The now displaced Cy3 will not be able to undergo BRET with Strep-Lucia effectively, resulting in decreased emission at 560 nm.

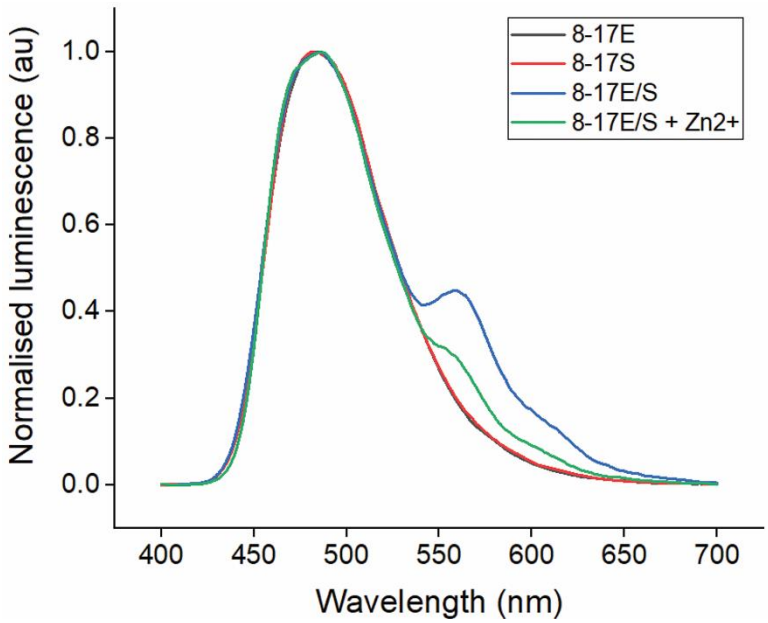

Figure 4.2. The luminescence spectra of samples containing DNAzyme formed by 8-17E, 8-17S or both with the final concentration of 10 nM. The spectra were smoothed and normalised to their respective maximum value for ease of comparison.

4.4.2 Optimisation of sensor conditions

After confirming the occurrence of BRET, the sensing parameters have to be optimised to maximise the sensor performance. The energy transfer efficiency via BRET is a multifactorial event that mainly influenced by the initial intermolecular distance between the BRET pair (*i.e.* Strep-Lucia on 8-17E and Cy3 on 8-17S), as well as the intrinsic emission of acceptor fluorophore (*i.e.* Cy3). Besides, since every 8-17E can only hybridise with a single 8-17S and conjugate with one Strep-Lucia, their hybridisation and conjugation efficiencies are pivotal for optimal BRET. These parameters were therefore optimised by studying the (1) strands modifications on 8-17E and 8-17S, respectively; (2) molar ratio of 8-17E and 8-17S during DNA hybridisation; as well as (3) molar ratio of Strep-Lucia and DNAzyme complex during conjugation step.

4.4.2.1 Strands modifications

As a general principle, the BRET efficiency is inversely proportional to the sixth power of distance between the BRET pair, with a commonly agreed working distance of no greater than 10 nm (Brown, Blumer and Hepler, 2015; Bajar *et al.*, 2016). Hence, alternating the relative position of Cy3 or introducing spacer between Cy3 and Strep-Lucia could increase the BRET efficiency. The effect of such modifications was evaluated by calculating and comparing their BRET ratios based on equation 4A. 3S and 5S were used to study the effect of Cy3 position on subsequent BRET, each representing Cy3 labelled at 3' and 5' ends individually. Samples containing 3S generally yielded weak to no BRET, which could be attributed to the intermolecular distance between the BRET pair. Note that an intact 8-17 DNAzyme without coordination with metal ions generally adapts a B-form conformation (Mazumdar *et al.*, 2009). Assuming a diameter of 0.34 nm per base pair in this form (Hatters *et al.*, 2001), the end to end diameter of the entire DNAzyme structure alone is predicted to be approximately 7.26 nm, based on a 22 base pair excluding the stem loop motif of 8-17E. With the inclusion of biotin at approximately 2 nm, the intermolecular distance between Cy3 at 3'-end and the Strep-Lucia is approximately ≥10 nm (Figure 4.1), leading to inefficient BRET. This concludes that Cy3 has to be located at 5'-end of the 8-17S strand.

However, streptavidin has been previously shown to quench Cy3 fluorescence in close proximity (Wang *et al.*, 2014). The quantum yield and fluorescence lifetime of Cy3 also determines how efficient this fluorophore can convert and re-emit the energy received from Strep-Lucia. For instance, after photoisomerization, a highly emissive *trans* Cy3 can return to ground state and turn into non-fluorescent *cis* isomer despite under continuous excitation (Levitus and

Ranjit, 2011). This *trans-cis* transition can be restricted by the microenvironment, mainly through steric interactions with nearby proteins as seen in protein induced fluorescence enhancement (PIFE) (Stennett *et al.*, 2015), or by strategically positioning of the fluorophore on dsDNA strand during DNA hybridisation (Morten *et al.*, 2018). A few modifications have been made by adding variation of spacers on 8-17E to elucidate how these could influence the subsequent BRET. There are two types of spacers with various lengths studied here, including polyethylene glycol (*i.e.* 9E and 18E) and poly(dT) (*i.e.* 3TE and 6TE) derivatives, each representing carbon-based and DNA-based spacers, with their numbers indicate the number of monomers. The polyethylene glycol-derived spacer is presumed to be inert on Cy3 emission or DNAzyme activity as it is essentially non-DNA and electrostatically neutral. As summarised in Figure 4.3, the combination of 0E5S showed highest BRET ratio compared to others. This indicates that the streptavidin moiety did not quench the Cy3 emission in this case. Introducing spacers on 8-17E, regardless of carbon or DNA derivatives, distances the BRET pair and reduces subsequent BRET efficiency, as demonstrated by their reduced BRET ratios. Interestingly, while incorporating poly(dT) spacers with different lengths led to similar BRET reduction, adding carbon spacers demonstrated gradual decrease in BRET efficiency as the polyethylene glycol doubled in length from 9 to 18 bases. The emission of Cy3 attached onto a DNA strand can also be altered by nearby nucleobases, for instance, its fluorescence is weaker when placing close to pyrimidine-rich sequence (Kretschy, Sack and Somoza, 2016). This implies that the effect of poly(dT) spacers on BRET might be due to the impact from its pyrimidine-based DNA rather than the spatial differences.

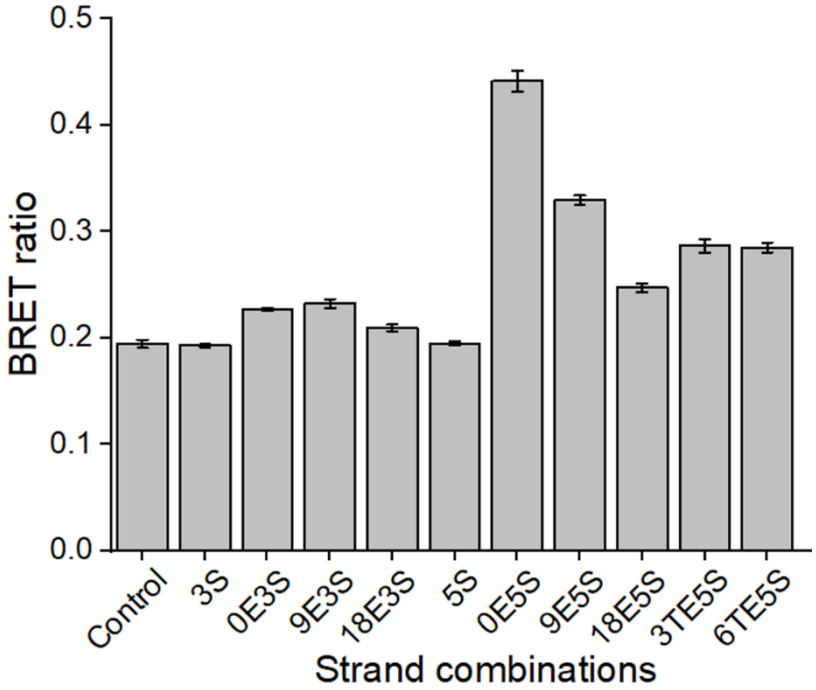

Figure 4.3. Averaged BRET ratio (n = 3) calculated based on equation 4A as a function of varying the combinations between spacers on 8-17E and Cy3 positions on 8-17S. Note that control in this study refers to Strep-Lucia samples without any DNAzyme strands.

4.4.2.2 Molar ratio of 8-17E:8-17S

Moving on, the sensor has also been optimised in terms of DNAzyme assembly (*i.e.* efficiency of DNA hybridisation) by altering the molar ratio between 8-17E and 8-17S. To enable controlled conjugation with Strep-Lucia in later stage, the molar ratio of the DNA strands was manipulated by changing the relative concentration of 8-17S under a fixed concentration of 8-17E at 10 nM. Since BRET only occurs when 8-17S and 8-17E strands are in close proximity, the resulting BRET ratio can be a direct indication on the efficiency of DNA strand hybridisation. Figure 4.4 shows the BRET ratios of 8-17E:8-17S prepared in various combination of molar ratios with 1:0 represents control samples without 8-17S at all. In general, as the amount of 8-17S increases, DNA hybridisation efficiency increases accordingly, with 8-17E:8-17S of the molar ratio 1:2 yields the best BRET ratio. Such stoichiometry with

higher amount of 8-17S could be due to the structural feature of a catalytic core motif in 8-17E that affects the hybridisation efficiency. Besides, modifications of Cy3 and biotin at each DNA strand may further contribute to the electro-steric hindrance that lowers the hybridisation efficiency. Assuming DNA molecules behave like particles with Brownian movement (Chan, Graves and McKenzie, 1995), higher amount of 8-17S increases its frequency of intermolecular collision with 8-17E strand, consequently improving rate of successful collisions and hybridisation efficiency. Nonetheless, there is no apparent improvement after increasing the relative concentration of 8-17S to 2 and above. This implies that the optimal DNAzyme hybridisation has already been achieved at the molar ratio of 8-17E:8-17S = 1:2.

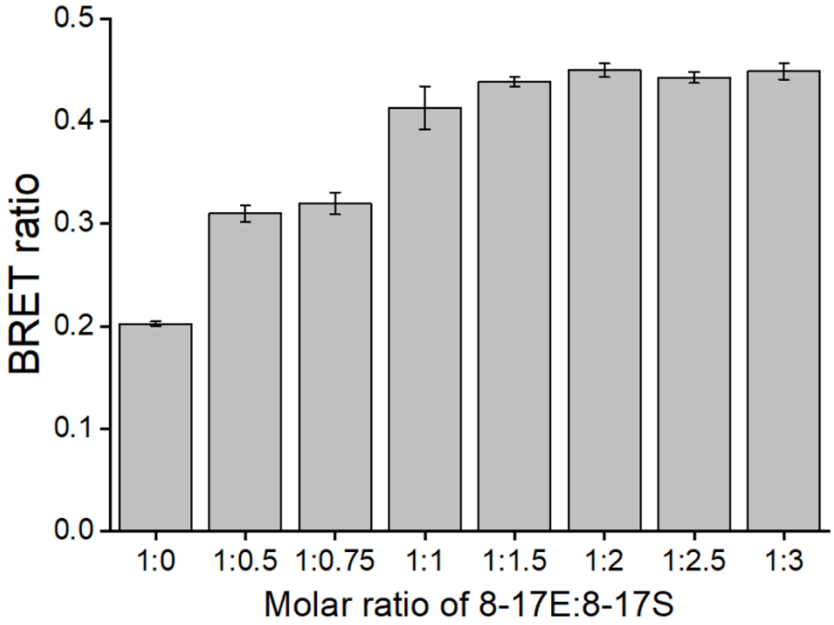

Figure 4.4. Averaged BRET ratio (n = 3) calculated based on equation 4A as a function of varying the molar ratio between 8-17E and 8-17S strands during DNA hybridisation.

4.4.2.3 Molar ratio of Strep-Lucia:DNAzyme complex

With the hybridisation of 8-17E:8-17S now optimised, the subsequent conjugation efficiency between the DNAzyme complex and Strep-Lucia was investigated. This is important as the BRET is highly dependent on the successful conjugation of Strep-Lucia with biotinylated 8-17E on DNAzyme complex. Noteworthily, the intrinsic streptavidin/biotin interaction has been reported with an exceptionally high association constant in the 10^{15} regime (González *et al.*, 1997). As there is no overhanging sequence on the DNAzyme complex, the presence of Cy3 might pose steric hindrance for optimal conjugation. Although this is somewhat negated by the observation from section 4.4.2.1 where effect of spacers was found non-beneficial. Note that the Strep-Lucia studied here has a reported molecular mass of 37 kDa (Ora *et al.*, 2016), suggesting a fusion protein comprised of a Lucia luciferase (23 kDa) and potentially a monomer subunit of streptavidin (14 kDa). To study the conjugation between Strep-Lucia bearing a monomeric streptavidin and the biotinylated 8-17E, a fixed amount of Strep-Lucia was incubated with different amount of DNAzyme complexes. As illustrated in Figure 4.5, there was a progressive albeit small increase in BRET ratio as the Strep-Lucia:DNAzyme complex increases from 1:0 to 1:1 molar ratio. The findings lead to two conclusions: (1) the streptavidin moiety of Strep-Lucia is indeed in monomeric form as the binding ratio between Strep-Lucia:DNAzyme complex was determined to be 1:1 and (2) its high affinity to bind with biotin is retained despite the co-expression of Lucia luciferase. Given such properties, the conjugation efficiency between Strep-Lucia and DNAzyme complex can thus achieve a near ideal 100 % since each Strep-Lucia can be conveniently conjugated with one DNAzyme complex individually as evidenced here.

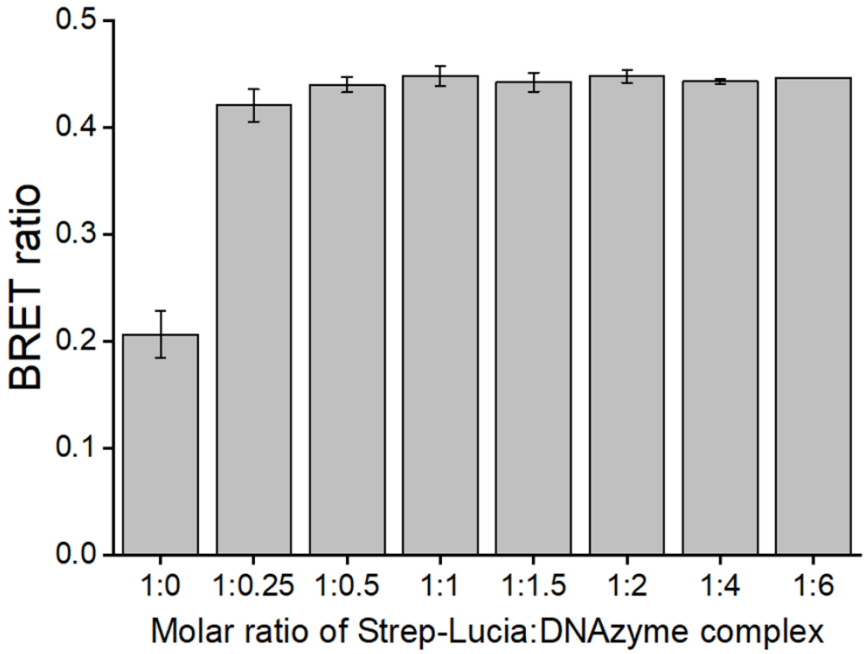

Figure 4.5. Averaged BRET ratio (n = 3) calculated based on equation 4A as a function of varying the molar ratio between Strep-Lucia and DNAzyme complex during conjugation.

4.4.3 Selectivity performance

Moving forward, in order to deploy the sensor for Zn^{2+} ions detection, its ability to identify this metal ion from others has to be first determined. The selectivity performance was evaluated by introducing the sensor to various metal ions at the same concentration, including both monovalent and divalent ions such as lithium (Li^{+}), sodium (Na^{+}), potassium (K^{+}), barium (Ba^{2+}), calcium (Ca^{2+}), magnesium (Mg^{2+}) and lead (Pb^{2+}) with the resulting activity analysed based on equation 4B. As summarised in Figure 4.6, only Zn^{2+} ions resulted the highest Δ BRET %, indicating their selective catalytic activity. Notably, the 8-17 DNAzyme is known to be catalytic not only when incubated with Zn^{2+}, but also with Pb^{2+} and Mg^{2+} ions. In fact, the affinity in activity of 8-17 DNAzyme with Pb^{2+} (K_d < 0.12 mM) is significantly lower as compared to that of Zn^{2+} (K_d = 1.15 mM) and Mg^{2+} (K_d = 53 mM), indicating the higher

affinity of the former to interact with 8-17 DNAzyme in driving the catalytic reaction (Kim *et al.*, 2007).

Contradictorily, the selectivity result observed here showed that there is no adverse interference from Pb^{2+}, possibly due to biotinylation or Strep-Lucia conjugation on the DNAzyme complex. Lu and co-workers (Kim *et al.*, 2007) have previously reported that the higher activity of Pb^{2+} could be due to its unique reaction route compared to the other two metal ions. While Zn^{2+} and Mg^{2+} ions were found to induce global folding configurational rearrangement on the DNAzyme prior to RNA transesterification, there was no Pb^{2+}-related global folding activity observed. This suggests that the Pb^{2+}-related activity of 8-17 DNAzyme might be hindered by the incorporation of BRET, such as the presence of Strep-Lucia. As Pb^{2+} is known to bind with a wide variety of biomolecules, especially low molecular weight and thiolate-rich proteins (Gonick, 2011; Cangelosi, Ruckthong and Pecoraro, 2017), the possibility of this metal ion getting sequestered and prevented from interacting with the DNAzyme complex cannot be ruled out. Nonetheless, the exact interactions of 8-17 DNAzyme with regards to Pb^{2+} ions are yet to be fully unveiled even to date. Based on the findings reported here, only the Pb^{2+}-containing sample exhibits a minimally enhanced BRET compared to control, resulting a negative Δ BRET % value. However, with regards to this study for Zn^{2+} detection, such small changes from Pb^{2+} can be considered to have negligible impact when compared to the value obtained from samples containing Zn^{2+} ions. Still, more thorough investigations are needed to provide substantial evidence on how BRET, as demonstrated here, could render the DNAzyme activity to be insensitive to Pb^{2+} ions.

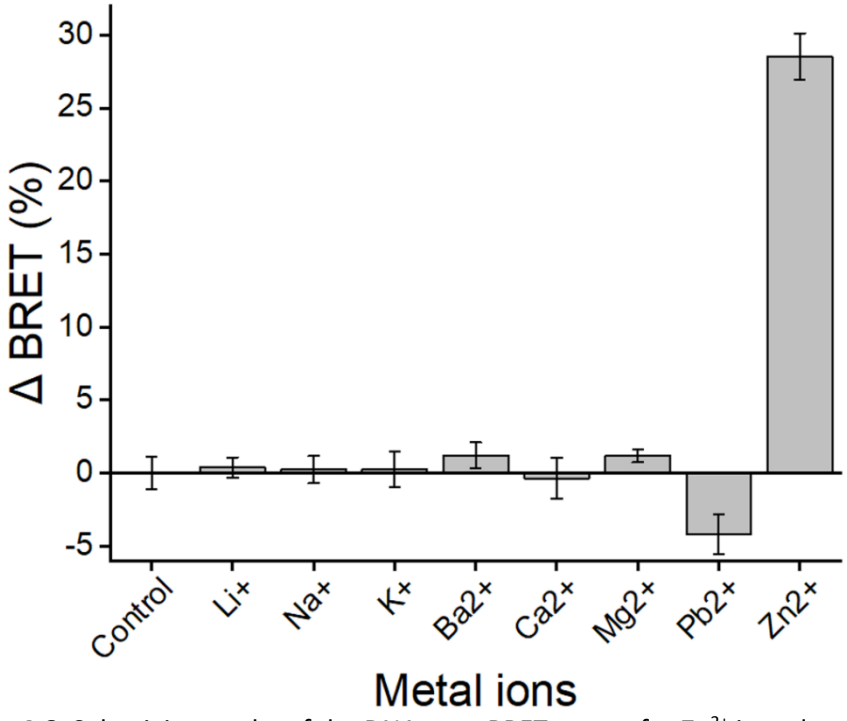

Figure 4.6. Selectivity results of the DNAzyme BRET sensor for Zn^{2+} ions detection against other metal ions. The metal ions were fixed at a final concentration of 3000 nM individually. The averaged Δ BRET (%) is calculated in relative to control (sample without metal ions) with n = 3 based on equation 4B.

4.4.4 Sensitivity performance

With the sensor demonstrated to be greatly selective, its performance in quantifying Zn^{2+} ion was then assessed. Figure 4.7 depicts the gradual changes in luminescence spectra and Δ BRET (%) value of Zn^{2+}-containing analyte samples calculated based on equation 4B. Using a final concentration of 10 nM DNAzyme, the sensor demonstrated good and reliable quantitative results by showing a gradual decrease in BRET (hence higher Δ BRET) with increasing final concentration of Zn^{2+} ions. With such small amount of probe, the linear range of detection was from 100 to 3200 nM of final Zn^{2+} ion concentration with 0.99 of R^2 value. Based on equation 4C, the LOD was calculated to be 62.58 nM. This achievement is indeed encouraging compared to other reported Zn^{2+}-related sensors, especially with regards to those derived from DNAzymes (Table 4.2).

Table 4.2. Comparison of the reported DNAzyme sensors for zinc ions detection

Reference	DNAzyme used	LOD	Detection range	Remarks
This work	8-17	62.58 nM	100 – 3200 nM	10 nM of DNAzyme complexes Reaction duration of 30 minutes No signal amplification
(Li *et al.*, 2000; Hwang *et al.*, 2014)	8-17	Not mentioned	Up to 500 µM	0.5 nM of DNAzyme complexes Used radioisotopes
(Li *et al.*, 2015)	8-17	0.47 nM	1 – 30 nM	Estimated 300 nM of DNAzyme complexes Used DNAzyme-functionalised citAuNPs
(Si *et al.*, 2018)	8-17	0.1 nM	0.25 – 2 nM	80 nM of DNAzyme complexes Signal amplified via hybridisation chain reaction
(Xu *et al.*, 2014)	9NL27	10 nM	50 nM – 50 µM	Signal amplified via PCR Long reaction duration of 4 hours

For instance, despite Lu group (Li *et al.*, 2000; Hwang *et al.*, 2014) reported a linear response to Zn^{2+} up to 500 µM with just 0.5 nM of putative hybridised 8-17 DNAzyme complexes, modification on the oligonucleotide strands with radioisotopes was required and the actual performance for Zn^{2+} ion quantification was not discussed in details. Similarly, an 8-17 DNAzyme-AuNPs nanoprobe based on AuNPs-induced fluorescence quenching reported by Tang and co-workers (Li *et al.*, 2015) showed a good linearity from 1 to 30 nM, with a detection limit of 0.47 nM for Zn^{2+} quantification. While the results are encouraging, a rather laborious procedure to prepare the DNAzyme-functionalised citAuNPs with an estimated final concentration

of 300 nM of active DNAzyme complexes were required. Later on, the group further proposed another 8-17 DNAzyme derived sensor in which a linear range of response had been observed from 0.25 to 2 nM with a detection limit of 0.1 nM using 80 nM of DNAzyme (Si *et al.*, 2018). They accomplished such achievement with signal amplification via hybridisation chain reaction that involves multiple hairpin DNAs and fluorophores labelling.

There was also another Zn^{2+} sensor comprised of 9NL27 (a different DNAzyme that has unprecedented specificity towards Zn^{2+} ions) (Chandra, Sachdeva and Silverman, 2009; Xiao, Allen and Silverman, 2011) reported by Xu and co-workers (Xu *et al.*, 2014) in which a dynamic range of detection was observed from 50 nM to 50 µM with LOD of 10 nM through PCR amplification. In their design, a typical reaction duration of 4 hours was required for proper cleavage of its substrate strand, as compared to 30 mins of reaction time achieved here. Such huge difference in cleavage duration might be a result of the different targeted cleavage site in which 9NL27 DNAzyme hydrolyses a DNA, instead of RNA substrate as seen in 8-17 DNAzyme.

From another perspective, compared to organic probes such as the phosphorescent zinc sensor (ZIrF) reported by Lippard group (You *et al.*, 2011) that could only quantify zinc up to 1 equivalent of the phosphorescent probe in a 1:1 stoichiometry ratio, the sensor hereby also demonstrated quantification of > 300 equivalent concentration of analytes. Considering there is no signal amplification or complicated reactions, the Zn^{2+} ion biosensor reported here shows very promising results, especially with the early implementation of BRET technique.

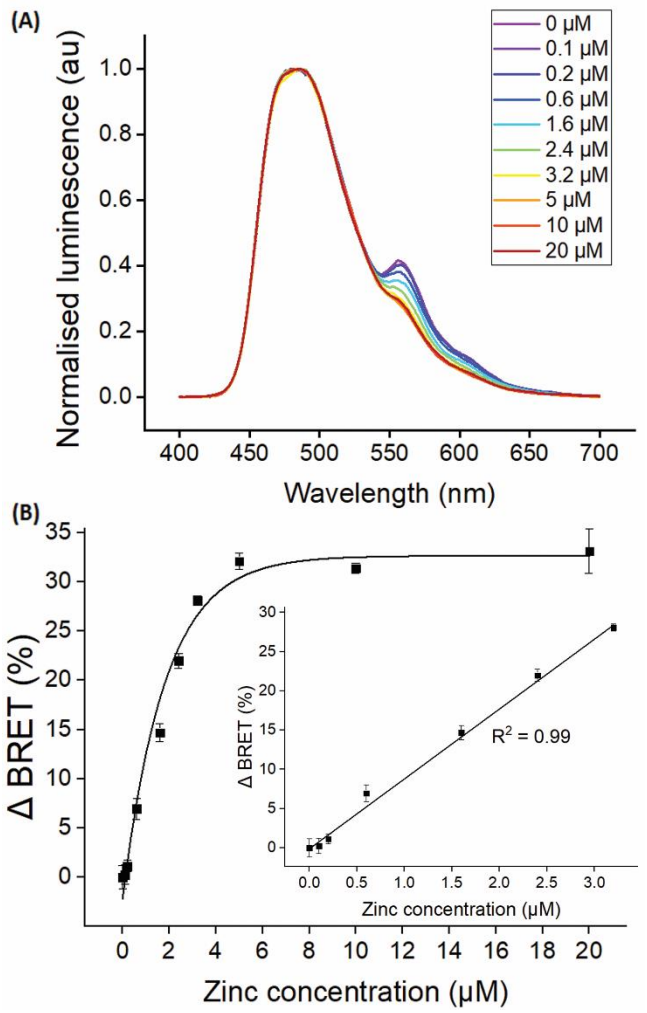

Figure 4.7. (A) The normalised luminescence spectra and **(B)** the averaged Δ BRET (%) with n = 3 calculated based on equation 4B of the DNAzyme BRET sensor in response to increasing concentration of Zn^{2+} ions. The concentration represents the final concentration of Zn^{2+} ions in the sample. The inset highlights the linear range from 100 to 3200 nM final concentration of Zn^{2+} ions.

4.5 Conclusion and future direction

In a nutshell, a DNAzyme-driven BRET-based sensor has been successfully designed based on the 8-17 DNAzyme by targeting Zn^{2+} ions as proof-of-concept study. The sensor utilises DNAzyme that catalyses RNA transesterification to cleave its substrate strand when the metal ion cofactor, Zn^{2+} ion is present. The consequent reduction in T_m leads to DNA dehybridisation as reflected by the drop in BRET efficiency due to increased intermolecular distance between the BRET pair of Cy3

fluorophore and Strep-Lucia luciferase. The changes in BRET ratio can thus be analysed to indicate the concentration of Zn^{2+} ions in a sample.

As for future direction, it should be beneficial to elucidate the interaction behind the observation in which the incorporation of BRET renders 8-17 DNAzyme insensitive to Pb^{2+} ions. To probe into this issue, possible approaches are to change the DNAzyme, bioluminescence protein, acceptor fluorophore or any combination of them. For example, instead of 8-17 DNAzyme, another Pb^{2+}-dependent DNAzymes such as the GR-5 DNAzyme (Breaker and Joyce, 1994) can be used. Such studies can therefore provide insights if the issue is an interference due to the Strep-Lucia luciferase, their complex formation with Cy3 or the 8-17 DNAzyme per se after being incorporated into BRET system. Moving forward, now that the sensor has been developed and evaluated for detection of Zn^{2+} in buffered solution, its potential for more sophisticated applications should be explored, such as *in vitro* and *in vivo* Zn^{2+} ion sensing. As a strong excitation light source is required to trigger the FRET, most fluorescence-derived *in vitro* and *in vivo* sensing suffers from a key limitation known as autofluorescence, the intrinsic fluorescence emitted by co-excited biological components (Cordina *et al.*, 2018) which can complicate the sensing reliability due to noisy background. The DNAzyme-driven BRET-based biosensor documented here is expected to avoid such limitation, given that the bioluminescence from a luciferase is much weaker compared to a commercialised laser. Although the BRET between Lucia luciferase and Cy3 fluorophore had been evidently proven to be compatible with 8-17 DNAzyme for zinc ion detection, further exploration into other DNAzyme-compatible BRET pairs should be advantageous. From the perspective of bioluminescence protein, Nanoluc luciferase has been previously reported in performing BRET with Cy3, showing a much higher BRET ratio than the Lucia-Cy3 BRET pair reported here (Engelen *et al.*, 2017). Other fluorophores such as TAMRA

could also be studied due to the fact that despite having similar excitation wavelength, TAMRA re-emit the fluorescence at slightly higher wavelength of 583 nm instead of 560 nm as for Cy3. If compatible with DNAzyme system, the resulting biosensor should have better screening resolution, thus improving the biosensor in terms of sensitivity performance. Furthermore, the sensing mechanism with BRET implementation studied here should be evaluated for generalisability in which other DNAzymes could be used for screening various targeted metal ions, such as sodium and uranyl ions which have their own dedicated DNAzymes being documented.

Lastly, this study presents the first demonstration of a metal ions detection biosensor derived from DNAzyme which exploits BRET phenomenon rather than conventional FRET with very promising selectivity and sensitivity performance.

CHAPTER 5

SUMMARY AND GENERAL CONCLUSION

The advantages of DNA nanotechnology for various forms of biosensing are well-reported but recent interest shifts towards exploring the unvisited mechanisms and bottlenecks that restrict their practical application. This is in conformity with the current research pursuit presented here, which aims to address the limitations by (1) incorporating cysAuNPs with non-modified DNA aptamer in rationally designing a colorimetric aptasensor for biomarker detection; and (2) implementing BRET technique into DNAzyme in developing a ratiometric metal ion biosensor.

Compared to other related studies, this thesis tried to tackle the issues from another perspective. Through the works presented here, the limitations associated with AuNPs functionalisation with DNA aptamer as well as FRET-dependent DNAzyme system had not only been addressed, but also presented an unexploited mode of detection and design of biosensor. Ultimately, the outcome from these studies should contribute to developing affordable, feasible and reliable biosensors for biomarkers and metal ions.

CHAPTER 6

FUTURE PROSPECTS

Nanotechnology has definitely presented a great opportunity for transformational work in numerous areas, particularly in the detection of biomarkers and metal ions as described in this thesis. Despite their huge improvement over the decades, their potential is yet to be fully disclosed. As for future prospect of the works presented here in this thesis, the following are noteworthy suggestions to some remaining aspects for investigation to further understand and widen their application horizon.

Regarding DNA aptamer and cysAuNPs, although UV-Vis spectroscopy appears to be a powerful tool in describing their interactions, more spectroscopic studies, such as surface-enhanced Raman spectroscopy and X-ray photoelectron spectroscopy, could be carried out to provide a more comprehensive understanding on their fundamental mode of interaction. Besides, both bare and citAuNPs have been previously studied for their electrochemistry properties, including but not limited to electrochemical impedance spectroscopy and voltammetry analysis (Callaghan *et al.*, 2010; Bonanni, Pumera and Miyahara, 2011). It would be beneficial to study the cysAuNPs and describe them from similar perspective to better understand how surface chemistry could contribute to their electrochemistry profile.

From another perspective, although DNAzymes are receiving more and more attention in recent year, their fundamental mode of action is still unclear. With the crystal structures of 8-17 DNAzyme being reported few years ago (Liu *et al.*, 2017), many forthcoming studies are expected. As the reports mostly concerned about 8-17 DNAzyme with regards to Pb^{2+} ions, it would be interesting if similar study can be performed highlighting Zn^{2+} ions since they have been previously documented to

have different reaction routes (Mazumdar *et al.*, 2009). This would also help to find out the underlying factor resulted in the BRET-based DNAzyme biosensor reported here to be irresponsive towards Pb^{2+} ions. Furthermore, as BRET has been proven to be a DNAzyme-compatible alternative for FRET, the prerequisite of bioluminescence protein might be a limiting factor for long term stability. For this, a fully DNA derived biosensor would be appreciated. Instead of having luciferase for bioluminescence, the widely applied G-quadruplex/hemin DNA nanostructure could be utilised for its peroxidase-mimicking activity that catalyse the chemiluminescent reaction of luminol in presence of hydrogen peroxide. By exploiting this as the luminescence energy source, a chemiluminescence resonance energy transfer (CRET) can be implemented for DNAzyme for a full DNA-based metal ion biosensor.

Regardless of upcoming studies, the prospective of DNA nanotechnology can be seen from the promising studies being reported from time to time. The future is hopeful, and the author is optimistic to see how impactful the related technologies can be to benefit human civilisation in general.

REFERENCES

Achenbach, J. *et al*. (2004) 'DNAzymes: from creation in vitro to application in vivo', *Current Pharmaceutical Biotechnology*, 5(4), pp. 321–336. doi: 10.2174/1389201043376751.

Aina, V. *et al*. (2010) 'Functionalization of sol gel bioactive glasses carrying Au nanoparticles: selective Au affinity for amino and thiol ligand groups', *Langmuir*, 26(24), pp. 18600–18605. doi: 10.1021/la1036647.

Al-Johani, H. *et al*. (2017) 'The structure and binding mode of citrate in the stabilization of gold nanoparticles', *Nature Chemistry*, 9(9), pp. 890–895. doi: 10.1038/nchem.2752.

Alizadeh, N. *et al*. (2018) 'Current advances in aptamer-assisted technologies for detecting bacterial and fungal toxins', *Journal of Applied Microbiology*, 124(3), pp. 644–651. doi: 10.1111/jam.13650.

Alkilany, A. M. *et al*. (2014) 'Colloidal stability of citrate and mercaptoacetic acid capped gold nanoparticles upon lyophilization: effect of capping ligand attachment and type of cryoprotectants', *Langmuir*, 30(46), pp. 13799–13808. doi: 10.1021/la504000v.

Amendola, V. *et al*. (2017) 'Surface plasmon resonance in gold nanoparticles: a review', *Journal of Physics: Condensed Matter*, 29(20), p. 203002. doi: 10.1088/1361-648X/aa60f3.

Aper, S. J. A., Dierickx, P. and Merkx, M. (2016) 'Dual readout BRET/FRET sensors for measuring intracellular zinc', *ACS Chemical Biology*, 11(10), pp. 2854–2864. doi: 10.1021/acschembio.6b00453.

Arts, R. *et al*. (2016) 'Detection of antibodies in blood plasma using bioluminescent sensor proteins and a smartphone', *Analytical Chemistry*, 88(8), pp. 4525–4532. doi: 10.1021/acs.analchem.6b00534.

Arvizo, R., Bhattacharya, R. and Mukherjee, P. (2010) 'Gold nanoparticles: opportunities and challenges in nanomedicine', *Expert Opinion on Drug Delivery*, 7(6), pp. 753–763. doi: 10.1517/17425241003777010.

Asadzadeh-Firouzabadi, A. and Zare, H. R. (2017) 'Application of cysteamine-capped gold nanoparticles for early detection of lung cancer-specific miRNA (miR-25) in human blood plasma', *Analytical Methods*, 9(25), pp. 3852–3861. doi: 10.1039/C7AY01098B.

Augustine, A. K., Nampoori, V. P. N. and Kailasnath, M. (2014) 'Rapid synthesize of gold nanoparticles by microwave irradiation method and its application as an optical limiting material', *Optik*, 125(22), pp. 6696–6699. doi: 10.1016/j.ijleo.2014.08.075.

Aung, K. M. M. *et al*. (2014) 'Studying forkhead box protein A1-DNA interaction and ligand inhibition using gold nanoparticles, electrophoretic mobility shift assay, and fluorescence anisotropy', *Analytical Biochemistry*, 448(1), pp. 95–104. doi: 10.1016/j.ab.2013.11.017.

Avino, A. *et al*. (2012) 'Thrombin binding aptamer, more than a simple aptamer: chemically modified derivatives and biomedical applications', *Current Pharmaceutical Design*, 18(14), pp. 2036–2047. doi: 10.2174/138161212799958387.

Aydin, S. (2015) 'A short history, principles, and types of ELISA, and our laboratory experience with peptide/protein analyses using ELISA', *Peptides*, 72, pp. 4–15. doi: 10.1016/j.peptides.2015.04.012.

Bajar, B. T. *et al*. (2016) 'A guide to fluorescent protein FRET pairs', *Sensors*, 16(9), pp. 1488. doi: 10.3390/s16091488.

Bene, L. and Damjanovich, L. (2019) 'Förster resonance energy transfer pioneers biomechanics: molecular-scale force meters for visualizing intracellular stress fields', *Cytometry A*, 95(8), pp. 819–822. doi: 10.1002/cyto.a.23780.

Berney, H. *et al*. (2000) 'A DNA diagnostic biosensor: development, characterisation and performance', *Sensors and Actuators B: Chemical*, 68(1), pp. 100–108. doi: 10.1016/S0925-4005(00)00468-8.

Bhumkar, D. R. *et al*. (2007) 'Chitosan reduced gold nanoparticles as novel carriers for transmucosal delivery of insulin', *Pharmaceutical Research*, 24(8), pp. 1415–1426. doi: 10.1007/s11095-007-9257-9.

Bi, S. *et al*. (2015) 'A hot-spot-active magnetic graphene oxide substrate for microRNA detection based on cascaded chemiluminescence resonance energy transfer', *Nanoscale*, 7(8), pp. 3745–3753. doi: 10.1039/C4NR06603K.

Bishop, K. J. M. *et al*. (2009) 'Nanoscale forces and their uses in self-assembly', *Small*, 5(14), pp. 1600–1630. doi: 10.1002/smll.200900358.

Blake, C. C. F. *et al*. (1965) 'Structure of hen egg-white lysozyme: a three-dimensional fourier synthesis at 2 Å resolution', *Nature*, 206(4986), pp. 757–761. doi: 10.1038/206757a0.

Bonanni, A., Pumera, M. and Miyahara, Y. (2011) 'Influence of gold nanoparticle size (2-50 nm) upon its electrochemical behavior: an electrochemical impedance spectroscopic and voltammetric study', *Physical Chemistry Chemical Physics*, 13(11), pp. 4980–4986. doi: 10.1039/c0cp01209b.

Bock, L. C. *et al.* (1992) 'Selection of single-stranded DNA molecules that bind and inhibit human thrombin', *Nature*, 355(6360), pp. 564–566. doi: 10.1038/355564a0.

Breaker, R. R. and Joyce, G. F. (1994) 'A DNA enzyme that cleaves RNA', *Chemistry & Biology*, 1(4), pp. 223–229. doi: 10.1016/1074-5521(94)90014-0.

Brewer, S. H. *et al*. (2005) 'Probing BSA binding to citrate-coated gold nanoparticles and surfaces', *Langmuir*, 21(20), pp. 9303–9307. doi: 10.1021/la050588t.

Bruesehoff P. J. *et al*. (2012) 'Improving metal ion specificity during in vitro selection of catalytic DNA', *Combinatorial Chemistry & High Throughput Screening*, 5(4), pp. 327–335. doi: 10.2174/1386207023330264.

Brown, N. E., Blumer, J. B. and Hepler, J. R. (2015) 'Bioluminescence resonance energy transfer to detect protein-protein interactions in live cells', *Protein-Protein Interactions*, pp. 457–465. doi: 10.1007/978-1-4939-2425-7_30.

Brust, M. *et al*. (1994) 'Synthesis of thiol-derivatised gold nanoparticles in a two-phase liquid-liquid system', *Journal of the Chemical Society, Chemical Communications*, 0(7), pp. 801–802. doi: 10.1039/C39940000801.

Brust, M. *et al*. (1995) 'Synthesis and reactions of functionalised gold nanoparticles', *Journal of the Chemical Society, Chemical Communications*, 16(16), pp. 1655–1656. doi: 10.1039/C39950001655.

Bülbül, G. *et al*. (2018) 'DNA assay based on nanoceria as fluorescence quenchers (NanoCeracQ DNA assay)', *Scientific Reports*, 8(2426), pp. 1–9. doi: 10.1038/s41598-018-20659-9.

Burdette, S. C. *et al*. (2001) 'Fluorescent sensors for Zn^{2+} based on a fluorescein platform: synthesis, properties and intracellular distribution', *Journal of the American Chemical Society*, 123(32), pp. 7831–7841. doi: 10.1021/ja010059l.

Burdette, S. C. *et al*. (2003) 'ZP4, an improved neuronal Zn^{2+} sensor of the Zinpyr family', *Journal of the American Chemical Society*, 125(7), pp. 1778–1787. doi: 10.1021/ja0287377.

Cai, Y. D. and Chou, K. C. (2005) 'Using functional domain composition to predict enzyme family classes', *Journal of Proteome Research*, 4(1), pp. 109–111. doi: 10.1021/pr049835p.

Callaghan, M. F. *et al*. (2010) 'An investigation of the impedance properties of gold nanoparticles', *Journal of Physics: Conference Series*, 224(1), pp. 1–5. doi: 10.1088/1742-6596/224/1/012058.

Cammann, K. (1977) 'Bio-sensors based on ion-selective electrodes', *Fresenius' Zeitschrift für analytische Chemie*, 287(1), pp. 1–9. doi: 10.1007/BF00539519.

Cangelosi, V., Ruckthong, L. and Pecoraro, V. L. (2017) 'Lead(II) binding in natural and artificial proteins', in Sigel, A., Sigel, H., and Sigel, R. K. O. (eds.) *Lead – Its Effects on Environment and Health*. Berlin, De Gruyter, pp. 271–317. doi: 10.1515/9783110434330-010.

Cao, R. and Li, B. (2011) 'A simple and sensitive method for visual detection of heparin using positively-charged gold nanoparticles as colorimetric probes', *Chemical Communications*, 47(10), p. 2865. doi: 10.1039/c0cc05094f.

Cardoso Avila, P. E. *et al*. (2017) 'Biological response of HeLa cells to gold nanoparticles coated with organic molecules', *Toxicology in Vitro*, 42(February), pp. 114–122. doi: 10.1016/j.tiv.2017.04.013.

Carter, K. P., Young, A. M. and Palmer, A. E. (2014) 'Fluorescent sensors for measuring metal ions in living systems', *Chemical Reviews*, 114(8), pp. 4564–4601. doi: 10.1021/cr400546e.

Cassandri, M. *et al*. (2017) 'Zinc-finger proteins in health and disease', *Cell Death Discovery*, 3(1), p. 17071. doi: 10.1038/cddiscovery.2017.71.

Catuogno, S. and Esposito, C. L. (2017) 'Aptamer cell-based selection: overview and advances', *Biomedicines*, 5(3). doi: 10.3390/biomedicines5030049.

Cepeda-Plaza, M., McGhee, C. E. and Lu, Y. (2018) 'Evidence of a general acid-base catalysis mechanism in the 8-17 DNAzyme', *Biochemistry*, 57(9), pp. 1517–1522. doi: 10.1021/acs.biochem.7b01096.

Chakraborty, S. *et al*. (2011) 'Contrasting effect of gold nanoparticles and nanorods with different surface modifications on the structure and activity of bovine serum albumin', *Langmuir*, 27(12), pp. 7722–7731. doi: 10.1021/la200787t.

Chan, V., Graves, D. J. and McKenzie, S. E. (1995) 'The biophysics of DNA hybridization with immobilized oligonucleotide probes', *Biophysical Journal*, 69(6), pp. 2243–2255. doi: 10.1016/S0006-3495(95)80095-0.

Chandra, M., Sachdeva, A. and Silverman, S. K. (2009) 'DNA-catalyzed sequence-specific hydrolysis of DNA', *Nature Chemical Biology*, 5(10), pp. 718–720. doi: 10.1038/nchembio.201.

Chang, C. C. *et al*. (2019) 'Gold nanoparticle-based colorimetric strategies for chemical and biological sensing applications', *Nanomaterials*, 9(6), pp. 1–24. doi: 10.3390/nano9060861.

Chen, C., Sun, X. M. and Li, B. H. (2011) 'Adsorption of waste beer yeast modified with Cibacron Blue F-3GA for lysozyme', *Chinese Journal of Analytical Chemistry*, 39(1), pp. 91–94. doi: 10.1016/S1872-2040(10)60410-0.

Chen, X. *et al*. (1998) 'DNA optical sensor: a rapid method for the detection of DNA hybridization', *Biosensors and Bioelectronics*, 13(3–4), pp. 451–458. doi: 10.1016/S0956-5663(97)00095-X.

Chen, Y. M. *et al*. (2008) 'Colorimetric detection of lysozyme based on electrostatic interaction with human serum albumin-modified gold nanoparticles', *Langmuir*, 24(7), pp. 3654–3660. doi: 10.1021/la7034642.

Chen, Y. *et al*. (2007) 'Characterization of spectral FRET imaging microscopy for monitoring nuclear protein interactions.', *Journal of Microscopy*, 228(2), pp. 139–52. doi: 10.1111/j.1365-2818.2007.01838.x.

Chen, Y. *et al*. (2017) 'Double-enzymes-mediated bioluminescent sensor for quantitative and ultrasensitive point-of-care testing', *Analytical Chemistry*, 89(10), pp. 5422–5427. doi: 10.1021/acs.analchem.7b00239.

Chen, Z. *et al*. (2011) 'Electrochemical impedance spectroscopy detection of lysozyme based on electrodeposited gold nanoparticles', *Talanta*, 83(5), pp. 1501–1506. doi: 10.1016/j.talanta.2010.11.042.

Chen, Z. *et al*. (2013) 'Detection of vascular endothelial growth factor based on gold nanoparticles and immunoreaction using resonance light scattering', *Plasmonics*, 8(2), pp. 605–611. doi: 10.1007/s11468-012-9442-5.

Chen, Z. B. *et al*. (2013) 'Colorimetric detection of potassium ions using aptamer-functionalized gold nanoparticles', *Analytica Chimica Acta*, 787, pp. 189–192. doi: 10.1016/j.aca.2013.05.020.

Cheng, A. K. H., Ge, B. and Yu, H.-Z. (2007) 'Aptamer-based biosensors for label-free voltammetric detection of lysozyme', *Analytical Chemistry*, 79(14), pp. 5158–5164. doi: 10.1021/ac062214q.

Clogston, J. D. and Patri, A. K. (2011) 'Zeta potential measurement.', in Methods in molecular biology (Clifton, N.J.), pp. 63–70. doi: 10.1016/b978-0-12-814182-3.00014-6.

Contreras-Trigo, B. *et al*. (2018) 'Slight pH fluctuations in the gold nanoparticle synthesis process influence the performance of the citrate reduction method', *Sensors*, 18(7), p. 2246. doi: 10.3390/s18072246.

Cordina, N. M. *et al*. (2018) 'Reduced background autofluorescence for cell imaging using nanodiamonds and lanthanide chelates', *Scientific Reports*, 8(1), pp. 1–14. doi: 10.1038/s41598-018-22702-1.

Costello, L. C. and Franklin, R. B. (1998) 'Novel role of zinc in the regulation of prostate citrate metabolism and its implications in prostate cancer', *The Prostate*, 35(4), pp. 285–296. doi: 10.1002/(SICI)1097-0045(19980601)35:4<285::AID-PROS8>3.0.CO;2-F.

Coté, G. L., Lec, R. M. and Pishko, M. V. (2003) 'Emerging biomedical sensing technologies and their applications', *IEEE Sensors Journal*, 3(3), pp. 251–266. doi: 10.1109/JSEN.2003.814656.

Cox, J. C. and Ellington, A. D. (2001) 'Automated selection of anti-protein aptamers', *Bioorganic and Medicinal Chemistry*, 9(10), pp. 2525–2531. doi: 10.1016/S0968-0896(01)00028-1.

Cuajungco, M. P. and Lees, G. J. (1997) 'Zinc metabolism in the brain: Relevance to human neurodegenerative disorders', *Neurobiology of Disease*, 4(3–4), pp. 137–169. doi: 10.1006/nbdi.1997.0163.

Cuenoud, B. and Szostak, J. W. (1995) 'A DNA metalloenzyme with DNA ligase activity', *Nature*, 375(6532), pp. 611–614. doi: 10.1038/375611a0.

Daghestani, H. N. and Day, B. W. (2010) 'Theory and applications of surface plasmon resonance, resonant mirror, resonant waveguide grating, and dual polarization interferometry biosensors', *Sensors*, 10(11), pp. 9630–9646. doi: 10.3390/s101109630.

Daniel, M. C. and Astruc, D. (2004) 'Gold nanoparticles: assembly, supramolecular chemistry, quantum-size-related properties, and applications toward biology, catalysis, and nanotechnology', *Chemical Reviews*, 104(1), pp. 293–346. doi: 10.1021/cr030698+.

Deng, B. *et al*. (2014) 'Aptamer binding assays for proteins: the thrombin example—a review', *Analytica Chimica Acta*, 837, pp. 1–15. doi: 10.1016/j.aca.2014.04.055.

Dhumale, V. A. *et al*. (2012) 'Reversible aggregation control of polyvinylpyrrolidone capped gold nanoparticles as a function of pH', *Materials Express*, 2(4), pp. 311–318. doi: 10.1166/mex.2012.1082.

de Lima, R., Seabra, A. B. and Durán, N. (2012) 'Silver nanoparticles: a brief review of cytotoxicity and genotoxicity of chemically and biogenically synthesized nanoparticles', *Journal of Applied Toxicology*, 32(11), pp. 867–879. doi: 10.1002/jat.2780.

Dirks, R. M. and Pierce, N. A. (2004) 'Triggered amplification by hybridization chain reaction', *Proceedings of the National Academy of Sciences of the United States of America*, 101(43), pp. 15275–15278. doi: 10.1073/pnas.0407024101.

Doane, T. L. *et al*. (2012) 'Nanoparticle ζ -potentials', *Accounts of Chemical Research*, 45(3), pp. 317–326. doi: 10.1021/ar200113c.

Donkers, R. L., Lee, D. and Murray, R. W. (2004) 'Synthesis and isolation of the molecule-like cluster Au38(PhCH2CH2S)24', *Langmuir*, 20(5), pp. 1945–1952. doi: 10.1021/la035706w.

Dykman, L. A. and Khlebtsov, N. G. (2011) 'Gold nanoparticles in biology and medicine: recent advances and prospects.', *Acta naturae*, 3(2), pp. 34–55. doi: 10.32607/20758251-2011-3-2-34-55.

Elci, S. G. *et al*. (2016) 'Surface charge controls the suborgan biodistributions of gold nanoparticles', *ACS Nano*, 10(5), pp. 5536–5542. doi: 10.1021/acsnano.6b02086.

Elghanian, R. *et al*. (1997) 'Selective colorimetric detection of polynucleotides based on the distance-dependent optical properties of gold nanoparticles', *Science*, 277(5329), pp. 1078–1081. doi: 10.1126/science.277.5329.1078.

Elia, P. *et al*. (2014) 'Green synthesis of gold nanoparticles using plant extracts as reducing agents', *International Journal of Nanomedicine*, pp. 4007–4021. doi: 10.2147/IJN.S57343.

Ellington, A. D. and Szostak, J. W. (1990) 'In vitro selection of RNA molecules that bind specific ligands', *Nature*, 346(6287), pp. 818–822. doi: 10.1038/346818a0.

Engelen, W. *et al*. (2017) 'Nucleic acid detection using BRET-beacons based on bioluminescent protein-DNA hybrids', *Chemical Communications*, 53(19), pp. 2862–2865. doi: 10.1039/c6cc10032e.

Erk, C. *et al*. (2012) 'Formation of gold nanoparticles in polymeric nanowires by low-temperature thermolysis of gold mesitylene', *Journal of Materials Chemistry*, 22(2), pp. 684–690. doi: 10.1039/c1jm14193g.

Evanko, D. (2004) 'Hybridization chain reaction', *Nature Methods*, 1(3), pp. 186–186. doi: 10.1038/nmeth1204-186a.

Faraday, M. (1857) ‘X. The bakerian lecture: experimental relations of gold (and other metals) to light’, *Philosophical Transactions of the Royal Society of London*, 147(0), pp. 145–181. doi: 10.1098/rstl.1857.0011.

Faulhammer, D. and Famulok, M. (1996) ‘The Ca^{2+} Ion as a cofactor for a novel RNA-cleaving deoxyribozyme’, *Angewandte Chemie*, 35(2324), pp. 2837–2841. doi: 10.1002/anie.199628371.

Feng, M. *et al*. (2019) ‘Enhancing catalytic activity of uranyl-dependent DNAzyme by flexible linker insertion for more sensitive detection of uranyl ion’, *Analytical Chemistry*, 91, pp. 6608–6615. doi: 10.1021/acs.analchem.9b00490.

Flynn-Charlebois, A. *et al*. (2003) ‘Deoxyribozymes with 2‘–5‘ RNA ligase activity’, *Journal of the American Chemical Society*, 125(9), pp. 2444–2454. doi: 10.1021/ja028774y.

Förster, T. (1946) ‘Energiewanderung und fluoreszenz’, *Die Naturwissenschaften*, 33(6), pp. 166–175. doi: 10.1007/BF00585226.

Förster, T. (1948) ‘Zwischenmolekulare energiewanderung und fluoreszenz’, *Annalen der Physik*, 437(1–2), pp. 55–75. doi: 10.1002/andp.19484370105.

Frederickson, C. J. *et al*. (2000) ‘Importance of zinc in the central nervous system: the zinc-containing neuron’, *The Journal of Nutrition*, 130(5), pp. 1471S-1483S. doi: 10.1093/jn/130.5.1471S.

Freeman, R., Liu, X. and Willner, I. (2011) ‘Chemiluminescent and chemiluminescence resonance energy transfer (CRET) detection of DNA, metal ions, and aptamer-substrate complexes using hemin/G-quadruplexes and CdSe/ZnS quantum dots’, *Journal of the American Chemical Society*, 133(30), pp. 11597–11604. doi: 10.1021/ja202639m.

Frens, G. (1973) 'Controlled nucleation for the regulation of the particle size in monodisperse gold suspensions', *Nature Physical Science*, 241(105), pp. 20–22. doi: 10.1038/physci241020a0.

Gabor, F. (2011) 'Characterization of nanoparticles intended for drug delivery', *Scientia Pharmaceutica*, 79(3), pp. 701–702. doi: 10.3797/scipharm.br-11-01.

Gao, F. *et al*. (2011) 'A DNA hybridization detection based on fluorescence resonance energy transfer between dye-doped core-shell silica nanoparticles and gold nanoparticles', *Analyst*, 136(19), pp. 3973–3980. doi: 10.1039/c1an15287d.

Ghosh, D. and Chattopadhyay, N. (2013) 'Gold nanoparticles: acceptors for efficient energy transfer from the photoexcited fluorophores', *Optics and Photonics Journal*, 3(1), pp. 18–26. doi: 10.4236/opj.2013.31004.

Gold, L. and Tuerk, C. (1990) 'Systematic evolution of ligands by exponential enrichment: RNA ligands to bacteriophage T4 DNA polymerase', *Science*, 249(4968), pp. 505–510. doi: 10.1126/science.2200121.

Goldblum, R. M. *et al*. (1982) 'Human milk banking. II. relative stability of immunologic factors in stored colostrum, *Acta Paediatrica*, 71(1), pp. 143–144. doi: 10.1111/j.1651-2227.1982.tb09387.x.

Goldburg, W. I. (1999) 'Dynamic light scattering', *American Journal of Physics*, pp. 1152–1160. doi: 10.1119/1.19101.

Gonick, H. C. (2011) 'Lead-binding proteins: a review', *Journal of Toxicology*, 2011, pp. 1–10. doi: 10.1155/2011/686050.

González, M. *et al*. (1997) 'Interaction of biotin with streptavidin. Thermostability and conformational changes upon binding', *Journal of Biological Chemistry*, 272(17), pp. 11288–11294. doi: 10.1074/jbc.272.17.11288.

Gorbenko, G. P., Ioffe, V. M. and Kinnunen, P. K. J. (2007) 'Binding of lysozyme to phospholipid bilayers: evidence for protein aggregation upon membrane association', *Biophysical Journal*, 93(1), pp. 140–153. doi: 10.1529/biophysj.106.102749.

Grabrucker, A. M., Rowan, M. and Garner, C. C. (2011) 'Brain-delivery of zinc-ions as potential treatment for neurological diseases: mini review.', *Drug delivery letters*, 1(1), pp. 13–23. doi: 10.2174/2210303111101010013.

Grimpe, B. (2011) 'Deoxyribozymes: new therapeutics to treat central nervous system disorders', *Frontiers in Molecular Neuroscience*, 4(September), pp. 1–5. doi: 10.3389/fnmol.2011.00025.

Gu, Y. *et al*. (2018) 'Quantification of DNA by a thermal-durable biosensor modified with conductive poly(3,4-ethylenedioxythiophene)', *Sensors*, 18(11). doi: 10.3390/s18113684.

Gür, F. N. *et al*. (2016) 'Toward self-assembled plasmonic devices: high-yield arrangement of gold nanoparticles on DNA origami templates', *ACS Nano*, 10(5), pp. 5374–5382. doi: 10.1021/acsnano.6b01537.

Haguenau, F. *et al*. (2003) 'Key events in the history of electron microscopy', *Microscopy and Microanalysis*, 9(2), pp. 96–138. doi: 10.1017/S1431927603030113.

Han, T. H. *et al*. (2013) 'Synthesis of positively charged gold nanoparticles using a stainless-steel mesh', *Journal of Nanoscience and Nanotechnology*, pp. 6140–6144. doi: 10.1166/jnn.2013.7660.

Han, T. H. *et al*. (2014) 'Optimization of positively charged gold nanoparticles synthesized using a stainless-steel mesh and its application for colorimetric hydrogen

peroxide detection', *Journal of Industrial and Engineering Chemistry*, 20(4), pp. 2003–2009. doi: 10.1016/j.jiec.2013.09.023.

Hatters, D. M. *et al*. (2001) 'Sedimentation analysis of novel DNA structures formed by homo-oligonucleotides', *Biophysical Journal*, 81(1), pp. 371–381. doi: 10.1016/S0006-3495(01)75706-2.

Helmfors, L. *et al*. (2015) 'Protective properties of lysozyme on β-amyloid pathology: implications for Alzheimer disease', *Neurobiology of Disease*, 83, pp. 122–133. doi: 10.1016/j.nbd.2015.08.024.

Henglein, A. and Meisel, D. (1998) 'Radiolytic control of the size of colloidal gold nanoparticles', *Langmuir*, 14(26), pp. 7392–7396. doi: 10.1021/la981278w.

Heo, J. H. *et al*. (2015) 'Ultrastable-stealth large gold nanoparticles with DNA directed biological functionality', *Langmuir*, 31(51), pp. 13773–13782. doi: 10.1021/acs.langmuir.5b03534.

Hirn, S. *et al*. (2011) 'Particle size-dependent and surface charge-dependent biodistribution of gold nanoparticles after intravenous administration', *European Journal of Pharmaceutics and Biopharmaceutics*, 77(3), pp. 407–416. doi: 10.1016/j.ejpb.2010.12.029.

Hollenstein, M. (2015) 'DNA catalysis: the chemical repertoire of DNAzymes', *Molecules*, 20(11), pp. 20777–20804. doi: 10.3390/molecules201119730.

Hostetler, M. J. *et al*. (1996) 'Monolayers in three dimensions: synthesis and electrochemistry of ω-functionalized alkanethiolate-stabilized gold cluster compounds', *Journal of the American Chemical Society*, 118(17), pp. 4212–4213. doi: 10.1021/ja960198g.

Hostetler, M. J., Templeton, A. C. and Murray, R. W. (1999) 'Dynamics of place-exchange reactions on monolayer-protected gold cluster molecules', *Langmuir*, 15(11), pp. 3782–3789. doi: 10.1021/la981598f.

Huang, J. *et al*. (2016) 'Fluorescence resonance energy transfer-based hybridization chain reaction for: in situ visualization of tumor-related mRNA', *Chemical Science*, 7(6), pp. 3829–3835. doi: 10.1039/c6sc00377j.

Huang, X. *et al*. (2006) 'A resonance energy transfer between chemiluminescent donors and luminescent quantum-dots as acceptors (CRET)', *Angewandte Chemie*, 45(31), pp. 5140–5143. doi: 10.1002/anie.200601196.

Huang, Y. *et al*. (2012) 'An amplified chemiluminescence aptasensor based on bi-resonance energy transfer on gold nanoparticles and exonuclease III-catalyzed target recycling', *Chemical Communications*, 48(97), pp. 11877–11879. doi: 10.1039/c2cc37130h.

Hussain, S. A. (2009) 'An introduction to fluorescence resonance energy transfer (FRET)', *Current Protocols in Cytometry*, 38(1). Available at: http://arxiv.org/abs/0908.1815.

Hwang, K. *et al*. (2014) 'Photocaged DNAzymes as a general method for sensing metal ions in living cells', *Angewandte Chemie*, 53(50), pp. 13798–13802. doi: 10.1002/anie.201408333.

Inoue, K. *et al*. (2002) 'Osteopenia and male-specific sudden cardiac death in mice lacking a zinc transporter gene, Znt5.', *Human Molecular Genetics*, 11(15), pp. 1775–84. doi: 10.1093/hmg/11.15.1775.

Itoh, H. *et al*. (2004) 'Photochemical assembly of gold nanoparticles utilizing the photodimerization of thymine', *Langmuir*, 20(5), pp. 1972–1976. doi: 10.1021/la0359777.

Jain, S., Hirst, D. G. and O'Sullivan, J. M. (2012) 'Gold nanoparticles as novel agents for cancer therapy', *The British Journal of Radiology*, 85(1010), pp. 101–113. doi: 10.1259/bjr/59448833.

Jayasena, S. D. (1999) 'Aptamers: an emerging class of molecules that rival antibodies in diagnostics', *Clinical Chemistry*, 45(9), pp. 1628–1650. Available at: http://www.ncbi.nlm.nih.gov/pubmed/10471678.

Jones, G. A. and Bradshaw, D. S. (2019) 'Resonance energy transfer: from fundamental theory to recent applications', *Frontiers in Physics*, 7(July), pp. 1–19. doi: 10.3389/fphy.2019.00100.

Kang, J. *et al*. (2016) 'A rapid colorimetric sensor of clenbuterol based on cysteamine-modified gold nanoparticles', *ACS Applied Materials & Interfaces*, 8(1), pp. 1–5. doi: 10.1021/acsami.5b09079.

Kavita, V. (2017) 'DNA biosensors-a review', *Journal of Bioengineering & Biomedical Science*, 07(02). doi: 10.4172/2155-9538.1000222.

Ke, Y., Castro, C. and Choi, J. H. (2018) 'Structural DNA nanotechnology: artificial nanostructures for biomedical research', *Annual Review of Biomedical Engineering*, 20(1), pp. 375–401. doi: 10.1146/annurev-bioeng-062117-120904.

Khandelwal, G. and Bhyravabhotla, J. (2010) 'A phenomenological model for predicting melting temperatures of dna sequences', *PLoS ONE*, 5(8), pp. 1–9. doi: 10.1371/journal.pone.0012433.

Kim, H.K. *et al*. (2007) 'Metal-dependent global folding and activity of the 8-17 DNAzyme studied by fluorescence resonance energy transfer', *Journal of the American Chemical Society*, 129(21), pp. 6896–6902. doi: 10.1021/ja0712625.

Kim, J. W. *et al*. (2009) 'An operationally simple colorimetric assay of hyaluronidase activity using cationic gold nanoparticles', *Analyst*, 134(7), pp. 1291–1293. doi: 10.1039/b822917a.

Kimling, J. *et al*. (2006) 'Turkevich method for gold nanoparticle synthesis revisited', *Journal of Physical Chemistry B*, 110(32), pp. 15700–15707. doi: 10.1021/jp061667w.

King, J. C., Shames, D. M. and Woodhouse, L. R. (2000) 'Zinc homeostasis in humans', *The Journal of Nutrition*, 130(5), pp. 1360S-1366S. doi: 10.1093/jn/130.5.1360S.

Kirby, R. *et al*. (2004) 'Aptamer-based sensor arrays for the detection and quantitation of proteins', *Analytical Chemistry*, 76(14), pp. 4066–4075. doi: 10.1021/ac049858n.

Kołodziejczak-Radzimska, A. and Jesionowski, T. (2014) 'Zinc oxide—from synthesis to application: a review', *Materials*, 7(4), pp. 2833–2881. doi: 10.3390/ma7042833.

Kondeková, M. *et al*. (2014) 'Analysis of lysozyme in cheese samples by on-line combination of capillary zone electrophoresis and mass spectrometry', *Food Chemistry*, 153, pp. 398–404. doi: 10.1016/j.foodchem.2013.12.078.

Kozuka, M. *et al*. (2015) 'Rapid and simple purification of lysozyme from the egg shell membrane', *Journal of Nutritional Science and Vitaminology*, 61(1), pp. 101–103. doi: 10.3177/jnsv.61.101.

Kretschy, N., Sack, M. and Somoza, M. M. (2016) 'Sequence-dependent fluorescence of Cy3- and Cy5-labeled double-stranded DNA', *Bioconjugate Chemistry*, 27(3), pp. 840–848. doi: 10.1021/acs.bioconjchem.6b00053.

Laity, J. H., Lee, B. M. and Wright, P. E. (2001) 'Zinc finger proteins: new insights into structural and functional diversity', *Current Opinion in Structural Biology*, 11(1), pp. 39–46. doi: 10.1016/S0959-440X(00)00167-6.

Lalander, C. H. *et al*. (2010) 'DNA-directed self-assembly of gold nanoparticles onto nanopatterned surfaces: controlled placement of individual nanoparticles into regular arrays', *ACS Nano*, 4(10), pp. 6153–6161. doi: 10.1021/nn101431k.

Lee, J. H. *et al*. (2012) 'Production of aqueous spherical gold nanoparticles using conventional ultrasonic bath', *Nanoscale Research Letters*, 7, pp. 1–7. doi: 10.1186/1556-276X-7-420.

Leitzmann, M. F. *et al*. (2003) 'Zinc supplement use and risk of prostate cancer', *JNCI: Journal of the National Cancer Institute*, 95(13), pp. 1004–1007. doi: 10.1093/jnci/95.13.1004.

Lemire, J., Mailloux, R. and Appanna, V. D. (2008) 'Zinc toxicity alters mitochondrial metabolism and leads to decreased ATP production in hepatocytes', *Journal of Applied Toxicology*, 28(2), pp. 175–182. doi: 10.1002/jat.1263.

Lequin, R. M. (2005) 'Enzyme immunoassay (EIA)/enzyme-linked immunosorbent assay (ELISA)', *Clinical Chemistry*, 51(12), pp. 2415–2418. doi: 10.1373/clinchem.2005.051532.

Levitus, M. and Ranjit, S. (2011) 'Cyanine dyes in biophysical research: the photophysics of polymethine fluorescent dyes in biomolecular environments', *Quarterly Reviews of Biophysics*, 44(1), pp. 123–151. doi: 10.1017/S0033583510000247.

Li, F. *et al*. (2012) 'Buffer enhanced bioluminescence resonance energy transfer sensor based on Gaussia luciferase for in vitro detection of protease', *Analytica Chimica Acta*, 724, pp. 104–110. doi: 10.1016/j.aca.2012.02.047.

Li, J. *et al*. (2000) 'In vitro selection and characterization of a highly efficient Zn(II)-dependent RNA-cleaving deoxyribozyme.', *Nucleic acids research*, 28(2), pp. 481–8. doi: 10.1093/nar/28.2.481.

Li, J. and Lu, Y. (2000) 'A highly sensitive and selective catalytic DNA biosensor for lead ions', *Journal of the American Chemical Society*, 122(42), pp. 10466–10467. doi: 10.1021/ja0021316.

Li, L. *et al*. (2010) 'An aptamer-based biosensor for the detection of lysozyme with gold nanoparticles amplification', *Sensors and Actuators B: Chemical*, 149(1), pp. 110–115. doi: 10.1016/j.snb.2010.06.015.

Li, L. *et al*. (2015) 'Simultaneous imaging of Zn^{2+} and Cu^{2+} in living cells based on DNAzyme modified gold nanoparticle', *Analytical Chemistry*, 87(9), pp. 4829–4835. doi: 10.1021/acs.analchem.5b00204.

Li, L. D. *et al*. (2011) 'Aptamer biosensor for label-free impedance spectroscopy detection of thrombin based on gold nanoparticles', *Sensors and Actuators, B: Chemical*, 157(1), pp. 189–194. doi: 10.1016/j.snb.2011.03.048.

Li, Q. *et al*. (2019) 'A cascade toehold-mediated strand displacement strategy for label-free and sensitive non-enzymatic recycling amplification detection of the HIV-1 gene', *Analyst*, 144(6), pp. 2173–2178. doi: 10.1039/c8an02340a.

Li, X. F. *et al*. (2019) 'Acute toxicity and hazardous concentrations of zinc to native freshwater organisms under different pH values in China', *Bulletin of Environmental*

Contamination and Toxicology, 103(1), pp. 120–126. doi: 10.1007/s00128-018-2441-2.

Li, Y. *et al*. (2018) 'Aptamers-based sensing strategy for 17 β -estradiol through fluorescence resonance energy transfer between oppositely charged CdTe quantum dots and gold nanoparticles', *Journal of Nanoscience and Nanotechnology*, 18(3), pp. 1517–1527. doi: 10.1166/jnn.2018.14235.

Liang, X. *et al*. (2011) 'Colorimetric detection of melamine in complex matrices based on cysteamine-modified gold nanoparticles', *Analyst*, 136(1), pp. 179–183. doi: 10.1039/C0AN00432D.

Liang, Y. *et al*. (2016) 'Fluorescence ELISA for sensitive detection of ochratoxin A based on glucose oxidase-mediated fluorescence quenching of CdTe QDs', *Analytica Chimica Acta*, 936, pp. 195–201. doi: 10.1016/j.aca.2016.06.018.

Liao, D. *et al*. (2013) 'Fluorescence turn-on detection of a protein using cytochrome c as a quencher', *Chemical Communications*, 49(82), pp. 9458–9460. doi: 10.1039/c3cc43985b.

Liao, J. Y., Song, Y. and Liu, Y. (2015) 'A new trend to determine biochemical parameters by quantitative FRET assays', *Acta Pharmacologica Sinica*, 36(12), pp. 1408–1415. doi: 10.1038/aps.2015.82.

Liu, B. *et al*. (2011) 'A FRET-based ratiometric sensor for mercury ions in water with multi-layered silica nanoparticles as the scaffold', *Chemical Communications*, 47(31), p. 8913. doi: 10.1039/c1cc12544c.

Liu, B. and Liu, J. (2017a) 'Freezing directed construction of bio/nano interfaces: reagentless conjugation, denser spherical nucleic acids, and better nanoflares',

Journal of the American Chemical Society, 139(28), pp. 9471–9474. doi: 10.1021/jacs.7b04885.

Liu, B. and Liu, J. (2017b) 'Methods for preparing DNA-functionalized gold nanoparticles, a key reagent of bioanalytical chemistry', *Analytical Methods*, 9(18), pp. 2633–2643. doi: 10.1039/C7AY00368D.

Liu, C. *et al*. (2018) 'Enzyme Biosensors for Point-of-Care Testing', in MEMS Sensors - Design and Application. InTech. doi: 10.5772/intechopen.73249.

Liu, F. K. (2012) 'Using size-exclusion chromatography to monitor variations in the sizes of microwave-irradiated gold nanoparticles', *ISRN Chromatography*, 2012, pp. 1–7. doi: 10.5402/2012/970685.

Liu, G. *et al*. (2018) 'Application of gold-nanoparticle colorimetric sensing to rapid food safety screening', *Sensors*, 18(12), pp. 1–16. doi: 10.3390/s18124166.

Liu, H. *et al*. (2017) 'Crystal structure of an RNA-cleaving DNAzyme', *Nature Communications*, 8(1), p. 2006. doi: 10.1038/s41467-017-02203-x.

Liu, J. and Lu, Y. (2006) 'Preparation of aptamer-linked gold nanoparticle purple aggregates for colorimetric sensing of analytes', *Nature Protocols*, 1(1), pp. 246–252. doi: 10.1038/nprot.2006.38.

Liu, L. *et al*. (2016) 'Multiplex electrochemiluminescence DNA sensor for determination of hepatitis B virus and hepatitis C virus based on multicolor quantum dots and Au nanoparticles', *Analytica Chimica Acta*, 916, pp. 92–101. doi: 10.1016/j.aca.2016.02.024.

Liu, M., Chang, D. and Li, Y. (2017) 'Discovery and biosensing applications of diverse RNA-cleaving DNAzymes', *Accounts of Chemical Research*, 50(9), pp. 2273–2283. doi: 10.1021/acs.accounts.7b00262.

Liu, S. *et al*. (2014) 'A label-free fluorescence detection strategy for lysozyme assay using $CuInS_2$ quantum dots', *Analyst*, 139(12), pp. 3048–3054. doi: 10.1039/c4an00160e.

Liu, X. *et al*. (2007) 'Extinction coefficient of gold nanoparticles with different sizes and different capping ligands', *Colloids and Surfaces B: Biointerfaces*, 58(1), pp. 3–7. doi: 10.1016/j.colsurfb.2006.08.005.

Liu, Y. *et al*. (2016) 'Chiroplasmonic assemblies of gold nanoparticles for ultrasensitive detection of 8-hydroxy-2'-deoxyguanosine in human serum sample', *Analytical Chemistry*, 88(12), pp. 6509–6514. doi: 10.1021/acs.analchem.6b01258.

Long, G. L. and Winefordner, J. D. (1983) 'Limit of detection: a closer look at the IUPAC definition', *Analytical Chemistry*, 55(7), pp. 712A-724A. doi: 10.1021/ac00258a001.

Lou, T., Qiang, H. and Chen, Z. (2017) 'Core-shell Cu@Au nanoparticles-based colorimetric aptasensor for the determination of lysozyme', *Talanta*, 163(August), pp. 132–139. doi: 10.1016/j.talanta.2016.10.095.

Lowe, C. R. (1984) 'Biosensors', *Trends in Biotechnology*, 2(3), pp. 59–65. doi: 10.1016/0167-7799(84)90011-8.

Lukman, S. *et al*. (2014) 'Hybrid assembly of DNA-coated gold nanoparticles with water soluble conjugated polymers for studying protein-DNA interaction and ligand inhibition', *RSC Advances*, 4(17), pp. 8883–8893. doi: 10.1039/c3ra46752j.

Luo, Y. *et al*. (2015) 'A novel colorimetric aptasensor using cysteamine-stabilized gold nanoparticles as probe for rapid and specific detection of tetracycline in raw milk', *Food Control*, 54, pp. 7–15. doi: 10.1016/j.foodcont.2015.01.005.

Luppa, P. B., Sokoll, L. J. and Chan, D. W. (2001) 'Immunosensors—principles and applications to clinical chemistry', *Clinica Chimica Acta*, 314(1–2), pp. 1–26. doi: 10.1016/S0009-8981(01)00629-5.

Ma, Y. *et al*. (2013) 'Colorimetric sensing strategy for mercury(ii) and melamine utilizing cysteamine-modified gold nanoparticles', *Analyst*, 138(18), pp. 5338–5343. doi: 10.1039/c3an00690e.

Machleidt, T. *et al*. (2015) 'NanoBRET-a novel BRET platform for the analysis of protein-protein interactions', *ACS Chemical Biology*, 10(8), pp. 1797–1804. doi: 10.1021/acschembio.5b00143.

Marras, S. A. E. (2002) 'Efficiencies of fluorescence resonance energy transfer and contact-mediated quenching in oligonucleotide probes', *Nucleic Acids Research*, 30(21), p. e122. doi: 10.1093/nar/gnf121.

Maye, M. M. *et al*. (2000) 'Heating-induced evolution of thiolate-encapsulated gold nanoparticles: a strategy for size and shape manipulations', *Langmuir*, 16(2), pp. 490–497. doi: 10.1021/la990892k.

Mazumdar, D. *et al*. (2009) 'Activity, folding and Z-DNA formation of the 8-17 DNAzyme in the presence of monovalent ions', *Journal of the American Chemical Society*, 131(15), pp. 5506–5515. doi: 10.1021/ja8082939.

McCall, K. A., Huang, C. and Fierke, C. A. (2000) 'Function and nechanism of zinc metalloenzymes', *The Journal of Nutrition*, 130(5), pp. 1437S-1446S. doi: 10.1093/jn/130.5.1437S.

Medintz, I. L. *et al*. (2003) 'A fluorescence resonance energy transfer sensor based on maltose binding protein', *Bioconjugate Chemistry*, 14(5), pp. 909–918. doi: 10.1021/bc020062+.

Merza, K. S. *et al*. (2012) 'Comparative study on methods for preparation of gold nanoparticles', *Green and Sustainable Chemistry*, pp. 26–28. doi: 10.4236/gsc.2012.21005.

Millan, K. M. and Mikkelsen, S. R. (1993) 'Sequence-selective biosensor for DNA based on electroactive hybridization indicators', *Analytical Chemistry*, 65(17), pp. 2317–2323. doi: 10.1021/ac00065a025.

Mirkin, C. A. *et al*. (1996) 'A DNA-based method for rationally assembling nanoparticles into macroscopic materials', *Nature*, 382(6592), pp. 607–609. doi: 10.1038/382607a0.

Morten, M. J. *et al*. (2018) 'Stacking-induced fluorescence increase reveals allosteric interactions through DNA', *Nucleic Acids Research*, 46(21), pp. 11618–11626. doi: 10.1093/nar/gky887.

Moscinski, L. C., Kasnic, G. and Saker, A. (1992) 'The significance of an elevated serum lysozyme value in acute myelogenous leukemia with eosinophilia', *American Journal of Clinical Pathology*, 97(2), pp. 195–201. doi: 10.1093/ajcp/97.2.195.

Muddineti, O. S., Ghosh, B. and Biswas, S. (2015) 'Current trends in using polymer coated gold nanoparticles for cancer therapy', *International Journal of Pharmaceutics*, pp. 252–267. doi: 10.1016/j.ijpharm.2015.02.038.

Mun, H. *et al*. (2014) 'Homogeneous assay of target molecules based on chemiluminescence resonance energy transfer (CRET) using DNAzyme-linked aptamers', *Biosensors and Bioelectronics*, 58, pp. 308–313. doi: 10.1016/j.bios.2014.02.008.

Mura, S. *et al*. (2015) 'Functionalized gold nanoparticles for the detection of nitrates in water', *International Journal of Environmental Science and Technology*, 12(3), pp. 1021–1028. doi: 10.1007/s13762-013-0494-7.

Muttaqin, Nakamura, T. and Sato, S. (2015) 'Synthesis of gold nanoparticle colloids by highly intense laser irradiation of aqueous solution by flow system', *Applied Physics A*, 120(3), pp. 881–888. doi: 10.1007/s00339-015-9314-x.

Nakamoto, M., Kashiwagi, Y. and Yamamoto, M. (2005) 'Synthesis and size regulation of gold nanoparticles by controlled thermolysis of ammonium gold(I) thiolate in the absence or presence of amines', *Inorganica Chimica Acta*, 358(14), pp. 4229–4236. doi: 10.1016/j.ica.2005.03.037.

Nash, J. A. *et al*. (2006) 'The peptidoglycan-degrading property of lysozyme Is not required for bactericidal activity in vivo', *The Journal of Immunology*, 177(1), pp. 519–526. doi: 10.4049/jimmunol.177.1.519.

Nasir, M. S. *et al*. (1999) 'The chemical cell biology of zinc: structure and intracellular fluorescence of a zinc-quinolinesulfonamide complex', *JBIC Journal of Biological Inorganic Chemistry*, 4(6), pp. 775–783. doi: 10.1007/s007750050350.

Negishi, Y. *et al*. (2004) 'Magic-numbered Au(n) clusters protected by glutathione monolayers (n = 18, 21, 25, 28, 32, 39): isolation and spectroscopic characterization.', *Journal of the American Chemical Society*, 126(21), pp. 6518–6519. doi: 10.1021/ja0483589.

Niidome, T. *et al*. (2004) 'Preparation of primary amine-modified gold nanoparticles and their transfection ability into cultivated cells', *Chemical Communications*, 10(17), pp. 1978–1979. doi: 10.1039/b406189f.

Nishida, K. *et al*. (2009) 'Zinc transporter Znt5/Slc30a5 is required for the mast cell-mediated delayed-type allergic reaction but not the immediate-type reaction', *Journal of Experimental Medicine*, 206(6), pp. 1351–1364. doi: 10.1084/jem.20082533.

Nowakowski, A. B. *et al*. (2015) 'Chemical-biological properties of zinc sensors TSQ and Zinquin: formation of sensor-Zn-protein adducts versus $Zn(Sensor)_2$ complexes', *Inorganic Chemistry*, 54(24), pp. 11637–11647. doi: 10.1021/acs.inorgchem.5b01535.

Nowakowski, A. B. and Petering, D. H. (2011) 'Reactions of the fluorescent sensor, Zinquin, with the zinc-proteome: adduct formation and ligand substitution', *Inorganic Chemistry*, 50(20), pp. 10124–10133. doi: 10.1021/ic201076w.

Ocaña, C. *et al*. (2015) 'Label free aptasensor for lysozyme detection: a comparison of the analytical performance of two aptamers', *Bioelectrochemistry*, 105, pp. 72–77. doi: 10.1016/j.bioelechem.2015.05.009.

Okitsu, K. *et al*. (2001) 'Formation of colloidal gold nanoparticles in an ultrasonic field: control of rate of gold (III) reduction and size of formed gold particles', *Langmuir*, 17(25), pp. 7717–7720. doi: 10.1021/la010414l.

Oliveira Brett, A. M. (2005) 'Chapter 4 DNA-based biosensors', in *Comprehensive Analytical Chemistry*, pp. 179–208. doi: 10.1016/S0166-526X(05)44004-0.

Oliveira, J. P. *et al*. (2020) 'A helpful method for controlled synthesis of monodisperse gold nanoparticles through response surface modeling', *Arabian Journal of Chemistry*, 13(1), pp. 216–226. doi: 10.1016/j.arabjc.2017.04.003.

Ora, A. *et al*. (2016) 'Cellular delivery of enzyme-loaded DNA origami', *Chemical Communications*, 52(98), pp. 14161–14164. doi: 10.1039/c6cc08197e.

Ortiz-Aguayo, D. and del Valle, M. (2018) 'Label-free aptasensor for lysozyme detection using electrochemical impedance spectroscopy', *Sensors*, 18(2). doi: 10.3390/s18020354.

Outten, C. E. (2001) 'Femtomolar sensitivity of metalloregulatory proteins controlling zinc homeostasis', *Science*, 292(5526), pp. 2488–2492. doi: 10.1126/science.1060331.

Pallares, R. M. *et al*. (2015) 'A plasmonic nanosensor with inverse sensitivity for circulating cell-free DNA quantification', *Chemical Communications*, 51(77), pp. 14524–14527. doi: 10.1039/c5cc05331e.

Pallares, R. M., Thanh, N. T. K. and Su, X. (2018) 'Tunable plasmonic colorimetric assay with inverse sensitivity for extracellular DNA quantification', *Chemical Communications*, 54(80), pp. 11260–11263. doi: 10.1039/C8CC05465G.

Patel, A. B., Miles, R. R. and Deininger, M. W. (2019) 'Lysozyme nephropathy in chronic myelomonocytic leukemia', *Clinical Case Reports*, 7(6), pp. 1263–1264. doi: 10.1002/ccr3.2188.

Peng, Y. *et al*. (2013) 'Aptamer-gold nanoparticle-based colorimetric assay for the sensitive detection of thrombin', *Sensors and Actuators, B: Chemical*, 177, pp. 818–825. doi: 10.1016/j.snb.2012.12.004.

Peter, C. *et al*. (2001) 'Optical DNA-sensor chip for real-time detection of hybridization events', *Analytical and Bioanalytical Chemistry*, 371(2), pp. 120–127. doi: 10.1007/s002160101006.

Petrukhin, O. M. and Maksimenko, O. O. (2008) 'Sensors in analytical chemistry', *Russian Journal of General Chemistry*, 78(12), pp. 2413–2417. doi: 10.1134/S1070363208120232.

Piro, B. and Reisberg, S. (2017) 'Recent advances in electrochemical immunosensors', *Sensors*, 17(4), p. 794. doi: 10.3390/s17040794.

Prasad, A. S. (2008) 'Zinc in human health: effect of zinc on immune cells', *Molecular Medicine*, 14(5–6), pp. 353–357. doi: 10.2119/2008-00033.Prasad.

Prasad, B. L. V. *et al*. (2002) 'Digestive ripening of thiolated gold nanoparticles: the effect of alkyl chain length', *Langmuir*, 18(20), pp. 7515–7520. doi: 10.1021/la020181d.

Prasad, B. L. V. *et al*. (2003) 'Digestive-ripening agents for gold nanoparticles: alternatives to thiols', *Chemistry of Materials*, 15(4), pp. 935–942. doi: 10.1021/cm0206439.

Qi, Y. *et al*. (2017) 'Simple and rapid chemiluminescence aptasensor for Hg^{2+} in contaminated samples: a new signal amplification mechanism', *Biosensors and Bioelectronics*, 87, pp. 439–446. doi: 10.1016/j.bios.2016.08.022.

Qin, Y. *et al*. (2011) 'Measuring steady-state and dynamic endoplasmic reticulum and Golgi Zn^{2+} with genetically encoded sensors', *Proceedings of the National Academy of Sciences of the United States of America*, 108(18), pp. 7351–7356. doi: 10.1073/pnas.1015686108.

Radenković, S. *et al*. (2017) 'The nature of the Au-N bond in gold(III) complexes with aromatic nitrogen-containing heterocycles: the influence of Au(III) ions on the ligand aromaticity', *New Journal of Chemistry*, 41(21), pp. 12407–12415. doi: 10.1039/c7nj02634j.

Rahimizadeh, K. *et al*. (2017) 'Development of cell-specific aptamers: recent advances and insight into the selection procedures', *Molecules*, 22(12), pp. 1–13. doi: 10.3390/molecules22122070.

Rahman, M. *et al*. (2015) 'Electrochemical DNA hybridization sensors based on conducting polymers', *Sensors*, 15(2), pp. 3801–3829. doi: 10.3390/s150203801.

Rahman, M. and Rebrov, E. (2014) 'Microreactors for gold nanoparticles synthesis: from Faraday to flow', *Processes*, 2(2), pp. 466–493. doi: 10.3390/pr2020466.

Rainey, K. H. and Patterson, G. H. (2019) 'Photoswitching FRET to monitor protein–protein interactions', *Proceedings of the National Academy of Sciences of the United States of America*, 116(3), pp. 864–873. doi: 10.1073/pnas.1805333116.

Ramírez-Segovia, A. S. *et al*. (2014) 'Glassy carbon electrodes sequentially modified by cysteamine-capped gold nanoparticles and poly(amidoamine) dendrimers generation 4.5 for detecting uric acid in human serum without ascorbic acid interference', *Analytica Chimica Acta*, 812, pp. 18–25. doi: 10.1016/j.aca.2013.12.025.

Ren, D. *et al*. (2019) 'A novel FRET biosensor based on four-way branch migration HCR for Vibrio parahaemolyticus detection', *Sensors and Actuators B: Chemical*, 296(October 2018), p. 126577. doi: 10.1016/j.snb.2019.05.054.

Rodríguez-Lorenzo, L. *et al*. (2012) 'Plasmonic nanosensors with inverse sensitivity by means of enzyme-guided crystal growth', *Nature Materials*, 11(7), pp. 604–607. doi: 10.1038/nmat3337.

Rodríguez, M. C. and Rivas, G. A. (2009) 'Label-free electrochemical aptasensor for the detection of lysozyme', *Talanta*, 78(1), pp. 212–216. doi: 10.1016/j.talanta.2008.11.002.

Saha, K. *et al*. (2012) 'Gold nanoparticles in chemical and biological sensing', *Chemical Reviews*, 112(5), pp. 2739–2779. doi: 10.1021/cr2001178.

Sakamoto, S. *et al*. (2018) 'Enzyme-linked immunosorbent assay for the quantitative/qualitative analysis of plant secondary metabolites', *Journal of Natural Medicines*, 72(1), pp. 32–42. doi: 10.1007/s11418-017-1144-z.

Salazar, O. and Asenjo, J. A. (2007) 'Enzymatic lysis of microbial cells', *Biotechnology Letters*, 29(7), pp. 985–994. doi: 10.1007/s10529-007-9345-2.

Santoriello, D. *et al*. (2017) 'Lysozyme-induced nephropathy', *Kidney International Reports*, 2(1), pp. 84–88. doi: 10.1016/j.ekir.2016.09.002.

Santoro, S. W. and Joyce, G. F. (1997) 'A general purpose RNA-cleaving DNA enzyme', *Proceedings of the National Academy of Sciences of the United States of America*, 94(9), pp. 4262–4266. doi: 10.1073/pnas.94.9.4262.

Sapkota, K. *et al*. (2019) 'Single-step FRET-based detection of femtomoles DNA', *Sensors*, 19(16). doi: 10.3390/s19163495.

Satsoura, D. *et al*. (2007) 'Circumvention of fluorophore photobleaching in fluorescence fluctuation experiments: a beam scanning approach', *ChemPhysChem*, 8(6), pp. 834–848. doi: 10.1002/cphc.200600589.

Sau, T. K. *et al*. (2001) 'Size controlled synthesis of gold nanoparticles using photochemically prepared seed particles', *Journal of Nanoparticle Research*, 3(4), pp. 257–261. doi: 10.1023/A:1017567225071.

Schaeublin, N. M. *et al*. (2011) 'Surface charge of gold nanoparticles mediates mechanism of toxicity', *Nanoscale*, 3(2), pp. 410–420. doi: 10.1039/c0nr00478b.

Schleh, C. *et al*. (2012) 'Size and surface charge of gold nanoparticles determine absorption across intestinal barriers and accumulation in secondary target organs after oral administration', *Nanotoxicology*, 6(1), pp. 36–46. doi: 10.3109/17435390.2011.552811.

Seeman, N. C. (1982) ‘Nucleic acid junctions and lattices’, *Journal of Theoretical Biology*, 99(2), pp. 237–247. doi: 10.1016/0022-5193(82)90002-9.

Seeman, N. C. (2017) ‘Structural DNA Nanotechnology: An Overview’, in *NanoBiotechnology Protocols*, pp. 143–166. doi: 10.1385/1-59259-901-X:143.

Serra, C. *et al*. (2002) ‘Expression and prognostic significance of lysozyme in male breast cancer’, *Breast Cancer Research*, 4(R16). doi: 10.1186/bcr537.

Sharma, A. K. *et al*. (2018) ‘Aggregation of cysteamine-capped gold nanoparticles in presence of ATP as an analytical tool for rapid detection of creatine kinase (CK-MM)’, *Analytica Chimica Acta*, 1024, pp. 161–168. doi: 10.1016/j.aca.2018.03.027.

Shin, H. S. *et al*. (2019) ‘Detection of Gram-negative bacterial outer membrane vesicles using DNA aptamers’, *Scientific Reports*, 9(1), pp. 1–8. doi: 10.1038/s41598-019-49755-0.

Shrivastava, A. and Gupta, V. (2011) ‘Methods for the determination of limit of detection and limit of quantitation of the analytical methods’, *Chronicles of Young Scientists*, 2(1), p. 21. doi: 10.4103/2229-5186.79345.

Si, H. *et al*. (2018) ‘Highly sensitive fluorescence imaging of Zn^{2+} and Cu^{2+} in living cells with signal amplification based on functional DNA self-assembly’, *Analytical Chemistry*, 90(15), pp. 8785–8792. doi: 10.1021/acs.analchem.7b05268.

Silverman, S. K. (2016) ‘Catalytic DNA: scope, applications, and biochemistry of deoxyribozymes’, *Trends in Biochemical Sciences*, 41(7), pp. 595–609. doi: 10.1016/j.tibs.2016.04.010.

Silvetti, T. *et al*. (2010) ‘Effects of lysozyme on the microbiological stability and organoleptic properties of unpasteurized beer’, *Journal of the Institute of Brewing*, 116(1), pp. 33–40. doi: 10.1002/j.2050-0416.2010.tb00395.x.

Singh, A. K. and Srivastava, O. N. (2015) 'One-step green synthesis of gold nanoparticles using black cardamom and effect of pH on its synthesis', *Nanoscale Research Letters*, 10(1), p. 353. doi: 10.1186/s11671-015-1055-4.

Singh, R. *et al*. (2011) 'Heavy metals and living systems: an overview', *Indian Journal of Pharmacology*, 43(3), p. 246. doi: 10.4103/0253-7613.81505.

Sonavane, G., Tomoda, K. and Makino, K. (2008) 'Biodistribution of colloidal gold nanoparticles after intravenous administration: effect of particle size', *Colloids and Surfaces B: Biointerfaces*, 66(2), pp. 274–280. doi: 10.1016/j.colsurfb.2008.07.004.

Song, K. M., Lee, S. and Ban, C. (2012) 'Aptamers and their biological applications', *Sensors*, 12(1), pp. 612–631. doi: 10.3390/s120100612.

Song, L. *et al*. (1995) 'Photobleaching kinetics of fluorescein in quantitative fluorescence microscopy', *Biophysical Journal*, 68(6), pp. 2588–2600. doi: 10.1016/S0006-3495(95)80442-X.

Song, P. *et al*. (2012) 'Label-free catalytic and molecular beacon containing an abasic site for sensitive fluorescent detection of small inorganic and organic molecules', *Analytical Chemistry*, 84(6), pp. 2916–2922. doi: 10.1021/ac203488p.

Stennett, E. M. S. *et al*. (2015) 'Demystifying PIFE: the photophysics behind the protein-induced fluorescence enhancement phenomenon in Cy3', *Journal of Physical Chemistry Letters*, 6(10), pp. 1819–1823. doi: 10.1021/acs.jpclett.5b00613.

Stoltenburg, R., Reinemann, C. and Strehlitz, B. (2005) 'FluMag-SELEX as an advantageous method for DNA aptamer selection', *Analytical and Bioanalytical Chemistry*, 383(1), pp. 83–91. doi: 10.1007/s00216-005-3388-9.

Su, J. *et al*. (2013) 'Target-induced charge reduction of aptamers for visual detection of lysozyme based on positively charged gold nanoparticles', *Chemical Communications*, 49(69), pp. 7659–7661. doi: 10.1039/c3cc43970d.

Su, R. *et al*. (2016) 'Highly selective and sensitive visual detection of oxytetracycline based on aptamer binding-mediated the anti-aggregation of positively charged gold nanoparticles', *Materials Letters*, 180, pp. 31–34. doi: 10.1016/j.matlet.2016.05.076.

Sujitha, M. V. and Kannan, S. (2013) 'Green synthesis of gold nanoparticles using citrus fruits (Citrus limon, Citrus reticulata and Citrus sinensis) aqueous extract and its characterization', *Spectrochimica Acta - Part A: Molecular and Biomolecular Spectroscopy*, 102, pp. 15–23. doi: 10.1016/j.saa.2012.09.042.

Sullenger, B. A. *et al*. (1990) 'Overexpression of TAR sequences renders cells resistant to human immunodeficiency virus replication', *Cell*, 63(3), pp. 601–608. doi: 10.1016/0092-8674(90)90455-N.

Sundaralingam, M. and Ponnuswamy, P. K. (2004) 'Stability of DNA duplexes with Watson-Crick base pairs: a predicted model', *Biochemistry*, 43(51), pp. 16467–16476. doi: 10.1021/bi048158+.

Tebbe, M. *et al*. (2015) 'Colloidally stable and surfactant-free protein-coated gold nanorods in biological media', *ACS Applied Materials and Interfaces*, 7(10), pp. 5984–5991. doi: 10.1021/acsami.5b00335.

Teichmann, M., Kopperger, E. and Simmel, F. C. (2014) 'Robustness of localized DNA strand displacement cascades', *ACS Nano*, 8(8), pp. 8487–8496. doi: 10.1021/nn503073p.

Templeton, A. C. *et al*. (1998) 'Reactivity of monolayer-protected gold cluster molecules: steric effects reactivity of monolayer-rrotected gold cluster molecules:

steric effects', *Journal of the American Chemical Society*, 120(8), pp. 1906–1911. doi: 10.1021/ja973863.

Thiha, A. and Ibrahim, F. (2015) 'A colorimetric enzyme-linked immunosorbent assay (ELISA) detection platform for a point-of-care dengue detection system on a lab-on-compact-disc', *Sensors*, 15(5), pp. 11431–11441. doi: 10.3390/s150511431.

Tichoniuk, M., Ligaj, M. and Filipiak, M. (2008) 'Application of DNA hybridization biosensor as a screening method for the detection of genetically modified food components', *Sensors*, 8(4), pp. 2118–2135. doi: 10.3390/s8042118.

Toomjeen, P. *et al*. (2019) 'Designing an aptasensor based on cysteamine-capped AuNPs for 8-Oxo-dG detection: a molecular dynamics approach and experimental validation', *Journal of Physical Chemistry B*, 123(5), pp. 1129–1138. doi: 10.1021/acs.jpcb.8b10436.

Tsai, D. H. *et al*. (2011) 'Adsorption and conformation of serum albumin protein on gold nanoparticles investigated using dimensional measurements and in situ spectroscopic methods', *Langmuir*, 27(6), pp. 2464–2477. doi: 10.1021/la104124d.

Turkevich, J., Stevenson, P. C. and Hillier, J. (1951) 'A study of the nucleation and growth processes in the synthesis of colloidal gold', *Discussions of the Faraday Society*, 11(c), pp. 55–75. doi: 10.1039/DF9511100055.

Umrao, S. *et al*. (2019) 'Smartphone-based kanamycin sensing with ratiometric FRET', *RSC Advances*, 9(11), pp. 6143–6151. doi: 10.1039/c8ra10035g.

Uppalapati, M. *et al*. (2016) 'A potent d-protein antagonist of VEGF-A is nonimmunogenic, metabolically stable, and longer-circulating in vivo', *ACS Chemical Biology*, 11(4), pp. 1058–1065. doi: 10.1021/acschembio.5b01006.

Vasilescu, A. *et al*. (2016) 'Aptamer-based electrochemical sensing of lysozyme', *Chemosensors*, 4(2), p. 10. doi: 10.3390/chemosensors4020010.

Vicente, N. B. *et al*. (2007) 'Photobleaching correction in fluorescence microscopy images', *Journal of Physics: Conference Series*, 90(1). doi: 10.1088/1742-6596/90/1/012068.

Vinkenborg, J. L. *et al*. (2009) 'Genetically encoded FRET sensors to monitor intracellular Zn^{2+} homeostasis', *Nature Methods*, 6(10), pp. 737–740. doi: 10.1038/nmeth.1368.

Vizoso, F. *et al*. (2001) 'Lysozyme expression by breast carcinomas, correlation with clinicopathologic parameters, and prognostic significance.', *Annals of surgical oncology*, 8(8), pp. 667–674. doi: 10.1007/s10434-001-0667-3.

Walkup, G. K. *et al*. (2000) 'A new cell-permeable fluorescent probe for Zn^{2+}', *Journal of the American Chemical Society*, 122(23), pp. 5644–5645. doi: 10.1021/ja000868p.

Wang, B. *et al*. (2017) 'Contribution of gold nanoparticles to the catalytic DNA strand displacement in leakage reduction and signal amplification', *Chemical Communications*, 53(79), pp. 10950–10953. doi: 10.1039/C7CC05832B.

Wang, C. and Yu, C. (2013) 'Detection of chemical pollutants in water using gold nanoparticles as sensors: a review', *Reviews in Analytical Chemistry*, 32(1), pp. 1–14. doi: 10.1515/revac-2012-0023.

Wang, H. *et al*. (2016) 'Effect of lysozyme on invasion and migration of human lung carcinoma A549 cells', *International Journal of Clinical and Experimental Pathology*, 9(8), pp. 8239–8246.

Wang, J. *et al*. (1996) 'DNA electrochemical biosensor for the detection of short DNA sequences related to the human immunodeficiency virus', *Analytical Chemistry*, 68(15), pp. 2629–2634. doi: 10.1021/ac9602433.

Wang, J. *et al*. (2014) 'Microfluidic biosensor for the detection of DNA by fluorescence enhancement and the following streptavidin detection by fluorescence quenching', *Biosensors and Bioelectronics*, 51, pp. 280–285. doi: 10.1016/j.bios.2013.07.058.

Wang, J. and Liu, B. (2009) 'Fluorescence resonance energy transfer between an anionic conjugated polymer and a dye-labeled lysozyme aptamer for specific lysozyme detection', *Chemical Communications*, (17), pp. 2284. doi: 10.1039/b820001g.

Wang, L. *et al*. (2006) 'Unmodified gold nanoparticles as a colorimetric probe for potassium DNA aptamers', *Chemical Communications*, (36), pp. 3780–3782. doi: 10.1039/b607448k.

Wang, M. *et al*. (2016) 'Unmodified and positively charged gold nanoparticles for sensitive colorimetric detection of folate receptor via terminal protection of small molecule-linked ssDNA', *Science China Chemistry*, 59(6), pp. 770–775. doi: 10.1007/s11426-016-5589-9.

Wang, W. *et al*. (2011) 'Aptamer-based PDMS-gold nanoparticle composite as a platform for visual detection of biomolecules with silver enhancement', *Biosensors and Bioelectronics*, 26(7), pp. 3110–3114. doi: 10.1016/j.bios.2010.10.034.

Wang, W. *et al*. (2017) 'Near-infrared photothermally activated DNAzyme–gold nanoshells for imaging metal ions in living cells', *Angewandte Chemie*, 56(24), pp. 6798–6802. doi: 10.1002/anie.201701325.

Wang, X. *et al*. (2019) 'A quencher-free DNAzyme beacon for fluorescently sensing uranyl ions via embedding 2-aminopurine', *Biosensors and Bioelectronics*, 135(March), pp. 166–172. doi: 10.1016/j.bios.2019.04.021.

Wang, Y. *et al*. (2019) 'Association between serum zinc levels and lung cancer: a meta-analysis of observational studies', *World Journal of Surgical Oncology*, 17(1), p. 78. doi: 10.1186/s12957-019-1617-5.

Wartell, R. M. and Benight, A. S. (1985) 'Thermal denaturation of DNA molecules: a comparison of theory with experiment', *Physics Reports*, 126(2), pp. 67–107. doi: 10.1016/0370-1573(85)90060-2.

Wei, G. T. (1999) 'Shape separation of nanometer gold particles by size-exclusion chromatography', *Analytical Chemistry*, 71(11), pp. 2085–2091. doi: 10.1021/ac990044u.

Wen, Z. B. *et al*. (2018) 'An ATP-fueled nucleic acid signal amplification strategy for highly sensitive microRNA detection', *Chemical Communications*, 54(77), pp. 10897–10900. doi: 10.1039/C8CC05525D.

Wu, A. H. *et al*. (2010) 'A reagentless DNA biosensor based on cathodic electrochemiluminescence at a C/CxO1-x electrode', *Talanta*, 81(3), pp. 934–940. doi: 10.1016/j.talanta.2010.01.040.

Wu, Z. S. *et al*. (2006) 'Optical detection of DNA hybridization based on fluorescence quenching of tagged oligonucleotide probes by gold nanoparticles', *Analytical Biochemistry*, 353(1), pp. 22–29. doi: 10.1016/j.ab.2006.01.018.

Wu, Z. *et al*. (2017) 'Imaging endogenous metal ions in living cells using a DNAzyme–catalytic hairpin assembly probe', *Angewandte Chemie*, 56(30), pp. 8721–8725. doi: 10.1002/anie.201703540.

Xia, H. *et al*. (2016) 'Revitalizing the Frens method to synthesize uniform, quasi-spherical gold nanoparticles with deliberately regulated sizes from 2 to 330 nm', *Langmuir*, 32(23), pp. 5870–5880. doi: 10.1021/acs.langmuir.6b01312.

Xia, X. *et al*. (2012) 'Quantifying the coverage density of poly(ethylene glycol) chains on the surface of gold nanostructures', *ACS Nano*, 6(1), pp. 512–522. doi: 10.1021/nn2038516.

Xiao, Y., Allen, E. C. and Silverman, S. K. (2011) 'Merely two mutations switch a DNA-hydrolyzing deoxyribozyme from heterobimetallic (Zn^{2+}/Mn^{2+}) to monometallic (Zn^{2+}-only) behavior', *Chemical Communications*, 47(6), pp. 1749–1751. doi: 10.1039/c0cc04575f.

Xing, H. *et al*. (2014) 'DNA aptamer technology for personalized medicine', *Current Opinion in Chemical Engineering*, 4, pp. 79–87. doi: 10.1016/j.coche.2014.01.007.

Xu, J. *et al*. (2014) 'Engineering a DNA-cleaving DNAzyme and PCR into a simple sensor for zinc ion detection.', *Analytical and bioanalytical chemistry*, 406(13), pp. 3025–9. doi: 10.1007/s00216-014-7732-9.

Xu, W. *et al*. (2014) 'A homogeneous immunosensor for AFB1 detection based on FRET between different-sized quantum dots', *Biosensors and Bioelectronics*, 56, pp. 144–150. doi: 10.1016/j.bios.2014.01.007.

Yadav, R., Patel, P. N. and Lad, V. N. (2018) 'High selective colorimetric detection of Cd^{2+} ions using cysteamine functionalized gold nanoparticles with cross-linked DL-glyceraldehyde', *Research on Chemical Intermediates*, 44(4), pp. 2305–2317. doi: 10.1007/s11164-017-3230-y.

Yang, Z. *et al*. (2018) 'Optical control of metal ion probes in cells and zebrafish using highly selective DNAzymes conjugated to upconversion nanoparticles', *Journal of the American Chemical Society*, 140(50), pp. 17656–17665. doi: 10.1021/jacs.8b09867.

Yao, X. *et al*. (2016) 'Colorimetric determination of lysozyme based on the aggregation of gold nanoparticles controlled by a cationic polymer and an aptamer', *Microchimica Acta*, 183(7), pp. 2353–2359. doi: 10.1007/s00604-016-1876-6.

Yasun, E. *et al*. (2015) 'BSA modification to reduce CTAB induced nonspecificity and cytotoxicity of aptamer-conjugated gold nanorods', *Nanoscale*, 7(22), pp. 10240–10248. doi: 10.1039/c5nr01704a.

Yee, C. K. *et al*. (1999) 'Novel one-phase synthesis of thiol-functionalized gold, palladium, and iridium nanoparticles using superhydride', *Langmuir*, 15(10), pp. 3486–3491. doi: 10.1021/la990015e.

Yeh, C. K. *et al*. (1997) 'A population-based study of salivary lysozyme concentrations and candidal counts', *Archives of Oral Biology*, 42(1), pp. 25–31. doi: 10.1016/S0003-9969(96)00104-5.

You, Y. *et al*. (2011) 'Phosphorescent sensor for biological mobile zinc', *Journal of the American Chemical Society*, 133(45), pp. 18328–18342. doi: 10.1021/ja207163r.

Zaichick, V. Y., Sviridova, T. V and Zaichick, S. V (1997) 'Zinc in the human prostate gland: normal, hyperplastic and cancerous', *International Urology and Nephrology*, 29(5), pp. 565–574. doi: 10.1007/BF02552202.

Zeng, S. *et al*. (2011) 'A review on functionalized gold nanoparticles for biosensing applications', *Plasmonics*, 6(3), pp. 491–506. doi: 10.1007/s11468-011-9228-1.

Zhai, J., Cui, H. and Yang, R. (1997) 'DNA based biosensors', *Biotechnology Advances*, 15(1), pp. 43–58. doi: 10.1016/S0734-9750(97)00003-7.

Zhang, J. *et al*. (2015) 'Low-cost and highly efficient DNA biosensor for heavy metal ion using specific DNAzyme-modified microplate and portable glucometer-based detection mode', *Biosensors and Bioelectronics*, 68, pp. 232–238. doi: 10.1016/j.bios.2015.01.001.

Zhang, J. *et al*. (2017) 'DNA aptamer-based activatable probes for photoacoustic imaging in living mice', *Journal of the American Chemical Society*, 139(48), pp. 17225–17228. doi: 10.1021/jacs.7b07913.

Zhang, X. *et al*. (2008) 'New strategy for quantifying biological zinc by a modified Zinpyr fluorescence sensor', *Journal of the American Chemical Society*, 130(47), pp. 15788–15789. doi: 10.1021/ja807156b.

Zhang, X. *et al*. (2012) 'Impacts of lead/zinc mining and smelting on the environment and human health in China', *Environmental Monitoring and Assessment*, 184(4), pp. 2261–2273. doi: 10.1007/s10661-011-2115-6.

Zhang, X. *et al*. (2012) 'Instantaneous attachment of an ultrahigh density of nonthiolated DNA to gold nanoparticles and its applications', *Langmuir*, 28(49), pp. 17053–17060. doi: 10.1021/la3035424.

Zhang, X. B. *et al*. (2010) 'Catalytic and molecular beacons for amplified detection of metal ions and organic molecules with high sensitivity', *Analytical Chemistry*, 82(12), pp. 5005–5011. doi: 10.1021/ac1009047.

Zhang, X., Servos, M. R. and Liu, J. (2012) 'Instantaneous and quantitative functionalization of gold nanoparticles with thiolated DNA using a pH-assisted and surfactant-free route', *Journal of the American Chemical Society*, 134(17), pp. 7266–7269. doi: 10.1021/ja3014055.

Zhang, Y. *et al*. (2018) 'An ultrasensitive electrochemiluminescence biosensor for multiple detection of microRNAs based on a novel dual circuit catalyzed hairpin assembly', *Chemical Communications*. 54(72), pp. 10148–10151. doi: 10.1039/C8CC06102E.

Zhang, Y., Lai, B. S. and Juhas, M. (2019) 'Recent advances in aptamer discovery and applications', *Molecules*, 24(5). doi: 10.3390/molecules24050941.

Zhao, S., Huang, Y., Liu, R., *et al*. (2010) 'A nonenzymatic chemiluminescent reaction enabling chemiluminescence resonance energy transfer to quantum dots', *Chemistry - A European Journal*, 16(21), pp. 6142–6145. doi: 10.1002/chem.201000478.

Zhao, S., Huang, Y., Shi, M., *et al*. (2010) 'Chemiluminescence resonance energy transfer-based detection for microchip electrophoresis', *Analytical Chemistry*, 82(5), pp. 2036–2041. doi: 10.1021/ac9027643.

Zhao, W., Lin, L. and Hsing, I.-M. (2009) 'Rapid synthesis of DNA-functionalized gold nanoparticles in salt solution using mononucleotide-mediated conjugation', *Bioconjugate Chemistry*, 20(6), pp. 1218–1222. doi: 10.1021/bc900080p.

Zhao, Y. W. *et al*. (2018) 'Application of aptamer-based biosensor for rapid detection of pathogenic Escherichia coli', *Sensors*, 18(8), pp. 1–16. doi: 10.3390/s18082518.

Zheng, H. *et al*. (2017) 'Highly sensitive aptamer-based colorimetric detection of melamine in raw milk with cysteamine-stabilized gold nanoparticles', *Journal of Nanoscience and Nanotechnology*, 17(2), pp. 853–861. doi: 10.1166/jnn.2017.12722.

Zheng, J. *et al*. (2013) 'Visual detection of glyphosate in environmental water samples using cysteamine-stabilized gold nanoparticles as colorimetric probe', *Analytical Methods*, 5(4), pp. 917–924. doi: 10.1039/C2AY26391B.

Zheng, M., Li, Z. and Huang, X. (2004) 'Ethylene glycol monolayer protected nanoparticles: synthesis, characterization, and interactions with biological molecules', *Langmuir*, 20(10), pp. 4226–4235. doi: 10.1021/la035981i.

Zhong, C. J. *et al*. (1999) 'Size and shape evolution of core-shell nanocrystals', *Chemical Communications*, (13), pp. 1211–1212. doi: 10.1039/a903165k.